FACIES DISTRIBUTION AND PALEOGEOGRAPHIC EVOLUTION OF PLEISTOCENE CARBONATES IN BONAIRE, NETHERLANDS ANTILLES

A Thesis

by

JONATHAN LUCAS SULAICA

Submitted to the Office of Graduate and Professional Studies of
Texas A&M University
in partial fulfillment of the requirements for the degree of

MASTER OF SCIENCE

Chair of Committee,	Juan Carlos Laya
Committee Members,	Michael Pope
	Niall Slowey
Head of Department,	Michael Pope

December 2015

Major Subject: Geology

ABSTRACT

The interaction between the Caribbean and South American plates produced irregular sea-floor topography on Bonaire (part of the Leeward Antilles Islands), which enables the deposition of calcium carbonate sediments. To better understand the nature and post-depositional history of these deposits, the distribution of carbonate facies across Bonaire was investigated. Direct observations (visual and photographic) of exposed Pleistocene carbonate rocks were made, then hand and core samples were collected. The samples were analyzed using thin-section petrography, X-ray diffraction, electron microprobe, and stable-isotope methods. Four terraces occur on Bonaire, and are associated with tectonic uplift and glacio-eustatic sea-level changes (the oldest, highest terrace located at the island center; the lowest, youngest terrace located along the island edge). Correlation to the dated terrace on adjacent islands indicates the youngest terrace is ~125 ky old (last interglacial highstand of sea level). Results from the visual observations and petrographic analysis (e.g., rock constituents, cement habit, mineralogy, and porosity) were used to delineate seven facies: *Acropora palmata* rudstone, *Montastrea annularis* framestone, Coralgal grainstone/packstone, Mixed Coral framestone, *Acropora cervicornis* floatstone, *Amphistegina sp.* grainstone, and Dolomite. Facies distribution is related to wave energy and water depth. Facies *Acropora palmata* rudstone and *Montastrea annularis* framestone are located on the windward side of the island (deposited in a high wave-energy, barrier reef environment). Facies Mixed Coral framestone and *Acropora cervicornis* floatstone are located on the

leeward side of the island (deposited in a low to medium-wave energy, fringing reef environment). Facies Coralgal grainstone/packstone are located on the platform interior (deposited in a low wave-energy, lagoonal environment). Facies *Amphistegina sp.* grainstone is located on the platform interior (deposited by eolian processes), and facies Dolomite is located at points across the island (formed by diagenesis of other facies). The dolomite displayed microcrystalline and sucrosic textures, and its $\delta^{18}O_{VPDB}$ values ranged from -0.7‰ to 2.7‰ and their mean value was 0.7‰. The proposed model of dolomitization is seepage reflux, during which dolomite forms as heavy brine solutions with heavy $\delta^{18}O$ made by evaporative processes seep into underlying carbonate rocks.

ACKNOWLEDGEMENTS

I am grateful for my advisor, Dr. Juan Carlos Laya for his guidance, support, expertise, and patience while working on this project. This was a very interesting project that I enjoyed working on, and am thankful for the experience. It was a pleasure working with you.

I am thankful for my other committee members, Dr. Michael Pope and Dr. Niall Slowey, for their support, expertise, and patience. I thank you both for your time and willingness to discuss my research, even during times when you were busy.

I would like to thank Dan A. Hughes Co. for their support by funding this project. This allowed longer duration in the field, as well as more samples to be acquired and different analysis to be performed on the samples, thus allowing the research to be more comprehensive and meaningful.

I also would like to thank classmates for their assistance performing this research, especially Philipp Tesch and Robet Widodo for their long hours in the field acquiring samples, and Bronwyn Moore, Robet Widodo, and Roy Conte for their help acquiring geochemical data and helping interpret diagenesis on the carbonates.

Many thanks to faculty members Dr. Ray Guillemente and Dr. Ethan Grossman for their time and expertise for performing lab work and helping understanding the results of geochemical data.

I would like to thank all my friends for their support and friendship. This has made my experience while in graduate school very much enjoyable.

Lastly, I would like to thank my Dad and Mom, and my sisters, Elisabeth, Adrianna, and Sophia for their love and always being there for me. This helped get me through some tough times and gave me drive to make me be the best person I can be.

TABLE OF CONTENTS

Page

Page

LIST OF FIGURES

FIGURE Page

FIGURE Page

LIST OF TABLES

INTRODUCTION

Bonaire Island is located in the southern Caribbean Sea, approximately 90 km north of Venezuela [Fig. 1]. It is one of the three islands that comprise the Netherlands or Leeward Antilles (commonly referred to as the ABC islands along with Aruba and Curacao). Bonaire is an example of an isolated carbonate platform (Read, 1985; Tucker and Wright, 1990). Controls on the formation and evolution of this type of platform include eustasy, tectonic subsidence and uplift, wind energy, wave energy, and tides (Deffeyes et al, 1965; Schellmann et al., 2002; Engel et al., 2012).

According to depositional environment models, during the Pleistocene a high energy regime created a barrier reef type environment with a protected lower energy lagoon between the barrier reef and the mainland (Bak, 1976; de Buisonje, 1964; Pomar, 2001; Bosence, 2005; James and Wood, 2010; James et al., 2010). This barrier reef environment is not common on the leeward side of islands, where low wave energy occurs and extensive fringing reef is permanently growing (van Duyl, 1985; Purkis, 2014). The leeward side has a sharp drop-off, with seaward-dipping slopes reaching up to 50 degrees and multiple horizontal benches interrupting the slope.

Climatic and oceanographic settings in Bonaire are ideal for coral growth. Situated in the low latitudes, corals are exposed to warm tropical waters throughout the year and the semi-arid climate regime results in only 52 cm/yr of rainfall annually so there is no river runoff. The waves impact the windward part of the island due to the continuous trade winds from the east (Haug and Tiedemann, 1998; Nisancioglu et al., 2003). Finally, tides within the Leeward Antilles are microtidal, with a range of

approximately 30 cm which provides stability for coral growth (De Haan and Zandeval, 1959).

Hermatypic coral species predominate in these reefs, which are abundant throughout the modern Caribbean Sea (Newell and Rigby, 1957; Wells 1957, 1967; Newell et al., 1959; Stehli and Wells, 1971; Milliman, 1974). The most abundant coral species include *Montastrea annularis*[1], *Acropora palmata*, *A. cervicornis*, *Diploria clivosa*, *D. labrinthiformis*, *Porites porites*, *P. astroides*, *Siderastrea sidera*, *S. radian*, and *Agaricia agaricites* (Bak, 1976; van Duyl, 1985; Kim and Lee, 1999; Pandolfi and Jackson, 2001). These corals' preferred growth environments depend upon both wave energy and water depth, and some corals may be sensitive to high wave energy.
The Pleistocene stratigraphy of Bonaire is directly related to glacio-eustatic sea-level change as well as tectonic uplift (Bandoian and Murray, 1974; Escalona and Mann, 2011; Hippolyte and Mann, 2011). These processes have created offlapping depositional patterns which are associated with inverse stratigraphy. In this setting, the youngest units are the lowest in elevation and located on the edge of the island, in contrast to the older Pleistocene units which are located toward the interior of the island and are higher in elevation (all occurring without influence from folding or faulting).

Previous studies focused on distribution of lithological units and described facies occurring on the island. Geologic maps of Bonaire include Cretaceous volcanics,

[1] Biologists have recently decided that the coral species referred to as *Montastrea annularis* in many previous studies is more properly referred to as *Montastrea faveolata*. I appreciate the reason for this change, but to maintain consistency with facies names used in published maps, and to avoid confusion when referring to the results of previous studies, this thesis will utilize the name *Montastrea annularis*.

Eocene limestone, Plio-Pleistocene inclined beds, Pleistocene terrace limestone, Pleistocene eolianite and Holocene carbonate sediments (Pijpers, 1933; de Buisonje, 1974; Bandoian and Murray, 1974). A revised geologic map was produced, adding the Cretaceous Rincon Limestone, redescribing the Eocene limestone as a conglomerate, limestone, and marl, as well as changing the previously described Plio-Pleistocene inclined beds (Seroe Domi Fm.) to Neogene (middle Miocene-Pliocene) (Hippolyte and Mann, 2011) (see Fig. 2). Fault kinematic analysis was also performed to collect mesoscale-fault data and reconstruct the regional Miocene and younger plate boundary tectonic forces that deformed the rocks (Hippolyte and Mann, 2011).

Outcrops located near the coast on the leeward and windward sides of the island were used to interpret depositional environments of carbonate deposits from described facies (Kim and Lee, 1999). The capitalized facies names refer to the facies delineated in the study (Kim and Lee, 1999). This interpretation includes windward environments comprising a barrier reef environment composed of *Acropora palmata* rudstone, a backreef lagoon composed of *Montastrea annularis* framestone, Diverse Coral rudstone composed of hemispherical, massive and spherical corals deposited off of the forereef slope, and Coralgal grainstone interpreted as calcareous beach sand. On the leeward side of the island, the facies included *Acropora cervicornis* floatstone as well as *Montastrea annularis* framestone.

In this study, the windward side also included *Acropora palmata* rudstone, *Montastrea annularis* Framestone, and the leeward side contained *Acropora cervicornis* floatstone facies, but the Coralgal grainstone was located in different locations than this

study (Kim and Lee, 1999). In addition, the present study describes a Mixed Coral framestone on the leeward side as well as facies from the 3rd- and 4th-terrace strata and discusses dolomite located within the 2nd-terrace cliffs, which Kim and Lee (1999) did not mention (for facies, see Fig. 3-5 and Table 1).

Few studies of dolomites in the Miocene-Pliocene units (including Seroe Domi Formation) and Holocene sediments were carried out. Dolomite from the third terrace in Bonaire was interpreted as Pliocene to determine original environment of formation, and it was suggested that initial dolomitization had a fresh to brackish water origin (Sibley, 1980). Petrographic analysis of "Pliocene" dolomites from Bonaire, Curacao, and Aruba characterized six dolomitic fabrics that were classified by mineralogy and size of material being dolomitized (Sibley, 1982). The dolomitic sediments in the Pekelmeer locality (southern Bonaire) were interpreted to form by the seepage reflux (Deffeyes et al., 1965). A porosity study of the Bonaire Plio-Pleistocene dolomites from the Seroe Domi Formation suggested porosity reduction occurred when limestone was dolomitized, reducing porosity from 25% to 11% (Lucia and Major, 1994). A geochemical study of the dolomite in the Pekelmeer locality was completed using $\delta^{18}O$ isotopes as an indicator for water salinity in an environment causing dolomitization. Results suggested that $\delta^{18}O$ alone cannot be used as an indicator for water salinity (Major et al., 1992). The stratigraphy and dolomitization history of the Seroe Domi Formation in Curacao (correlative to the Seroe Domi Formation in Bonaire) was determined using $^{87}Sr/^{86}Sr$ methods, which indicated relative ages of the different dolomites (Fouke et al., 1996).

The purpose of this study is to investigate the facies distribution of Pleistocene carbonate rocks across the entire isolated platform of Bonaire, and interpret their depositional environment. In addition, this thesis will interpret the stratigraphy and reconstruct the paleogeography of the Pleistocene carbonate rocks, as well as provide brief discussion of its diagenesis including dolomitization.

GEOLOGIC BACKGROUND

Tectonics

The island Bonaire is located in the southern area of the Caribbean Plate which is characterized by a Paleogene and Neogene terrigeneous deposits and Neogene carbonate banks deposited on top of deformed and metamorphosed oceanic crust and island arc (Gorney et al., 2007). The Caribbean plate is moving eastward relative to the surrounding plates (Miller et al., 2009; Ladd, 1976; Mann and Burke, 1984; Pindell et al., 2001).

There are differing hypotheses about the origin of the Caribbean Plate. One hypothesis involves the Caribbean Plate being derived from the paleogeographic Gulf of Mexico (James, 2006), while another hypothesis describes the Caribbean Plate originating from the Pacific Ocean. The most common model of the origin of the Caribbean Plate is from the Pacific Ocean, moving relatively eastward to South America continuously from the Cretaceous to the present (Jordan, 1975; Pindell et al., 1988; Perez et al., 2001; Trenkamp et al., 2002). This movement has created transtensional, transpressional, and convergent plate boundaries; influencing tectonic subsidence, uplift and subduction forming volcanic island arcs along the plate boundaries. The convergent plate boundary occurs further east with the Greater Antilles volcanic island arc, but the boundary near the ABC islands experienced transtensional and transpressional forces (Escalona and Mann, 2011). North of the Netherlands Antilles, the Caribbean Plate underthrusts the South American Plate at a shallow angle (Kellogg, 1984; Audemard, 1993; Levander et al, 2006). South of this thrust boundary is an accretionary wedge

resulting from the underthrusting of sedimentary rocks of the Caribbean Plate known as the South Caribbean Plate Boundary Zone (Silver et al., 1975; Biju-Duval et al., 1982).

The basement of the carbonate succession is the Washikemba Formation. Composed of rhyolite and dacite with some pumpellyite alteration, the Washikemba Fm. was dated using $^{40}Ar/^{39}Ar$ techniques (Thompson et al., 2004). With ages >90 Ma, Argon dating suggests the Washikemba Fm. was not formed on the Caribbean Plateau but instead in the intra-American proto-Great Arc (Thompson et al., 2004; Van Der Lelij, 2009). As the Caribbean Plate moved east relative to the South American Plate, it underwent both subsidence due to transtensional processes, as well as exhumation due to transpressional processes. Approximately 35 Ma, the Bonaire and Falcon Basins opened up and ~25 Ma, a second phase of transtensional rifting of the Bonaire and Falcon Basins occurred which led to submergence of the Bonaire platform (Gorney et al., 2007). Approximately 15 Ma, the Bonaire Basin becomes transpressive, which exhumed the platform (Gorney et al., 2007).

Stratigraphy

The stratigraphy of Bonaire was described by Pijpers (1933), Bandoian and Murray (1974), de Buisonje (1974), and Hippolyte and Mann (2011). The succession began with the Cretaceous volcanic Washikemba Fm., overlain by a thin succession of Cretaceous Maastrichtian Rincon limestone deposits. During the Eocene, the island was exposed due to tectonic uplift, weathered and eroded down to the pre-existing volcanics, and formed the Soebi Blanco conglomerate. Miocene carbonate is exposed on the northern side of the island, closer to the leeward coast. Miocene-Pliocene carbonate of

the Seroe Domi locally displayed high-angle dips up to 30 degrees away from the island's center. Pleistocene carbonate deposition occurred next, forming terraced strata, which is the most abundantly exposed carbonate on Bonaire (Fig. 6).

Terraces occur on both windward and leeward sides of the island, but the windward terraces are broad and much more pronounced due to the strong waves produced by the nearly constant trade winds (Alexander, 1961; Bandoian and Murray 1974; Herweijer et al., 1977; Herweijer and Focke, 1978). As sea-level fell, the strong waves carved out a cliff face in the rocks, and formed the terrace. Four terraces are recognized on the surface, with elevations at the top of the cliffs from each terrace level approximately 10 m, 25 m, 50 m, and 80 m [Figs. 7 and 8].

DATA AND METHODS

Hand samples and 2-in diameter cores were acquired from multiple locations on Bonaire. The total number of samples is 119, with 62 hand samples and 57 cores (2" diameter and approximately 18" long; for sample locations, see Fig. 9). The cores were collected using a Tanaka TED-270PFDH dual handle gas-powered core drill. These samples are mostly Pleistocene carbonate, but some Miocene samples were collected on the northwest side of the island. These samples were used to construct a facies distribution map of Bonaire, and investigate their diagenetic history.

A facies scheme was delineated based upon descriptions of hand samples, core samples, and thin sections, and observations of outcrops. A facies map was constructed to show the spatial relationship between the facies and their location on the island. Topographic maps were used to build profiles across the island. The facies map and profiles were used to generate geological cross-sections. No subsurface data was available, so subsurface geology is interpreted based on outcrop observations.

Paleogeography maps were constructed based on the morphology of the island of Bonaire and associated with each other in relation to relative time. Four paleogeography maps were constructed based on the distribution of the four terraces described on Bonaire.

Fifty-six thin sections were prepared, with 23 made at Texas A&M University, and 33 made by an independent company Quality Thin Section, Arizona. The samples prepared from the independent company were impregnated by blue stain to show porosity. All thin sections were stained with Alizarin Red S to assess the amount of

dolomitization within samples, and stained with potassium ferricyanide to observe ferrous calcite within the samples. These thin sections were studied using a Zeiss Axioplan 2 petrographic microscope to describe components within samples. Petrographic images were captured by Axiovision® 4.8 software. Dunham's (1962) carbonate rock classification texture scheme was used to describe the rocks. Cathololuminescence (CL) was performed on polished thin section samples to observe cements and their growth patterns with a Technosyn Cold Cathode Luminescence Model 8200 MkII. A vacuum pump was required to remove air by pumping down the vacuum chamber for 3 hours before analysis. After pumping down, the vacuum was set at approximately at -0.05 torr, the cathode power was set between 10-20 kV, which established a gun current set between 200 and 300 amperes. The microscope used to view the sample was the Leitz Laborlux D. The microscope had the camera Coolsnap-Pro_{cf} mounted above it which was used to capture the CL image.

A Cameca SX50 scanning electron microprobe was used to determine elemental composition of the samples. Thin sections were polished and carbon coated before being placed inside the microprobe. Energy dispersive spectroscopy (EDS) was used to verify mineral phases within the rock. After standardizing for calcite and dolomite, wavelength dispersive spectroscopy (WDS) was used to measure mineral composition. Abundances of Ca and Mg were observed for presence of dolomite as well as abundances of high-Mg and low-Mg calcite (HMC and LMW, repectively).

X-Ray diffraction (XRD) analysis was performed on powdered coral and whole rock samples to determine presence of dolomite, as well as to detect other mineralogies

within the samples such as aragonite and calcite. Approximately 0.1g of sample was drilled into powder, and crushed with mortar and pestle to eliminate all fragments from samples. Powder was then placed on a glass slide and flattened into a thin layer. The slide was then placed into a Rigaku Geigerflex XRD machine, where X-ray intensity as a function of 2-theta angle was measured. This allows relative sizes of peaks, which correspond to specific minerals were measured.

Fourteen samples were drilled to analyze their carbon and oxygen isotope ($\delta^{13}C$ and $\delta^{18}O$) compositions. Those analyses were performed at the Texas A&M University Stable Isotope Geosciences Facility using a Thermo 253 mass spectrometer with a Kiel IV Carbonate Device. Approximately 50µg of powder from each sample was analyzed and the $\delta^{13}C$ and $\delta^{18}O$ values were reported in per mil units relative to the Vienna PeeDee Belemnite (VPDB) standard.

RESULTS

Facies Analysis

Based upon the characteristics of the hand and core samples, 7 carbonate facies were differentiated. These facies include: *Amphistegina sp*. grainstone, *Montastrea annularis* framestone, *Acropora cervicornis* floatstone, *Acropora palmata* rudstone, Mixed Coral framestone, Coralgal grainstone/packstone, and Dolomite (Table 1, Figs. 3-5). These facies indicate similar energy processes occurred locally in the Pleistocene as they do today. Facies commonly located on the windward side of the island include *A. palmata* rudstone, *M. annularis* framestone, and Coralgal grainstone/packstone. Facies located predominantly on the leeward side of the island include *A. cervicornis* floatstone, Coralgal grainstone/packstone, and Mixed Coral framestone [Fig. 10]. Capitalized facies names refer to the delineated facies described on Bonaire.

Facies Distribution

The facies distribution was influenced mostly by variations of wave energy across the platform. Carbonate facies located on the windward (east) side of the island include *Montastrea annularis* framestone, *Acropora palmata* rudstone, dolomite, and Coralgal grainstone/packstone. These facies have a depositional pattern from distal to proximal of a single depositional cycles of the platform center includes *Acropora palmata* rudstone, *Montastrea annularis* framestone, and Coralgal grainstone/packstone. Dolomite is located within the 3rd terrace strata on the windward side. Carbonate facies located on the leeward (west) side include *Acropora cervicornis* floatstone, Mixed Coral framestone, as well as Coralgal grainstone/packstone [Fig. 11]. Dolomite occurs within

the 3rd terrace strata at Santa Barbara and 2nd terrace at Tolo. Progression of the leeward facies from proximal to distal in relation to the platform center based on one depositional cycle includes Mixed Coral framestone, *Acropora cervicornis* floatstone, and Coralgal grainstone/packstone. The platform interior is largely composed of Coralgal grainstone/packstone that is dolomitized in some locations, which includes the majority of the 4th terrace strata. *Amphistegina sp*. grainstone is an eolianite facies also located within the platform interior at three localities in the center of the island.

Dolomite occurs within the cliffs of the 2nd terrace on the northwest part of Bonaire on both windward and leeward sides. Dolomite from the 3rd terrace is exposed at the Seru Grandi and Santa Barbara locations. The 2nd terrace dolomite and 3rd terrace dolomite is genetically related to 3rd terrace strata. There are two textures associated with the dolomite: microcrystalline and sucrosic dolomite.

Petrographic Analysis

Bioclastic components within different facies viewed from thin sections include coralline red algae (Corallinacea family, both articulated and encrusting), benthic foraminifera (such as *Amphistegina sp.*), green algae and its calcified flakes (*Halimeda sp.*), bivalves, bryozoans, and coral fragments. Most of the bioclasts were fragmented while being reworked from different mechanical processes (Fig. 12 and Table 2).

There are varying types and abundances of cements and carbonate mud matrix. Carbonate mud matrix is present within the coralgal grainstone/packstone facies. The limestone within the beds of the 3rd and 4th terraces are recrystallized, having abundant meteoric cementation, as well as dolomitization precluding porosity (5-10%) within the

samples. The beds composing the 2nd terrace have less cementation (due to these being younger than the 3rd and 4th terrace beds). Dissolution is evident as well as cementation in the 2nd terrace samples, with more preserved porosity than samples from the 3rd and 4th terraces. First, the cements precipitated as fibrous and bladed types and nucleated on the walls of the grain growing outwards. The second-stage of cementation occurred when equant spar cement fully filled the pores. Beds composing the 1st terrace have undergone more dissolution than cementation. These beds are the youngest, so they have not been exposed to meteoric diagenesis as long as the other beds. Some cementation occurs within the 1st terrace beds inland, away from the influence of waves or ocean spray. These are fibrous cements and appear to have undergone only one stage of growth (Fig. 13).

The dolomite facies can be subdivided into two groups based on crystal texture within the matrix of the samples. The first dolomite texture occurs in the 2nd terrace and has a microcrystalline arrangement with some partially dissolved articulated red algae. The second dolomite type occurs in the 3rd and 4th terrace and consists of a coarser-crystalline sucrosic texture with the characteristic rhombic geometry. In addition, no bioclasts could be observed and some calcite spar remains within the 4th terrace dolomite. Visual porosity is approximately 5% within the samples from both textured dolomite.

Geochemical Analysis

X–Ray diffraction (XRD) was performed on rock and coral samples to determine presence of calcite, aragonite, and dolomite. Coral samples are from the 1st and 2nd

terraces of the windward side with six from the 1st terrace and 11 from the 2nd terrace. Analysis indicated that all corals from the 2nd terrace had replaced their mineralogy from aragonite to calcite [Fig. 14]. Only one sample from the 1st terrace had all original aragonite replaced by calcite, 2 samples were partially replaced with 25% abundance of calcite [Fig. 15], and 3 samples were completely composed of aragonite. Samples from Boca Onima, Tolo, and Santa Barbara were believed to be composed of dolomite. These samples were confirmed to be dolomite by X-Ray diffraction [Fig. 16].

Ten samples were analyzed with the Electron Microprobe. Examining the values of these samples in the order of deposition, with the first being the Seroe Domi Formation sample. The notable values for this sample are approximately 99% abundance of $CaCO_3$ and 1% abundance of $MgCO_3$. The values for the 4th terrace sample mimic the values for the Seroe Domi sample. The 4 non-dolomite samples from the 2nd terrace include an increased abundance of $MgCO_3$ to average approximately 1.5%, and $CaCO_3$ average abundance of 98.4%, and minute amounts (between 0.05-0.20%) of Si, Fe, Na, and Sr. The 1st terrace sample continues an increased abundance of $MgCO_3$ at approximately 3.3%, $CaCO_3$ abundance approximately 96.4%. All limestone samples are composed of LMC. The 3 dolomite samples are from the 2nd terrace, and composed approximately of 55% $CaCO_3$ and 45% $MgCO_3$. This dolomite has a non-stoichiometric relationship.

Both limestone and dolomite samples were analyzed for stable isotopes $\delta^{13}C$ and $\delta^{18}O$ [Fig. 17]. Whole rock powder drilled from limestone samples from terraces 1, 2, and 4 were used to determine isotopic signatures. Values from each of the terraces are

highly varied for both $\delta^{13}C$ and $\delta^{18}O$. Terrace 1 – values of $\delta^{13}C$ are -3.6‰ and -1.0‰. Values for $\delta^{18}O$ are -0.5‰ and 0.5‰. Terrace 2 – values of $\delta^{13}C$ vary from -5.8‰ to -2.5‰. Values of $\delta^{18}O$ vary from -3.8‰ to –4.9‰. Terrace 4 - values of $\delta^{13}C$ vary from –3.9‰ to -3.5‰. Values of $\delta^{18}O$ vary from -0.7‰ to -0.5‰.

When comparing the average isotopic values of C and O and relating them to their respective terrace, there was a depletion of heavy $\delta^{13}C$ and $\delta^{18}O$ isotopes from the 1^{st} to 2^{nd} terrace within limestone samples. The dolomite samples had $\delta^{13}C$ values from -0.77‰ to 3.13‰ and $\delta^{18}O$ values from 1.20‰ to 3.65‰. Dolomite samples were from the second terrace on both the windward and leeward side of the island.

DISCUSSION

Depositional Environments

Bonaire is composed of a variety of depositional environments that depending on the location on the platform. The windward side is comprised of high-energy barrier reef environment. The central part of the platform contains a low-medium energy lagoon environment. The leeward side of the island comprises of a low-medium energy fringing reef environment. The exposed central part of the platform also contains eolianites as a result of west-flowing winds. These depositional environments were interpreted based on coral assemblages and bioclastic compositions. The western Aves Island (approx. 60 km east of Bonaire, see Fig. 18) was used as an analogue to Bonaire's earliest Pleistocene deposition because it has similar depositional environments as Bonaire.

Barrier Reef

The barrier reef is composed most abundantly of the coral *Acropora palmata* (Mesolella et al., 1970; Scatterday, 1977), which thrives in high wave-energy environments. Especially, high-energy waves may fragment *A. palmata*, generating rubble deposits. The corals will undergo rapid growth by diverting the majority of its energy towards growth, increasing its survivability (Glatfelter et al., 1978; Lirman, 2000; Klaus et al., 2012). As rapid growth ensues, it will eventually create a crest on the reef that works as a barrier protecting the internal areas from wave energy. This process produces a protected lagoon environment where more sensitive head corals and fragile organisms can grow and grains can be deposited in the platform interior. The barrier reef environment is located on the eastern side of Bonaire, and is the most distally

located shallow marine depositional environment on the windward side of the island (see Figs. 19-22).

Lagoon

The lagoonal environment is located landward of the barrier reef in the platform interior where low-medium wave energy occurred (Fig. 21 and 22). During deposition of 4th terrace strata, the lagoon covered a major part of the interior platform, including *Montastrea annularis* framestone landward of the barrier reef, and Coralgal grainstone/packstone facies over the central part of the platform. Both facies were deposited due to the presence of low to medium wave energy. As the island emerged the spatial expanse of this environment increasingly became associated with the windward side that was located between the barrier reef and the exposed island. The lagoonal environment was described by de Buisonje (1974) as either a coral-rich bottom that was abundant with head corals *Montastrea annularis, Siderastrea siderastrea, and Diploria sp*., a grain-rich bottom from coral rubble and bioclasts fragments, or a rocky bottom with just carbonate rock exposed. Bare rock exposures on the ground would likely have only occurred where wave energy was still too high for grains to deposit. Evidence of the coral and grain-rich bottom occurs within the terraces.

Terraces 1-3 are composed, at least in some portion, of head corals, typically *Montastrea annularis* (Scatterday, 1977). The 2nd terrace also has abundant bioclastic grains which include very fine grain sand composed of fragments of green and red algae, coral, foraminifera, bryozoans, and bivalves. The most abundant facies in the lagoon is

Coralgal grainstone/packstone facies as indicated by the 3rd and 4th terraces being composed mainly of this facies.

Fringing Reef

The fringing reef depositional environment was located in areas of low-medium wave energy on the leeward side of the island. This environment occurred in slightly deeper waters and with higher energy compared to the platform interior. This environment also includes the top of the slope off the platform containing fringing reefs. This environment comprises corals *A. palmata*, *A. cervicornis*, *M. annularis*, *S. siderastrea, Diploria sp*, as well as other head corals (Focke, 1978; van Duyl, 1985). The arrangement of the corals from shallow to deep begins with *A. palmata* in the shallowest waters, only up to 4-5 meters deep (Chappell, 1980), followed by *A. cervicornis* between depths 15 and 30 m (Goreau and Wells, 1967; Mesolella, 1967). Head corals have a wider depth range of growth and can grow at depths up to 100 meters, but the optimal depth for growth for many head corals is between 10 – 60 m (Goreau and Wells, 1967; Mesolella, 1967) where there is decreased stress from wave action (Barnes, 1973; Chappell, 1980). Decreased stress is important for the head corals because they do not regenerate as rapidly as *Acropora sp.* (Dustan, 1975). In addition, bioclastic grains occur in the shallow marine environment and are randomly arranged both along strike and down slope. These grains (composed of fragments of red algae, foraminifera, and bivalves) are most abundant where slopes are less steep, which goes from the shoreline to about 5-10 m depth. These abundant grains are also found at a

horizontal sub-sea bench at an approximate 30m depth. Corals are more abundant than skeletal grains on the slope, but bioclasts were deposited between corals on the slope.

Eolianite

High-angle cross-bedded deposits of fine-grained grainstone occur in the central part of Bonaire. This grainstone is composed of bioclastic fragments, mainly of benthic foraminifera (*Amphistegina sp.*), bryozoans, and bivalves, and can be up to 40 m thick. These beds are topographically the highest carbonate strata on the island, located on top of the 3rd and 4th terrace strata. The beds are never located on top of strata from the 1st or 2nd terrace, so it was suggested by de Buisonje (1974) that this grainstone was derived from beach sands on the windward coast after deposition of the 3rd terrace strata. The grains were carried by the strong and constant trade winds from the east and deposited on the center of the island.

Tectonic Implications

Bonaire is located in the South Caribbean Plate Boundary Zone (SCPBZ), which has been experiencing transpression since the Miocene. The Caribbean Plate is moving southeast relative to the South American Plate. Within the SCPBZ, the Caribbean Plate converges with the South American Plate, and shallow subduction of the Caribbean Plate beneath the South American Plate occurs. The subduction occurs north of Bonaire (known as the South Caribbean Deformation Belt (SCDB)), and has created an accretionary wedge among the sedimentary rocks within the SCPBZ as a result of tectonic uplift.

Bonaire terrace formation was partially a product of tectonic uplift, but, as a result of this uplifting, it is possible that a subsidence process occurred on the southern part of the island. For that reason, the 1st terrace strata on the northern side of Bonaire is approximately 9 m above sea level whereas the same strata on the southern side disappears beneath the modern Pekelmeer lagoon. The reason for this process is that the distance between the north part of the island and the South Caribbean Deformation Belt subduction zone is approximately 120 km north of Bonaire. The shallow subduction occurring on the SSCB pushes the Bonaire block upward. It is possible that the northern side of Bonaire was more influenced by the subduction processes than the southern side, allowing for more uplift due to it being the nearest location to the subduction area. This, in effect, is believed to have influenced syntectonic deposition. Clinoforms prograding to the south are present in Seru Grandi (northern Bonaire), illustrating this process.

Seismic interpretation indicates that reverse faulting occurred in relation to subduction of the Caribbean Plate north of Bonaire in the South Caribbean Deformed Belt (Gorney et al., 2007; Escalona and Mann, 2011). However, in the Caribbean Arc Basin where the Netherlands Antilles are located, grabens formed due to transverse motion of the Caribbean Plate (Fig. 23). These grabens formed during the Paleogene to Early Miocene. The seismic transects illustrate normal faults within the basement (Cretaceous) through Early to Late Miocene times which shows thick sedimentary successions due to high clastic sediment input via the paleo Orinoco delta and other river deltas (Gorney et al., 2007; Escalona and Mann, 2011). South of Bonaire and Curacao, inverse faulting has occurred since the Miocene due to subduction from the South

Caribbean Deformation Belt. Inversed faulting induced by the shallow-angle subduction is the mechanism for terraced limestone formation on the Netherlands Antilles (Gorney et al., 2007; Escalona and Mann, 2011).

Curacao and Aruba are both within the same tectonic regime, experiencing similar tectonic uplifting as Bonaire. As a result, a similar pattern of deposition and erosion formed on these islands. Furthermore, Curacao and Aruba also experience an increase in subsidence from north to south, as in Bonaire.

In addition to the Netherlands Antilles, other Caribbean islands have experienced tectonic uplift due to convergent tectonic regime. Barbados is located at the northern part of the South American Plate which subducts beneath the Caribbean Plate, forming an accretionary prism. Barbados experienced Pleistocene uplift and contains multiple terrace levels dated from 82 ky (3-20 m elev.), 105 ky (6-30 m elev.), and 125 ky (36-60 m elev.) (Matthews, 1973). It can be inferred from this example that comparing the 36-60 m elevation of the MIS 5 aged carbonate rocks in Barbados to the up to 10 m elevation MIS 5 carbonate rocks in Bonaire that Barbados has experienced faster uplift rates than Bonaire.

Age Constraint for Pleistocene Deposits

The 1st terrace strata relates with elevation from sea-level close to 10 m. Both windward and leeward terraces are very pronounced. A wave-cut notch on both sides can be seen approximately 2 m above sea-level in some areas. Mineralogy within the strata is still mainly the original limestone in most locations. Samples from the 1st terrace strata in Curaçao, which is correlative to the 1st terrace in Bonaire, were dated by

Electron Spin Resonance (ESR) methods and Uranium-series (Schellmann et al., 2002; Muhs et al., 2012). Both studies produced dates to be approximately 125 ky which coincides with the MIS 5e interglacial period (Hornbach et al., 2010). Though there is no data to constrain ages of the 2^{nd}-4^{th} terraces, it is likely that these terraces were deposited during the preceding interglacial cycles. Terrace 2 may have been deposited during the MIS 7 (~200-220 ky), Terrace 3 may have been deposited during the MIS 9 (~330 ky), and Terrace 4 may have been deposited during the MIS 11 interglacial (~405 ky). Ages are from peak transgressions, which are based on paleosea-level reconstruction from $\delta^{18}O$ benthic foraminifera data (Shackleton and Opdyke, 1973; Waelbroeck et al., 2002 [Fig. 24]; Lisiecki and Raymo, 2005; Muhs et al., 2012 [Fig. 25]).

Platform Development and Paleogeographic Evolution

Volcanic Basement

The volcanic basement is exposed in two main regions, in the northwest and east parts of the island. The northwest volcanics have three major high-elevation localities, with the rest of the volcanic exposure averaging around 40 m. One of the physiographic features is a conical hill with an elevation up to 130 m on the southwest part of this volcanic region. The other two localities are linear ridges parallel to each other from the northwest to the center of that region. The maximum elevations for these ridges are 180 m and 130 m. These ridges are oriented southeast toward the eastern volcanic region. Between the two volcanic regions is carbonate strata from the 3^{rd} and 4^{th} terraces in which elevations are between 70 and 140 m. The eastern volcanics are topographically lower of which the maximum elevation is about 70m and average elevation is 25-30 m.

Based on these observations, it can be assumed that as the island was being uplifted, shallow water carbonate deposition began in the northwest region of Bonaire where the platform was shallowest. As uplift continued, the geographical extent of this carbonate deposition migrated to the southeast as the platform became shallower with water depth.

1st Phase Pleistocene Deposition and Paleogeography

The western Aves Island (approx. 60 km east of Bonaire, see Fig. 18) and the current Bonaire Island morphology were used as analogues. The western Aves Island was used for the analogue for the 4th terrace paleogeography [Fig. 26] because it contains a well-developed barrier reef on the windward (east) side with northwest–southeast extent of approximately 15 km protecting a lagoon from high-energy waves, and shallow marine waters on the leeward side including a fringing reef. There are exposed carbonate rocks on the rim of the platform, whose highest elevation is only a few meters, which is similar to what is expected of Bonaire during deposition of 4th terrace strata. This strata would be equivalent to phase 1 of Pleistocene carbonate deposition, and likely occurred during the MIS 11 (~405 ky).

When Bonaire's 4th terrace strata was deposited, the underlying Cretaceous volcanic basement could have been exposed as much as ~80 m above sea level in a few locations. (Miocene carbonates may also have been exposed as well, but these were eroded). The volcanic basement was elongated northwest to southeast, and carbonate deposition reflects this pattern (as seen by terrace 4 strata). The volcanic exposures would have been located on the northwest side of Bonaire. The basement to the southeast was not elevated enough to be subaerially exposed during the time the 4th

terrace was deposited. There is no evidence of Miocene shallow-water carbonate deposition in the exposed southeastern volcanic locality, so it is likely that the southeastern volcanics were submerged too deep to deposit shallow-water carbonate. It is estimated that the shallowest the southeastern volcanics were was approximately 60 m, which means deposition from the 4th terrace strata only occurred in the northwestern half of the island.

Trade winds from the east created high wave-energy which influenced barrier reef growth on the windward side of Bonaire. A similar setting is envisaged as the western Aves Island where the barrier reef provided protection from high wave-energy allowing for deposition with a shallow-water lagoon to be deposited. Fringing reefs grew on the leeward slopes of the platform.

2nd Phase Pleistocene Deposition and Paleogeography

At the time of deposition for the 3rd terrace strata (MIS 9, ~330ky), the shallow carbonate platform began to resemble the boomerang-shape of the current Bonaire platform. There was greater uplift of the volcanics to the northwest than in the southeast. The southeast basement could have been shallow enough (approximately 20 m deep sub-sea) to allow production of shallow-water carbonate. A large shallow lagoon formed in the northwest where it was protected from high-energy waves. The barrier reef would have extended further south allowing elongation of the lagoon and fringing reef development, as well as grainstone-packstone type sedimentation south on the leeward slopes (Fig. 27).

Skeletal grains and sedimentary structures occur within most of the 3rd terrace strata, however, corals indicative of a barrier reef environment (*Acropora palmata*) only occur on the windward side at Boca Onima. Continuing southeast, erosion occurred progressively further inland, resulting in complete erosion of the *Acropora palmata* rudstone and *Montastrea annularis* framestone facies. With these facies eroded, Coralgal grainstone/packstone is exposed at the terrace cliff-face with cross-stratification towards the top of the cliff.

The leeward facies is primarily coralgal grainstone/packstone, with no apparent cross-stratification. It is likely that the 4th terrace carbonate rocks provided protection from the strong wave energy from the windward side of the island, allowing small amounts of carbonate mud to deposit and pervasive bioturbation to occur.

Fine-grained sucrosic dolomite occurs at Santa Barbara in the west-central part of Bonaire. The massive dolomite bodies occur on an east-facing vertical cliff face. Some microcrystalline dolomite also occurs on the windward side at the Seru Grandi and Boca Onima localities.

3rd Phase Pleistocene Deposition and Paleogeography

During 3rd phase of Pleistocene deposition (MIS 7, ~200-220ky), the platform may have enlarged to the south, as well as widened to the east and west. Assuming little erosion of the volcanics and using current topography, very shallow waters (< 20 m) covered much of the platform allowing for increased carbonate deposition laterally, especially around the southeastern volcanic exposure. Much of the island was protected from high wave energy by the barrier reef and exposed rocks which allowed the platform

interior to develop into a lagoon. The lagoonal environment likely covered much of the internal parts of the platform over the current northwest volcanics region as well as the windward side of the island, landward of the barrier reef. The leeward side of the carbonate platform was open to the ocean with low-medium wave energy, but deposition in this environment likely occurred in slightly deeper waters because of the leeward slope of the platform (Fig. 28).

4th Phase Pleistocene Deposition and Paleogeography

After continued uplift, a greater area of Bonaire was exposed including greater physiographic features of the two volcanic regions and older carbonate rocks. Maximum sea-level during this time (MIS 5e, ~125 ky) was 6 m higher than current sea-level, which means with strata 10 m above current sea-level, Bonaire may have been uplifted approximately 4 m since MIS 5e. A barrier reef grew on the windward side of the carbonate platform with a low-medium energy lagoon forming between the reef and land. This lagoon supported mostly head coral species such as *Diploria sp.* and *Montastrea annularis*. The leeward side of Bonaire was largely protected from high-energy waves, by the leeward fringing reefs west of the eastern volcanic region. This protection is related to the morphology of the island forming an asymmetric "boomerang-shape". The morphology is related to the northwest to southeast orientation of volcanic exposure and a north-south trend of barrier reef growth (Fig. 29).

Distribution of Miocene Seroe Domi Formation

The Miocene Seroe Domi Formation was previously described and mapped on Bonaire by Pijpers (1933), de Buisonje (1974), Bandoian and Murray (1974), and

Hippolyte and Mann (2011). The Miocene strata was defined as high-angled (from 5-30 degrees), dipping away from the volcanic basement at Gotomeer in the northwestern part of the island. This strata was described as slope deposits (de Buisonje, 1974). The reefal and grain-rich lagoonal lithologies, which were likely deposited on the northwestern volcanic rocks, have since weathered away. These geological maps have described strata of the 3rd and 4th terraces from the leeward side of the island as Miocene strata, likely because it is along strike with the Miocene slope deposits. There are multiple problems with the Seroe Domi Formation being exposed as they were described in these geological maps:

1. Miocene outcropping at Gotomeer included high-angled beds, but beds to the east along strike did not have high-angle dips.
2. In some locations the beds were composed of *in situ* corals from a shallow marine environment instead of a slope.
3. Leeward strata of Bonaire was interpreted as Miocene, wheras strata from the windward side, of the same elevation and lithology, was described as Pleistocene.

The Miocene succession may continue along strike, but only in the subsurface. High-angled Miocene dipping strata at most locations are overlain by Pleistocene strata. The Miocene strata is described as medium-bedded, wheras the Pleistocene strata are more massive, except in the Coralgal grainstone/packstone, where cross-stratification occurs within laminae sets. It is inferred that most of the Miocene carbonate rocks originally deposited on the northwestern section of the island were eroded away. The

only Miocene carbonate rocks on the island were unconformably overlain by Pleistocene carbonate rocks.

Control on Deposition of Pleistocene Carbonate

Pleistocene depositional processes were influenced by oceanic currents, wind patterns, and sea level changes. Oceanographic processes influencing deposition include the direction and depth of ocean currents as well as nutrient levels in the waters. The wind pattern was influenced by the cooling and warming of the poles. Patterns related to the Coriolis effect shifted convection currents including the ITCZ (Intertropical Convergence Zone) north or south as the ice sheets expanded and shrank (Chiang and Bitz, 2005; Martinez et al., 2007). The Caribbean Current flows almost directly west approximately 200-300 km north of South America in the southern Caribbean Sea (Gordon, 1967, Martinez et al., 2007) (Fig. 30), and then diverts north as it approaches Central America. Later it flows through the Yucatan and Florida Straits, eventually joining the Gulf Stream. The Caribbean Current is relatively shallow, approximately 100 m below the surface and it is composed of surface water and deeper Subtropical Under Water (SUW) (Fig. 31-32) that originates from the tropical North Atlantic Ocean) (Gordon, 1967; Bornmalm et al., 1999; Kameo et al., 2004). The west-flowing trade winds have a moderate influence on shallow ocean current travel, especially in the southern Caribbean, where ocean current reflects wind pattern direction (Gordon, 1967).

Surface winds are controlled by west-flowing trade winds (Fig. 34) that are related to converging trade winds of the intertropical convergence zone (ITCZ). The location of the ITCZ is seasonally controlled, located more northerly during the northern

hemisphere's autumn and winter (October-December), and southerly during the northern hemisphere's spring and summer (May-July) (Hastenrath, 1975, Martinez et al., 2007) (Fig. 30), however, there are alternating cycles between wet years and dry years (Hastenrath, 1975). Weather patterns also are related to the location of the ITCZ. Weather to the north of the ITCZ is dryer, and weather to the south of the ITCZ is more humid and experiences more rainfall (Martinez et al., 2007). The ITCZ is located north of the equator in the South America/Caribbean region, fluctuating between 4º and 12º north. This asymmetry of the ITCZ is caused by a relation to physical instabilities and feedbacks that intensifies the initial onset of the ITCZ in either the northern or southern hemisphere (Philander et al., 1995). For instance, cold surface waters associated with upwelling at the equator prevents the ITCZ from traveling south (Pike, 1971). The position of the ITCZ is related to a positive feedback of atmospheric heating consistent with moist deep convection and a boundary-layer of convergence of moisture that feeds and intensifies the convection (Charney, 1971; Waliser and Somerville, 1974). The asymmetry of landmass between the northern and southern hemispheres and coastal geometries in the tropics may also affect the position and strength of the ITCZ (Philander et al., 1995).

Computer models indicate increased high latitude ice cover may have produced southward excursions of the ITCZ (Chiang and Bitz, 2005), and paleotemperature estimates of the last glacial maximum derived from the analysis of marine sediment cores are consistent with an ITCZ excursion (Arbuszewski et al., 2013). If the ITCZ also shifted south of its current position during older glacial periods, it is likely that

Bonaire would have the same semi-arid climate during older glacial lowstands, based on the assumption of current arid conditions north of the ITCZ (Hastenrath, 1975; Martinez et al., 2007). This means that similar depositional systems and diagenetic processes affecting the rock during glacial periods would occur similarly during interglacial periods.

The closure of the Panamanian Seaway, approximately 2.75 Ma, caused the surface ocean current direction to flow in an increasingly northward path after it passed present-day Colombia (Haug and Tiedemann, 1998; Schneider and Schmittner, 2006). Between 2.75 Ma and present-day, the paleoceanography of Bonaire did not alter much (Bornmalm et al., 1999). A westerly flow would be consistent during the Late Pleistocene and incorporate nutrients from the Orinoco and Amazon Rivers that would outflow into the Atlantic Ocean, similar to current conditions. The Orinoco River may have flowed north in the Miocene and drained into the Caribbean Sea at modern-day Venezuela, but uplifting of the Andean tectonics could have caused a shift of drainage patterns to the east (Hoorn et al., 1995; Hippolyte and Mann, 2011).

A thermocline occurs within the SUW waters, creating a barrier from water mixing between waters on the surface and the deep nutrient-filled waters (Kameo et al., 2004). The shallow Caribbean waters are depleted in nutrients, however there are still nutrient sources to the shallow Caribbean waters, including output from the Amazon and Orinoco Rivers, as well as upwelling along the northern coast of South America (Fig. 33). After the waters from the rivers leave their deltas, they travel north past Trinidad, where they are eventually incorporated into the Caribbean current waters (Van Andel,

1967; Muller-Karger and Castro, 1992; Hu et al., 2004). Also, upwelling occurs in shallow waters along the northern coastline of South America as a result of the strong trade winds pushing the surface water with it, allowing deeper, more nutrient-abundant waters to reach the surface.

In addition to nutrient sourcing from rivers, upwelling also was a nutrient source for Bonaire. Strong wind-driven coastal upwelling occurs mostly between 61ºW and 74ºW, except between 68ºW and 70ºW where downwelling occurs (Muller-Karger and Castro, 1992; Reuda-Roa and Muller-Karger, 2013). Strong upwelling episodes in the southern Caribbean Cariaco Basin from ~12,600 years ago were related to a rapid rise in sea-level, and subsequent upwelling ~10,000 years ago may be related to intensified trade winds (Peterson et al., 1991). These events likely occurred within the Pleistocene during Bonaire's carbonate deposition. Wind currents in the Caribbean often have small variations in their flow north and south, so it is likely that some of the nutrient-rich upwelled waters arrived at Bonaire.

Diagenetic Processes in Pleistocene Carbonates, Bonaire

Meteoric Diagenesis

Carbonate rocks in Bonaire formed in a semi-arid climate; therefore most of the island is not susceptible to extensive dissolution. With evaporation rate exceeding rainfall rate throughout most of the year, most dissolved calcite precipitates into porosity-destroying cements at the surface (Marshall, 1992). Mechanical weathering and dissolution does occur from continued wave action, which is the most effective force for erosion and is perhaps the origin of terrace formation (Bandoian and Murray, 1974).

There are numerous caves within the 2nd terrace strata, and it is suggested that these form by dissolution from saltwater-freshwater interaction in a mixing zone, or it may be related to a more humid conditions.

The older deposits were subjected to meteoric diagenesis for longer time periods, and therefore all original aragonite was replaced with calcite in the 3rd and 4th terrace strata. LMC is present in the older terraces. Samples from the 3rd terrace were not tested for geochemical data, so it is assumed that strata from the 3rd terrace will have similar results due to a similar exposure history as the 4th-terrace strata. Strata from the 2nd terrace is younger, so there is some preservation of the first stage of meteoric dissolution. However, much cementation has also occurred, filling in porosity as rimmed cements. Aragonitic corals from the 2nd terrace has also been replaced by LMC calcite to replace a metastable aragonite with a stable calcite (Matthews, 1968; Constantz, 1986). The 1st terrace strata corals are still mainly composed of aragonite. In addition, samples from this strata indicate more preserved porosity than strata from the second terrace. 1st terrace rocks show increased porosity from dissolution, preferentially from the metastable aragonite. The 1st terrace also contains some LMC cements, but fewer cements than the older strata.

Stable isotopes $\delta^{13}C$ and $\delta^{18}O$ were examined from limestone samples from terrace strata 1, 2, and 4. Some results from terrace 3 strata were acquired in another study (Kim, 1998). In this study, both terrace 2 (termed middle terrace 1 by Kim (1998)) and terrace 3 (termed middle terrace 2) (Kim, 1998) data was grouped together (Kim, 1998).

Terrace 4 samples were partially dolomitized and show values a trend of positive values $\delta^{18}O$ values ranging from -0.7‰ to 2.7‰ VPDB, averaging to 0.7‰ VPDB, and $\delta^{13}C$ values ranging from -4.0‰ to 2.7‰ VPDB with an average of -1.7‰ VPDB. The middle terrace results expressed similar $\delta^{18}O$ values ranging from -4.8‰ to -3.6‰ VPDB, averaging -4.3‰, and $\delta^{13}C$ values ranging between -9.2‰ and -3.64‰ VPDB, averaging at -6.1‰ VPDB. Terrace 1 samples show negative $\delta^{18}O$ and $\delta^{13}C$ values, with $\delta^{18}O$ values of -4.2‰ and -0.5‰ VPDB, averaging to -2.4‰, and $\delta^{13}C$ of -1.0‰ and -3.7‰ VPDB with an average of -2.4‰ VPDB. Negative values associated with isotopic $\delta^{18}O$ and $\delta^{13}C$ analysis are associated with subaerially exposed meteoric diagenesis.

Potential factors controlling the $\delta^{18}O$ values of exposed carbonate rocks generally include temperature, evaporation, and mineralogy. However, in the case of Bonaire, temperature remains relatively constant throughout the year, so $\delta^{18}O$ values are not likely to change much due to this variable. Paleotemperature for the past ~2.5 Ma should remain within a similar range due to Bonaire moving along the same latitude line near the equator, and deposition only occurring over the platform during highstands. The $\delta^{18}O$ of aragonite is enriched relative to that of calcite (Tarutani et al., 1969; Grossman and Ku, 1986; Kim and O'Neil, 1997), which may account for the 1st terrace samples having a heavier average $\delta^{18}O$ value than the 2nd and 3rd terrace average $\delta^{18}O$ value for limestone samples. Also, a decrease in $\delta^{18}O$ could be related to lighter oxygen from rainwater being incorporated into the crystal lattices of the calcium carbonate (Kim, 1998). Based on the presence of dolomite, samples from terraces 3 and 4 have

positive $\delta^{18}O$ values and have much heavier isotopic values than the lowest two terraces. It is likely that the heavier $\delta^{18}O$ values are a product of evaporative processes on the surface (Hudson, 1977).

$\delta^{13}C$ values range from -5.8‰ to 1.5‰ VPDB. The only anomalies are two samples that coincide with the positive $\delta^{18}O$ from terrace 4. These heavy isotopic values could be related to evaporation (e.g. Kim, 1998), or related to dissolved inorganic carbon (DIC) having a localized abundance of $\delta^{13}C$ (Kim, 1998).

Dolomitization

Dolomitization of modern sediments was observed in southern Bonaire in the Pekelmeer hypersaline lagoon (Deffeyes et al., 1965). The mechanism of dolomitization suggested is seepage reflux, which is the process of dense hypersaline brines seeping into the subsurface (Deffeyes, et al., 1965; Tucker and Wright, 1990; Lucia and Major, 1994). It is assumed that the dolomitization model occurring in the Pekelmeer lagoon also produced the Pleistocene dolomite due to Bonaire being in a similar setting during the Pleistocene.

Hypersalinity is a result of limited influx of new seawater into the system, and evaporation induced saturation of dissolved ions within the brines (Machel and Mountjoy, 1986; Klosowska, 2004). These waters have higher Mg^{2+}/Ca^{2+} ratios and will replace calcite for dolomite until they have precipitated enough Mg^{2+} and dissolved enough Ca^{2+} to approach equilibrium. Higher Mg^{2+} abundance within the hypersaline water is due to Ca^{2+} binding with sulfate used to form gypsum as the brines become increasingly saturated with dissolved ions. Seepage reflux is the model suggested to be

the mechanism that produced the dolomites in this study on the 2nd, 3rd, and 4th terraces. In this model, a coral-rubble levee separates the internal hypersaline lagoon from the ocean that sources the saline water. Water is introduced by microtidal high tides and seepage through the coral rubble. If this process occurred, dolomite crystals did not form out of an aqueous solution, but instead, it formed by way of metasomatism from pre-existing crystalline calcium carbonate (Degens and Epstein, 1963). Gypsum and other evaporites have not been described within the Pleistocene strata, but the lack of evaporites could simply be a consequence of loss due to weathering upon exposure to the atmosphere as sea level fell after the evaporites were deposited.

Dolomite from the 2nd terrace was described as having a different texture than that in the 3rd and 4th terraces. The 2nd terrace dolomite outcrops only on the 2nd terrace, and is genetically related to 3rd terrace strata. The 2nd terrace strata onlaps onto the 3rd terrace strata. But because the 2nd terrace dolomite outcrops at the 2nd terrace cliff on the windward and leeward sides of the island, it was referred to as 2nd terrace dolomite.

The 2nd terrace dolomite is microcrystalline, with some articulated red algae being partially dolomitized. Originally, it was though that red algae was composed of HMC, and seawater leached the excess Mg^{2+} ions from the algae, and incorporated it into the dolomite crystal lattice (Ries, 2006). However, electron microprobe analysis on Bonaire samples indicated that the red algae contained LMC with abundances of Mg^{2+} between 1 and 2 mole%. It was realized through this method that dolomitization did not occur by seawater leaching.

Compared to the dolomite in the 2nd terrace, the dolomite from the 3rd and 4th terraces has coarser, rhombohedral crystals with sucrosic texture, and no bioclasts are preserved. The dolomite from the 3rd terrace is located within the island's interior at the cliff of the 3rd terrace, east of Santa Barbara. The 4th terrace dolomite is located in the central part of the island, comprising most of the 4th terrace strata. This dolomite body is composed mostly of dolomite, but ~30% fine-crystalline calcite spar still remains.

In terms of texture, the 3rd terrace dolomite has coarser crystals, which suggests it was allowed a longer time to develop than the 2nd terrace dolomite. The 2nd terrace dolomite is located near the exterior of the island whereas the 3rd terrace dolomite is located in the middle of the island. This is interpreted as follow: as sea level began to fall during the last two glaciations, the interior lagoon where the 3rd terrace dolomite likely did not experience as strong of wave action as the 2nd terrace dolomite, which allowed for more rock preservation. This coarser 3rd terrace dolomite was also likely closer to the island's surface and endured a longer exposure to the hypersaline fluids.

The 4th terrace dolomite is much more expansive than the other dolomite units, therefore the locations of the seepage reflux brines must have been over a larger area. In order for the seepage reflux brines to efficiently dolomitize a large area, water needs to be able to flow over an area without large obstacles deterring flow, and there needs to only be a small volume of sea water being introduced into the system at a time. Limited volume of water input can be achieved by one or a few small inlets, or by large and effective coral rubble mounds. This event likely occurred after peak transgression as sea

level began to fall, allowing smaller volumes of water to cover the platform which would influence increased concentrations of Mg^{2+}.

Seepage reflux dolomitization is interpreted to be the process forming dolomite at the Pekelmeer, with its isotopically heavy values of $\delta^{18}O$ (2.1 – 3.7‰ VPDB, with an average value of 2.9‰ VPDB). The heavy $\delta^{18}O$ values indicate evaporation helped produce the dolomite across the island (Budd, 1996). There would have been a minimal influx of new waters into the lagoon, and evaporation would lead to the creation of denser brines, causing seepage reflux. However, $\delta^{18}O$ results for Pekelmeer dolomites may not always indicate evaporation and hypersalinity (Major et al., 1992). Dolomite $\delta^{18}O$ values from the Pekelmeer average to approximately 1‰ PDB, which is much lower than dolomites precipitated under arid hypersaline conditions, including Abu Dhabi sabkha dolomite at 2.8‰ PDB (McKenzie, 1981), Qatar sabkha dolomite at 3.5‰ PDB (Lloyd, 1966), and Solar Lake Egypt dolomite at 9‰ PDB (Aharon, 1977). These results indicate that the dolomite formed on Bonaire may not have formed solely as a result of evaporative processes. Instead, factors such as presence or absence of microbes, platform morphology, and water chemistry may influence the formation of this dolomite.

CONCLUSIONS

The morphology of Bonaire and its carbonate deposition was influenced spatially by tectonic uplift, glacio-eustatic sea-level changes, and strong wave energy. Four Pleistocene carbonate terraces formed from deposition and subsequent erosion, as tectonic uplift increases elevation of the carbonate rocks and allows further subaerial exposure. Corals are the main macrofossils within the terrace strata, and associated bioclasts were used to identify different depositional environments (barrier reef, lagoon, and fringing reef). The windward side of Bonaire is subject to wind and high wave energy, influencing growth of the barrier reef, with its abundant *Acropora palmata*. This reef crest blocks the high wave energy, allowing more delicate corals, such as *Montastrea annularis*, to grow in the protected lagoon. This protected lagoon extends towards the platform interior, as well as in locations where protection is offered by subaerially exposed carbonate and volcanic rocks. The fringing reef environment on the leeward side is also protected from high wave energy, but is characterized by deeper waters than the lagoonal environment, and is composed of fringing reefs and upper slope deposits. Within the Pleistocene terraces, seven carbonate facies were delineated, six of which relate to dominant bioclasts within the limestone (*Acropora palmata* rudstone, Montastrea *annularis* framestone, *Acropora cervicornis* floatstone, Mixed Coral framestone, coralgal grainstone/packstone, and *Amphistegina sp.* grainstone). The seventh facies is the Dolomite facies, which formed by diagenesis.

As the strata gets older, there is a trend of increasing meteoric diagenesis in terms of calcite cementation. Whole rock isotopic analysis indicate negative values for $\delta^{18}O$

and $\delta^{13}C$ throughout the Pleistocene terraces. These were interpreted as $\delta^{18}O$ relating to increased ^{16}O introduced into the crystal lattice from rainwater, and $\delta^{13}C$ related to normal meteoric cement values. Aragonite still remains within the 1st terrace strata, but older strata has aragonite replaced with LMC.

Dolomite occurs within Pleistocene strata on the leeward and windward sides of Bonaire. This dolomite is microcrystalline on the 2nd terrace cliffs and sucrosic texture within the island's interior. The origin of the dolomite units is not clear. Seepage reflux is the proposed model of dolomitization, but there may be other factors that have yet to be determined which influenced the production of dolomite.

REFERENCES

Aharon, P., Kolodny, Y., and Sass, E., 1977. Recent hot brine dolomitization in the "Solar Lake," Gulf of Elat, isotopic, chemical, and mineralogical study. Journal of Geology 85, 27-48.

Alexander, C.S., 1961. The Marine Terraces of Aruba, Bonaire, and Curacao, Netherlands Antilles. Annals of the Association of American Geographers 51 (1), 102-123.

Arbuszewski, J.A., deMenocal, P.B., Cleroux, C., Bradtmiller, L., and Mix, A., 2013. Meridional shifts of the Atlantic intertropical convergence zone since the Last Glacial Maximum. Nature Geoscience 6, 959-962.

Audemard, F.A., 1993. Neotectonics, Seismotectonics and seismic hazard in northwestern Venezuela (fault system Oca-Ancon). PhD thesis, University of Montpellier II, France.

Bak, R.P.M., 1976. Coral Reefs and Their Zonation in Netherlands Antilles. Caribbean Marine Biological Institute, 3-16.

Bandoian, C.A., and Murray, R.C., 1974. Pliocene-Pleistoene Carbonate Rocks of Bonaire, Netherlands Antilles. Geological Society of America Bulletin, v. 85 p. 1243-1252.

Barnes, D.J., 1973. Growth in Colonial Scleractinians. Bulletin of Marine Sciences 23 (2), 280-298.

Biju-Duval, B. Mascle, A., Montadert, L., and Wanneson, J., 1982. Episutural Oligo-Miocene basins along the north Venezuela margin. Watkins. J., Drake, C. (Eds.),

Studies in Continental Margin Geology, American Association of Petroleum Geologists Memoir 34, 347-358.

Bosence, D., 2005. A genetic classification of carbonate platforms based on their basinal and tectonic settings in the Cenozoic. Sedimentary Geology 175, 49-72.

Bornmalm, L., 1999. Changes in Circulation and Trophic Levels in the Pliocene Caribbean Sea: Evidence from Benthic Foraminifer Accumulation Rates. Journal of Foraminiferal Research 3 (3), 209-221.

Budd, D.A., 1997. Cenozoic dolomites of carbonate islands: their attributes and origin. Earth-Science Reviews 42, 1-47.

Chappell, J., 1980. Coral morphology, diversity and reef growth. Nature 286, 249-252.

Charney, J.G., 1971. Tropical cyclogenesis and the formation of the Intertropical Convergence Zone. Mathematical Problems of Geophysical Fluid Dynamics, Lectures in Applied Mathematics 13, 355-368.

Chiang, J.C.H., and Bitz, C.M., 2005. Influence of high latitude ice cover on the marine Intertropical Convergence Zone. Climate Dynamics 25, 447-496.

Constantz, B.R., 1986. The Primary Surface Area of Corals and Variations in Their Susceptibility to Diagenesis. Reef Diagenesis, 53-76.

De Buisonje, P.H., 1964. Marine terraces and sub-aeric sediments on the Netherlands Leeward Islands, Curacao, Aruba, and Bonaire, as indications of Quaternary changes in sea level and climate, I and II. Proceeding, Series B, Physical Sciences 67 (1), 60-79.

De Buisonje, P.H., 1974. Neogene and Quaternary geology of Aruba, Curacao, and Bonaire: Ph.D. Dissertation: Utrecht. Natuurwetenshappelijke Studiekring.

De Haan, D., and Zaneveld, J.S., 1959. Some notes on tides in Annabaii Harbour, Curacao, Netherlands Antilles. Bulletin of Marine Science 9 (2), 224-236.

Deffeyes, K.S., Lucia, F. Jerry, and Weyl, P.K., 1965. Dolomitization of Recent and Plio-Pleistocene Sediments by Marine Evaporite Waters on Bonaire, Netherlands Antilles. EPR Publication 348, Shell Development Company, pp 71-88.

Degens, E.T., and Epstein, S., 1964. Oxygen and carbon isotope ratios in coexisting calcites and dolomites from recent and ancient sediments. Geochimica et Cosmochimica Acta 28, 23-44.

Dunham, Robert J., 1962. Classification of Carbonate Rocks According to Depositional Textures. AAPG Memoir, Classification of Carbonate Rocks – A Symposium, pp 108-121.

Dustan, P., 1975. Growth and Form in the Reef-Building Coral *Montastrea annularis*. Marine Biology 33, 101-107.

Engel, M., Bruckner, H., Furstenberg, S., Frenzel, P., Konopczak, A.M., Scheffers, A., Kelletat, D., May, S.M., Schabitz, F., and Daut, G., 2012. A prehistoric tsunami induced long-lasting ecosystem changes on a semi-arid tropical island – the case of Boka Bartol (Bonaire, Leeward Antilles). The Science of Nature – Naturwissenschaften 100 (1), 51-67.

Escalona, A., and Mann, P., 2011. Tectonics, basin subsidence mechanisms, and paleogeography of the Caribbean – South American plate boundary zone. Marine and Petroleum Geology 28, 8-39.

Focke, J.W., 1978. Holocene development of coral fringing reefs, leeward off Curacao and Bonaire (Netherlands Antilles). Marine Geology 28, 31-41.

Fouke, B.W., Beets, C.J., Meyers, W.J., Hanson, G.N., and Melillo, A.J., 1996. $^{87}Sr/^{86}Sr$ Chronostratigraphy and Dolomitization History of the Seru Domi Formation, Curacao (Netherlands Antilles). Facies 35, 293-320.

Glatfelter, E.H., Monahan, R.K., and Glatfelter, W.B., 1978. Growth Rates of five Reef-Building Corals in the Northeast Caribbean. Bulletin of Marine Science 28 (4), 728-734.

Google Earth V 7.1.2.2041. (May 2nd, 2014). Bonaire, Netherlands Antilles. 12º 10' 12" N, 68º 15' 0" W. Digital Globe 2015, CNES/Astrium 2015. [July 6th, 2015].

Gordon, A.L., 1967. Circulations of the Caribbean Sea. Journal of Geophysical Research 72 (24), 6207-6223.

Goreau, T.F., and Wells, J.W., 1967. The Shallow-Water Scleractinia of Jamaica: Revised List of Species and their Vertical Distribution Range. Bulletin of Marine Science 17 (2), 442-453.

Gorney, D., Escalona, A., Mann, P., and Magnani, M.B., 2007. Chronology of Cenozoic tectonic events in western Venezuela and the Leeward Antilles based on integration of offshore seismic reflection data and on-land geology. American Association of Petroleum Geologists Bulletin 91 (5), 653-684.

Grossman, E.L., and Ku, T., 1986. Oxygen and Carbon Isotope Fractionation in Biogenic Aragonite: Temperature Effects. Chemical Geology (Isotope Geoscience Section) 59, 59-74.

Hastenrath, S., 1975. Variations in Low-Latitude Circulation and Extreme Climatic Events in the Tropical Americas. Journal of Atmospheric Science 33, 202-215.

Haug, G.H., and Tiedemann, R., 1998. Effect of the formation of the Isthmus of Panama on Atlantic Ocean thermohaline circulation. Nature 393, 673-676.

Herweijer, J.P., de Buisonje, P.H., and Zonneveld, J.I.S., 1977. Neogene and Quaternary Geology and Geomorphology. Guide to geological excursions on Curacao, Bonaire, and Aruba 2, 39-55.

Herweijer, J.P., and Focke, J.W., 1978. Late Pleistocene Depositional and Denudational History of Aruba, Bonaire and Curacao (Netherlands Antilles). Netherlands Journal of Geosciences 57 (2), 177-187.

Hidaka, K., 1958. Computation of the wind stresses over the oceans. Recent Oceanography Works Japan 4, 77-123.

Hippolyte, J., and Mann, P., 2011. Neogene-Quaternary tectonic evolution of the Leeward Antilles islands (Aruba, Bonaire, Curacao) from fault kinematic analysis. Marine and Petroleum Geology 28, 259-277.

Hoorn, C., Guerrero, J., Sarmiento, G.A., and Lorente, M.A., 1995. Andean tectonics as a cause for changing drainage patterns in Miocene northern South America. Geology 23 (3), 237-240.

Hornbach, M.J., Mann, P., Taylor, F.W., and Bowen, S.W., 2010. Estimating the Age of Near-Shore Carbonate Slides Using Coral Reefs and Erosional Markers. A Case Study from Curacao, Netherlands Antilles: The Sedimentary Record 8 (1).

Hu, C., Montgomery, E.T., Schmitt, R.W., Muller-Karger, F.E., 2004. The dispersal of the Amaxon and Orinoco River water in the tropical Atlantic and Caribbean Sea. Observation from space and S-PALACE floats: Deep-Sea Research Part II. 51, 1151-1171.

Hudson, J.D., 1977. Stable isotope and limestone lithification. Journal of the Geological Society 133, 637-660.

James, K.H., 2006. Arguments for and against the Pacific origin of the Caribbean Plate: discussion, fining for an inter-American origin. Geologica Acta 4 (1-2), 279-302.

James, N.P., Kendall, A.C., and Pufahl, P.K., 2010. Introduction to Biological and Chemical Sedimentary Facies Models. Canadian Society of Petroleum Geologists, Facies Models 4, 323-339.

James, N.P., and Wood, R., 2010. Reefs. Canadian Society of Petroleum Geologists, Facies Models 4, 421-447.

Jordan, T.H., 1975. The Present-Day Motions of the Caribbean Plate. Journal of Geophysical Research 80 (32), 4433-4439.

Kameo, K., Shearer, M.C., Droxler, A.W., Mita, I., Watanabe, R., and Sato, T., 2004. Glacial-interglacial surface water variations in the Caribbean Sea during the last 300 ky based on calcareous nannofossil analysis. Palaeogeography, Palaeoclimatology, Palaeoecology 212, 65-76.

Kellogg, J. N., 1984. Cenozoic tectonic history of the Sierra de Perija, Venezuela-Colombia, and adjacent basins, In: Bonini, W., Hargraves, R., Shagam, R. (Eds.), The Caribbean-South American Plate Boundary and Regional Tectonics. Geological Society of American Memoir 162, 239-261.

Kim, K.H., 1998. Integrated analysis and interpretations of the early diagenetic records imprinted on the uplifted Pleistocene coral reef limestones, Bonaire, Netherlands Antilles. PhD Dissertation, University of Houston, United States of America.

Kim, K.H., and Lee, D., 1999. Distribution and Depositional Environments of Coralline Lithofacies in Uplifted Pleistocene Coral Reefs of Bonaire, Netherlands Antilles. Journal of Paleontology of Korea 15 (2), 115-133.

Kim, S., and O'Neil, J.R., 1997. Equilibrium and nonequilibrium oxygen isotope effects in synthetic carbonates. Geochimica et Cosmochimica Acta 61 (16), 3461-3475.

Klaus, J.S., McNeill, D.F., Budd, A.F., and Coates, A.G., 2012. Neogene reef coral assemblages of the Bocas del Toro region, Panama: the rise of *Acropora palmata*. Coral Reefs 31, 191-203.

Klosowska, B.B., Troelstra, S.R., van Hinte, J.E., Beets, D., van der Borg, K., and de Jong, A.F.M., 2004. Late Holocene environmental reconstruction of St. Michiel saline lagoon, Curacao (Dutch Antilles). Radiocarbon 46 (2), 765-774.

Ladd, J.W., 1976. Relative Motion of South America with respect to North America and Caribbean tectonics. Geological Society of America Bulletin 87, 969-976.

Levander, A., Schmitz, M., Ave Lallemant, H.G., Zelt, C.A., Sawyer, D.S., Magnani, M.B., Mann, P., Christeson, G., Wright, J.E., Palvis, G.L., Pindell, J., 2006.

Evolution of the southern Caribbean plate boundary. EOS Transactions of the American Geophysical Union 87, 100-101.

Lirman, D., 2000. Fragmentation in the branching coral *Acropora palmata* (Lamarck): growth, survivorship, and reproduction of colonies and fragments. Journal of Experimental Marine Biology and Ecology 251, 41-57.

Lisiecki, L.E., and Raymo, M.E., 2005. A Plio-Pleistocene stack of 57 globally distributed benthic $\delta^{18}O$ records. Paleoceanography 20, PA 1003.

Lucia, F. J., and Major, R. P., 1994. Porosity Evaluation through hypersaline reflux dolomitization. Special Publications International Association of Sedimentologists 21, 325-341.

Lloyd, R.M., 1966. Oxygen isotope enrichment of sea water by evaporation. Geochimica et Cosmochimica Acta 30, 801-814.

Machel, H.., and Mountjoy, E.W., 1986. Chemistry and Environments of Dolomitization – A Reappraisal. Earth-Science Reviews 23, 175-222

Major, R. P., Lloyd, M.R., and Lucia, J.F., 1992. Oxygen isotope composition of Holocene dolomite formed in a humid hypersaline setting. GEOLOGY 20, 586-588.

Mann, P., and Burke, K., 1984. Neotectonics of the Caribbean. Reviews of Geophysics and Space Physics 22 (4), 309-362.

Marshall, J.D., 1992. Climatic and oceanographic isotope signals from the carbonate rock record and their preservation. Geological Magazine 129 (2), 143-160.

Martinez, J.I., Mora, G., and Barrows, T.T., 2007. Paleoceanographic conditions in the western Caribbean Sea for the last 560 kyr as inferred from planktonic foraminifera. Marine Micropaleontology 64, 177-188.

Matthews, R.K., 1968. Carbonate Diagenesis: Equilibration of Sedimentary Mineralogy to the Subaerial Environment; Coral Cap of Barbados, West Indies. Journal of Sedimentary Petrology 38 (4), 1110-1119.

Matthews, R.K., 1973. Relative Elevation of Late Pleistocene High Sea Level Stands. Barbados Uplift Rates and their Implications: Quaternary Research 3, 147-153.

McKenzie, J.A., 1981. Holocene dolomitization of calcium carbonate sediments from the coastal sabkhas of Abu Dhabi, U. A. E.: A stable isotope study. Journal of Geology 89, 185-198.

Mesolella, K.J., 1967. Zonation of uplifted Pleistocene coral reefs on Barbados, West Indies. Science 156, 638-640.

Mesolella, K.J., Sealy, H.A., Matthews, R.K., 1970. Facies Geometries within Pleistocene Reefs of Barbados, West Indies. The American Association of Petroleum Geologists Bullet, 54 (10), 1899-1917.

Miller, M.S., A. Levander, F. Niu, A. Li, 2009. Upper Mantle structure beneath the Caribbean-South American plate boundary from surface wave tomography. Journal of Geophysical Research 114, 1-13.

Milliman, J. D., 1974. Recent Sedimentary Carbonates 1, Marine Carbonates. New York, Springer-Verlag, p. 375.

Muhs, D.R., Pandolfi, J.M., Simmons, K.R., Schumann, R.R., 2012. Sea-level history of past interglacial periods from uranium-series dating of corals, Curacao, Leeward Antilles islands. Quaternary Research 78, 157-169.

Muller-Karger, F.E., and Castro, R.A., 1993. Mesoscale processes affecting phytoplankton abundance in the southern Caribbean Sea. Continental Shelf Research 14 (2), 199-221.

Newell, N. D. Imbrie, J., Purdy, E.G., and Thurber, D.L., 1959. Organism communities and bottom facies, Great Bahama Bank. Bulletin of American Museum of Natural History 117, 177-228.

Newell, N. D., and Rigby, J. K., 1959. Geological studies on the Great Bahama Bank, in Le Blanc, R. J. and Breeding, J. G. eds., Regional Aspects of Carbonate Deposition: a Symposium with Discussion. Society of Economic Paleontologists and Mineralogists Special Publication 5, 15-72.

Nisancioglu, K.H., Raymo, M.E., and Stone, P.H., 2003. Reorganization of Miocene deep water circulation in response to the shoaling of the Central American Seaway. Paleoceanography 18 (1), 1006.

Pandolfi, J.M., and Jackson, J.B.C., 2001. Community Structure of Pleistocene Coral Reefs of Curacao, Netherlands Antilles 71 (1), 49-67.

Perez, O., Bilham, R., Bendick, R., Velandia, J. R., Hernandez N., Moncayo, C., Hoyer, M., and Kozuch, M., 2001. Velocity field across the southern Caribbean plate boundary and estimates of Caribbean-South American plate motion using GPS geodesy 1994-2000. Geophysical Research Letters 28, 2987-2990.

Peterson, L.C., Overpeck, J.T., Kipp, N.G., and Imbrie, J., 1991. A high-resolution Late Quaternary upwelling record from the anoxic Cariaco Basin, Venezuela. Paleoceanography 6 (1), 99-119.

Philander, S.G.H., Gu, D., Halpern, D., Lambert, G., Lau, N.C., Li, T., and Pacanowski, R.C., 1995. Why the ITCZ is Mostly North of the Equator. Journal of Climate 9, 2958-2972.

Pijpers, P. J., 1933. Geology and paleontology of Bonaire (N.W.I.) [Ph.D. dissert.]. Utrecht, Netherlands, Univ. Utrecht.

Pike, A.C., 1971. The intertropical convergence zone studied with an interacting atmosphere and ocean model. Monthly Weather Review 99, 469-477.

Pindell, J.L., Cande, S.C., Pitmann III, W.C., Rowley, D.B., Dewey, J.F., Labrecque, J., and Haxby, W., 1988. A plate-kinematic framework for models of Caribbean evolution. Tectonophysics 155, 121-138.

Pindell, J., and Kennan, L., 2001. Kinematic Evolution of the Gulf of Mexico and Caribbean. Transactions of the Gulf Coast Section Society of Economic Paleontologists and Mineralogists (GCSSEPM) 21st Annual Bob F. Perkins Research Conference, Petroleum Systems of Deep-Water Basins, Houston, Texas, pp 2-5.

Pomar, L., 2001. Types of carbonate platforms: a genetic approach. Basin Research 13, 313-334.

Purkis, S.J., Rowlands, G.P., Kerr, J.M., 2014. Unravelling the influence of water depth and wave energy on the facies diversity of shelf carbonates. Sedimentology (2014) 1, 1-25.

Read, J.F., 1985. Carbonate Platform Facies Models. The American Association of Petroleum Geologists Bulletin 69 (1), 1-21.

Ries, J.B., 2006. Mg fractionation in crustose coralline algae: Geochemical, biological, and sedimentological implications of secular variation in the Mg/Ca ratio of seawater. Geochimica et Cosmochimica Acta 70, 891-900.

Roos, P.J., 1971. The shallow-water stony corals of the Netherlands Antilles. Studies on the fauna of Curacao and other Caribbean islands 130, 1-108.

Rueda-Roa, D.T., and Muller-Karger, F.E., 2013. The southern Caribbean upwelling system: Sea surface temperature, wind forcing and chlorophyll concentration patterns. Deep-Sea Research I 78, 102-114.

Scatterday, J.W., 1977. Low-water Emergence of Caribbean Reefs and Effect of Exposure on Coral Diversity-Observations off Bonaire, Netherlands Antilles. SG 4. Reefs and Related Carbonates--Ecology and Sedimentology, pp 155-169.

Schellmann, G., Radtke, U., Scheffers, A., Whelan, F., and Kelletat, D., 2002. ESR Dating of Coral Reef Terraces on Curacao (Netherlands Antilles) with Estimates of Younger Pleistocene Sea Level Elevations. Journal of Coastal Research 204, 947-957.

Schneider, B., and Schmittner, A., 2006. Simulating the impact of the Panamanian seaway closure on ocean circulation, marine productivity and nutrient cycling. Earth and Planetary Science Letters 246, 367-380.

Sibley, D.F., 1980. Climatic Control of Dolomitization, Seroe Domie Formation (Pliocene), Bonaire, N.A. SEPM Special Publication 28, 247-258.

Sibley, D.F., 1982. The Origin of Common Dolomite Fabrics: Clues from the Pliocene. Journal of Sedimentary Petrology 52 (4), 1087-1100.

Silver, E., Case, J., MacGillavry, H., 1975. Geophysical study of the Venezuelan borderland. Geological Society of American Bulletin 86, 213-226.

Shackleton, N.J., and Opdyke, N.D., 1973. Oxygen Isotope and Palaeomagnetic Stratigraphy of Equatorial Pacific Core V28-238: Oxygen Isotope Temperatures and Ice Volumes on a 10^5 Year and 10^6 Year Scale. Quaternary Research 3, 39-55.

Stehli, F.G., and Wells, J.W., 1971. Diversity and Age Patterns in Hermatypic Corals. Systematic Zoology 20 (2), 115-126.

Stehli, F.G., and Wells, J.W., 1971. Diversity and Age Patterns in Hermatypic Corals. Systematic Zoology 20 (2), 115-126.

Tarutani, T., Clayton, R.N., Mayeda, T.K., 1969. The effect of polymorphism and magnesium substitution on oxygen isotope fractionation between calcium carbonate and water. Geochimica et Cosmochimica Acta 33, 987-996.

Thompson, P. M. E., Kempton, P.D., White, R.V., Saunders, A.D., Kerr, A.C., Tarney, J., and Pringle, M.S., 2004. Elemental, Hf-Nd isotopic and geochronological

constraints on an island arc sequence associated with the Cretaceous Caribbean plateau: Bonaire, Dutch Antilles. Lithos 74, 91-116.

Tucker, M.E., and Wright, V.P., 1990. Carbonate Sedimentology. Blackwell Publishing, USA, UK, and Australia.

Trenkamp, R., Kellogg, J.N., Freymueller, J.T., and Mora, H.P., 2002. Wide plate margin deformation, southern Central American and northwestern South America, CASA GPS observations. Journal of South American Earth Sciences 15, 157-171.

Van Der Lelij, R., Spikings, R.A., Kerr, A., Kounov, A., Cosca, M., Chew, D., and Villagomez, D., 2009. Thermochronology and Tectonics of the Leeward Antilles: evolution of the Southern Caribbean Plate Boundary Zone. PhD dissertation, University of Geneva, Switzerland.

van Andel, T.J.H., 1967. The Orinoco Delta. Journal of Sedimentary Petrology 37 (2), 297-310.

van Duyl, F.C., 1985. Atlas of the Living Reefs of Curacao and Bonaire. Foundation for Scientific Research in Surinam and the Netherlands Antilles 117, 1-90.

Waelbroeck, C., Labeyrie, L., Michel, E., Duplessey, J.C., McManus, J.F., Lambeck, K., Balbon, E., Labracherie, M., 2002. Sea-level and deep water temperature changes derived from benthic foraminifera isotopic records. Quaternary Science Reviews 21, 295-305.

Waliser, D.E., and Somerville, R.C.J., 1994. Preferred latitude of the intertropical convergence zone. Journal of Atmospheric Science 51, 1397-1415.

Wells, J.W., 1957. Corals; annotated bibliography, *in* Ladd, H. S., ed., Paleoecology. Geological Society of America Memoir, 773-782.

Wells, J.W., 1967. Corals as bathometers. Marine Geology 5, 349-365.

APPENDIX A: FIGURES AND TABLES

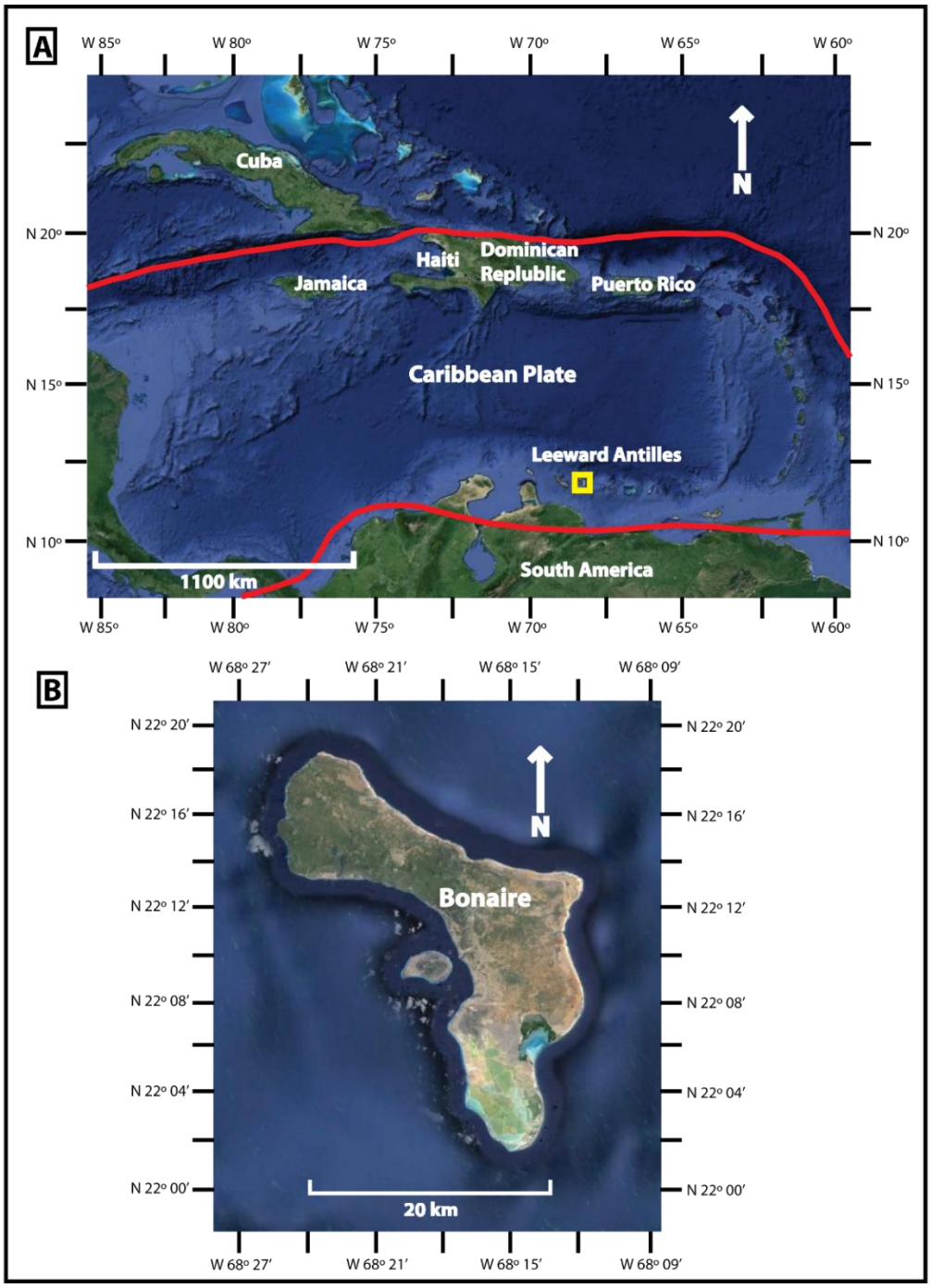

Figure 1: (A) Location of Bonaire (yellow box) with respect to Caribbean Plate (outlined in red) and South America. (B) Island of Bonaire. (Satellite images provided by Google Earth).

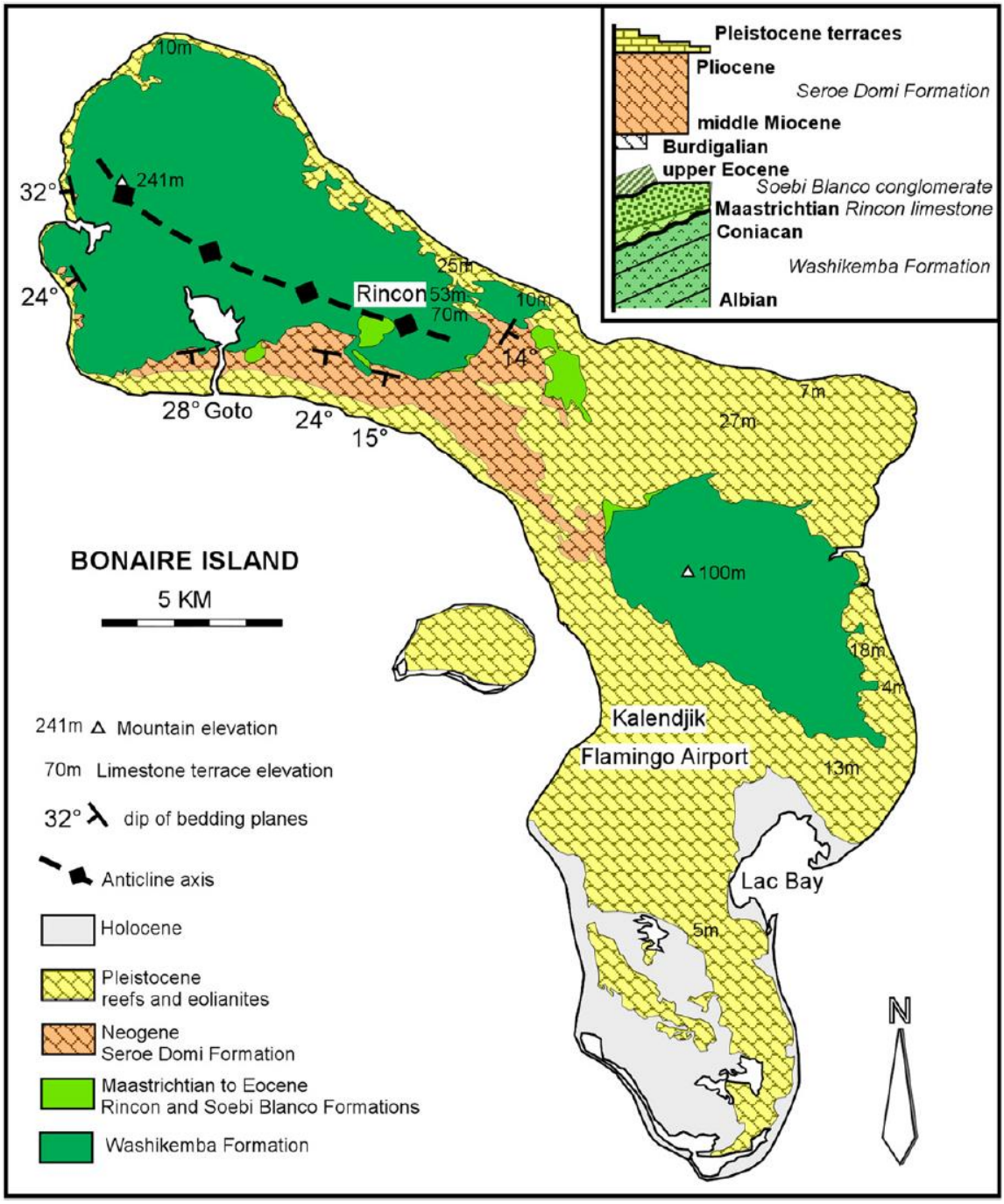

Figure 2: Geologic map illustrating possible structural features on the island, including an anticline in the northwest. Reprinted from Hippolyte and Mann (2011).

Figure 3: Images and descriptions for *Amphistegina sp.* grainstone, *Montastrea annularis* framestone, and *Acropora cervicornis* floatstone. Thin section of fine-gr. *Amphistegina sp.* grainstone is represented include *Amphistegina sp.* foraminifera (f) and meteoric cement (c) (A). *Montastrea annularis* Framestone is represented by the abundance of *Montastrea annularis*, shown by outcrop photograph (B). *Acropora cervicornis* Floatstone is represented by a thin section (C) and outcrop photograph (D). The thin section (C) illustrates abundance of red algae fragments (R). The outcrop (D) contains dissolved voids of original *A. cervicornis* branches, of which some have been infilled with sediment.

Amphistegina sp. Grainstone

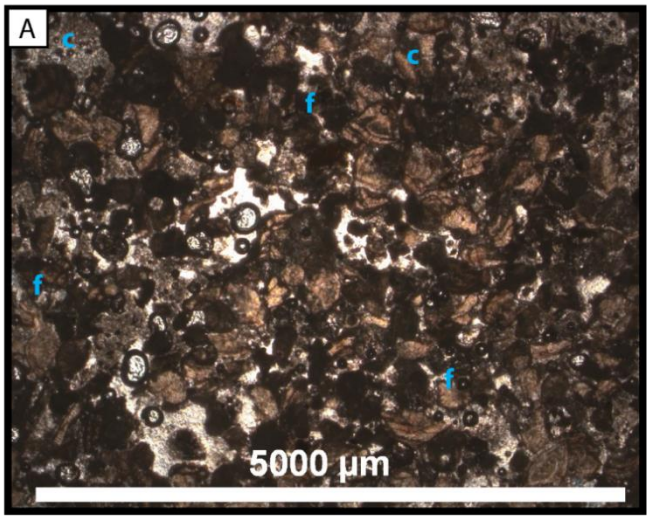

Montastrea Annularis Framestone

Acropora cervicornis Floatstone

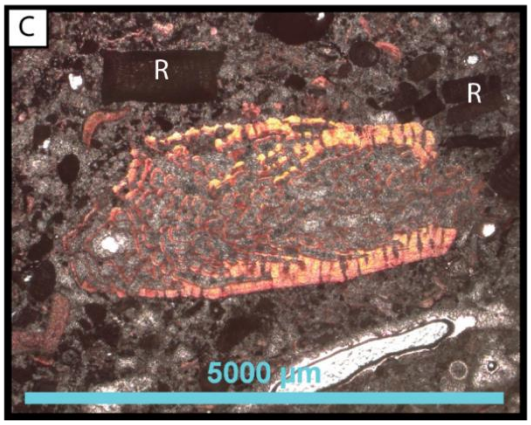

Figure 4: Images and descriptions for *Acropora palmata* rudstone, Mixed Coral framestone, and Coralgal grainstone/packstone facies. *Acropora palmata* rudstone is denoted by lenticular voids of dissolved *A. palmata* branches, and is best exemplified by outcrop study, of which the photograph (A) derives. Mixed Coral Framestone is also best exemplified by outcrop study. B) Head coral *Montastrea annularis*. C) zonation from bottom to top a zone composed of head corals including *M. annularis* and *Diploria sp.* Overlaying this zone is a zone abundant in *A. cervicornis.* Above *A. cervicornis* is an *A. palmata* zone, which is the uppermost unit. The Coralgal grainstone/packstone facies is shown in outcrop (D) and thin section (E). Bedforms may be observed in outcrop, including cross-stratification in the top meter of outcrops (Fig. 4 D outlines with the black lines). The thin section illustrates the main bioclasts in this facies are red algae fragments (R).

Acropora palmata Rudstone

Mixed Coral Framestone

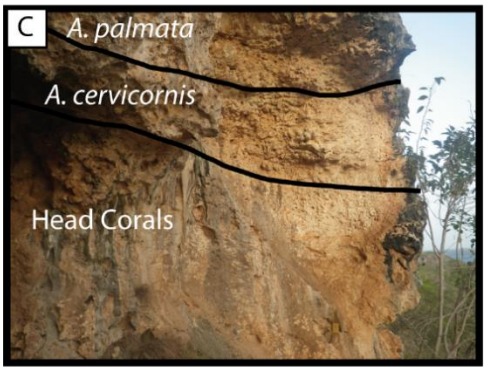

Coralgal Grainstone/Packstone

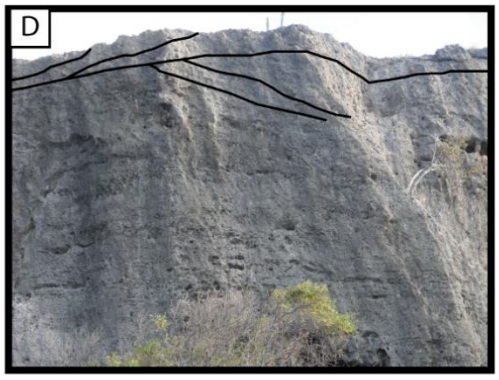

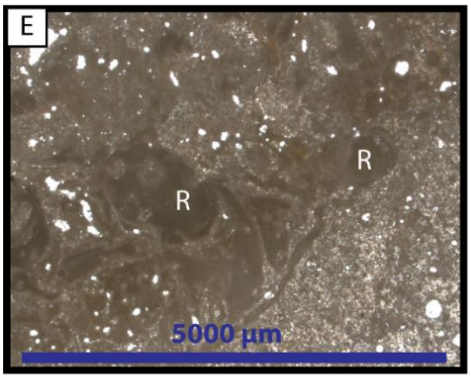

Figure 5: Images and descriptions for Dolomite facies. Sample 9-3-1 (A) illustrates dolomite with microcrystalline matrix and partially recrystallized red algae fragments. Sample 20BON2 (B) illustrates a coarser sucrosic texture from the 4th terrace. Sample 19BON4 (C) is dolomite with sucrosic texture from the 4th terrace. A core sample 9-3-1 (D) is cut in half to show the fresh white exposure, as well as its apparent crystalline composition. In outcrop (Seru Grandi location) (E), the dolomite which was originally white, weathers to a gray color.

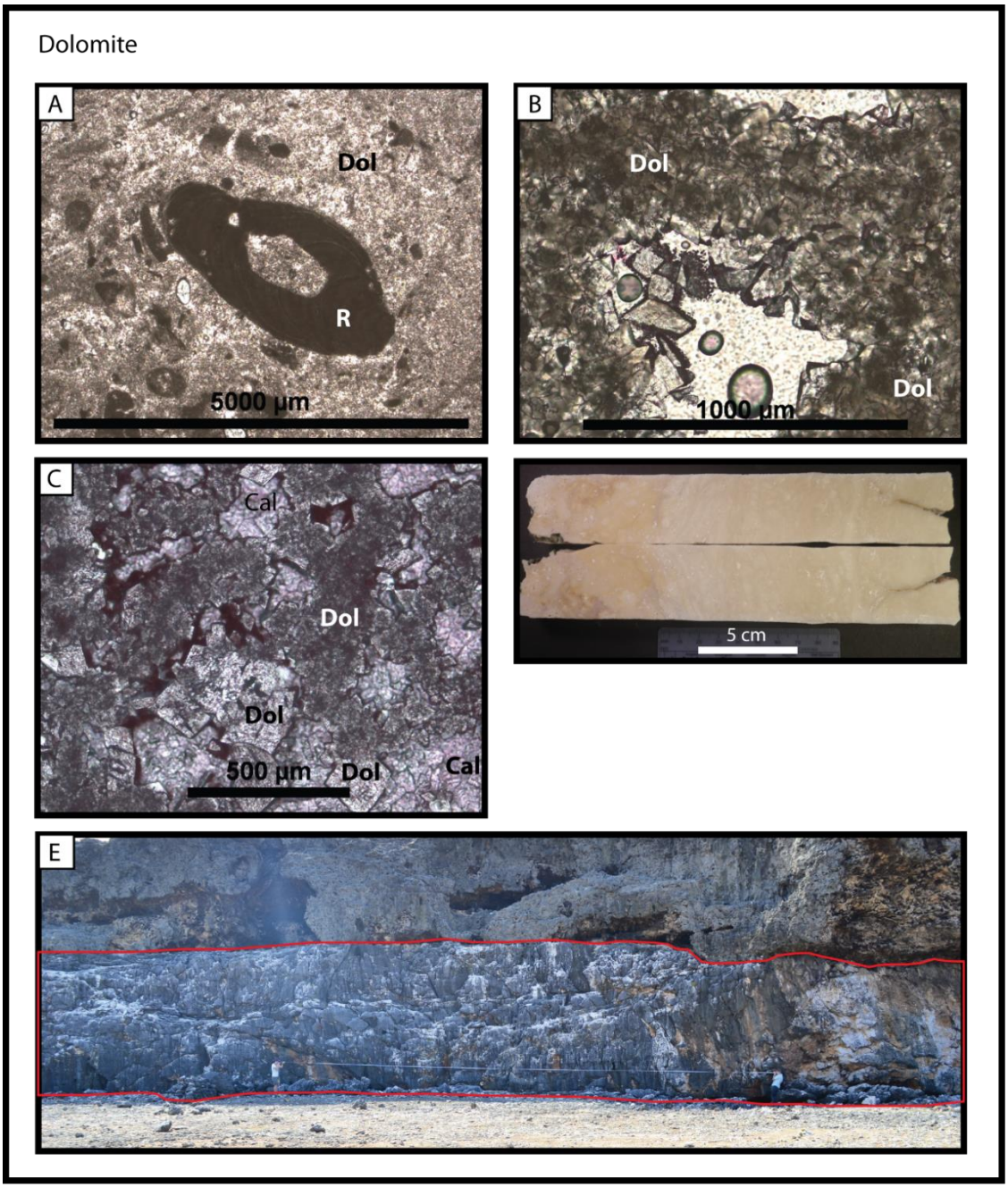
Dolomite
A
Dol
R
5000 µm
B
Dol
1000 µm
Dol
C
Cal
Dol
Dol
500 µm
Dol
Cal
5 cm
E

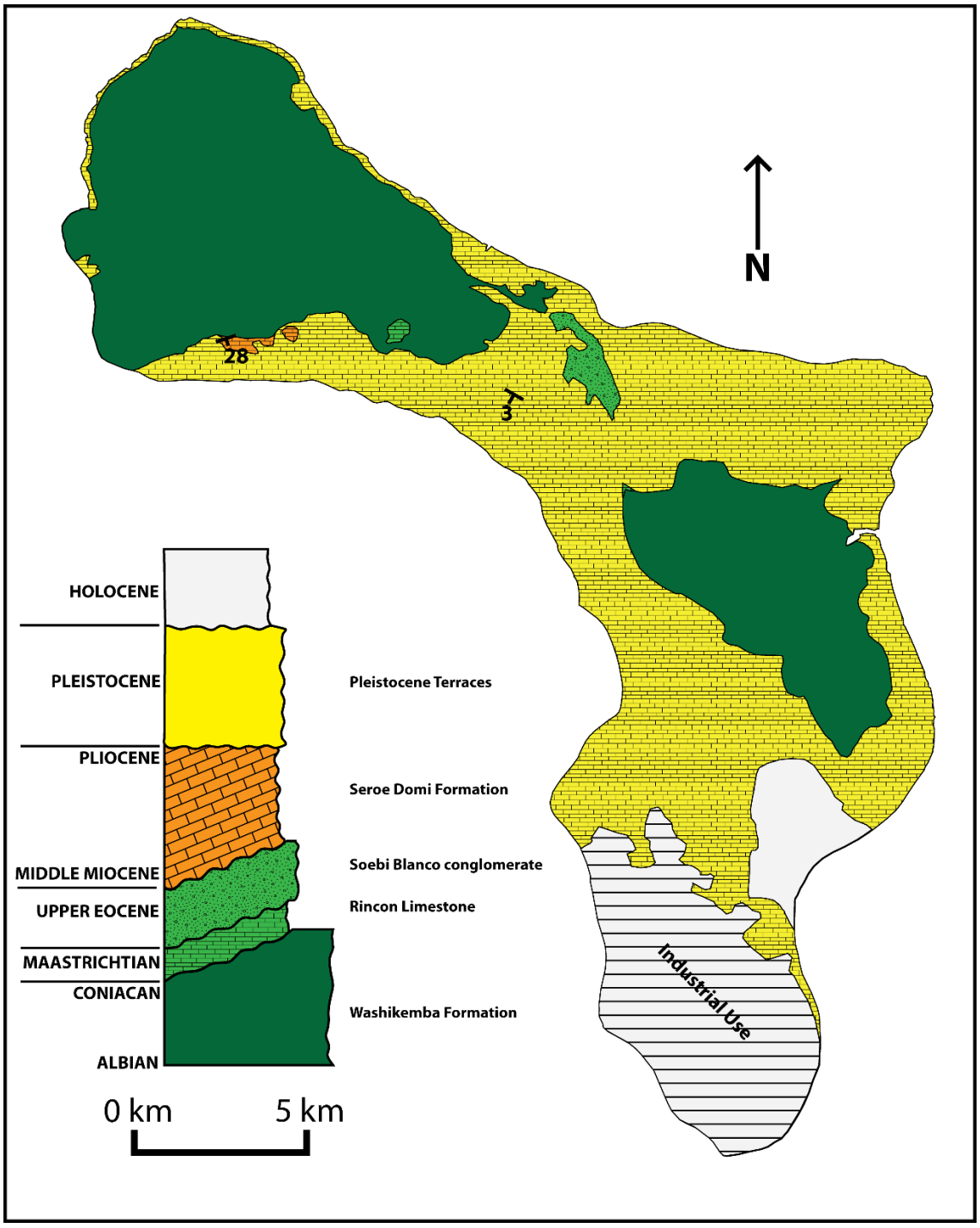

Figure 6: Geologic map and associated stratigraphic column of Bonaire. Modified from Hippolyte and Mann (2011).

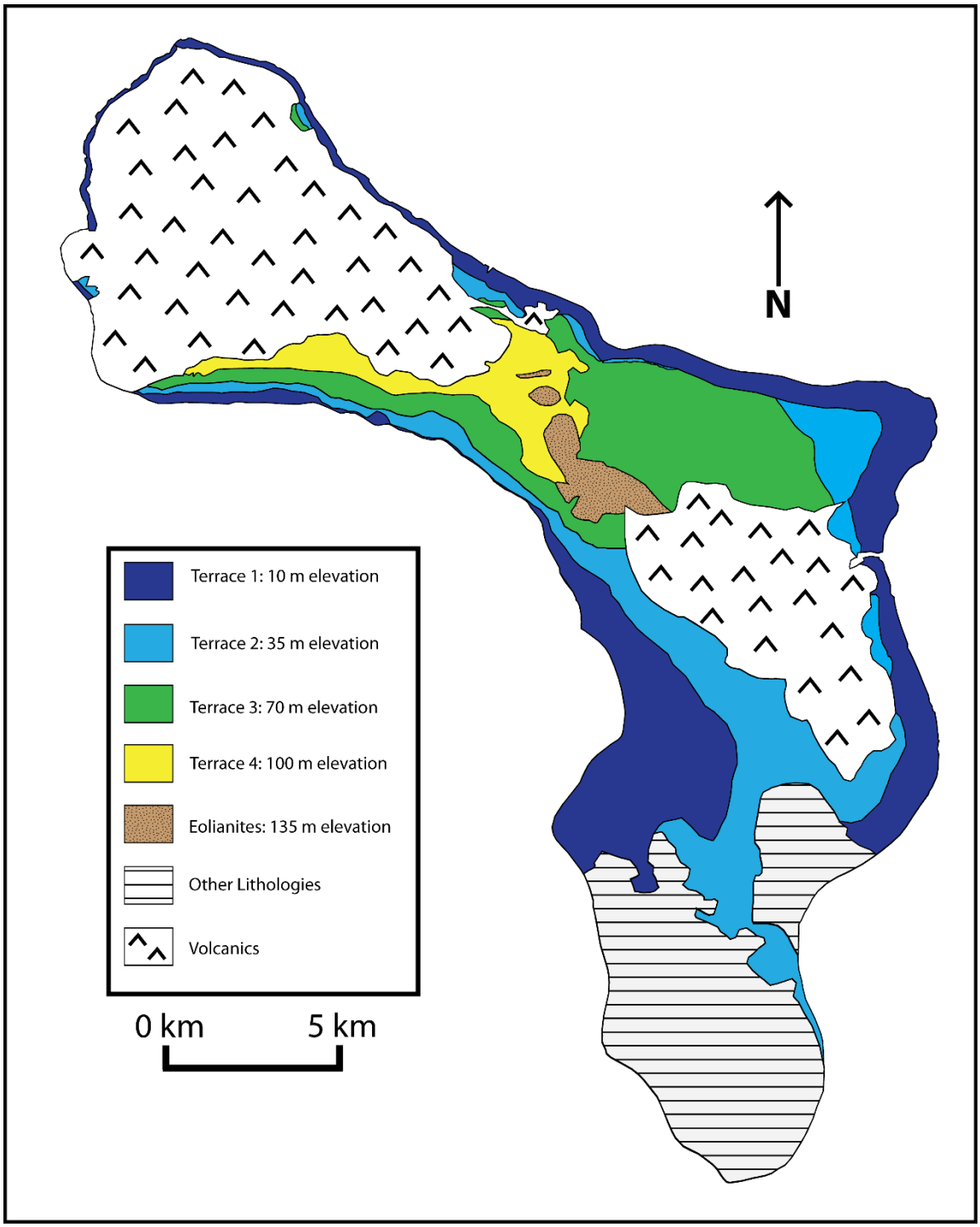

Figure 7: Map illustrating 4 Pleistocene carbonate terraces and eolianite units delineated in this study. The eolianite units do not depict an additional terrace level, and are likely to be Pleistocene age deposits.

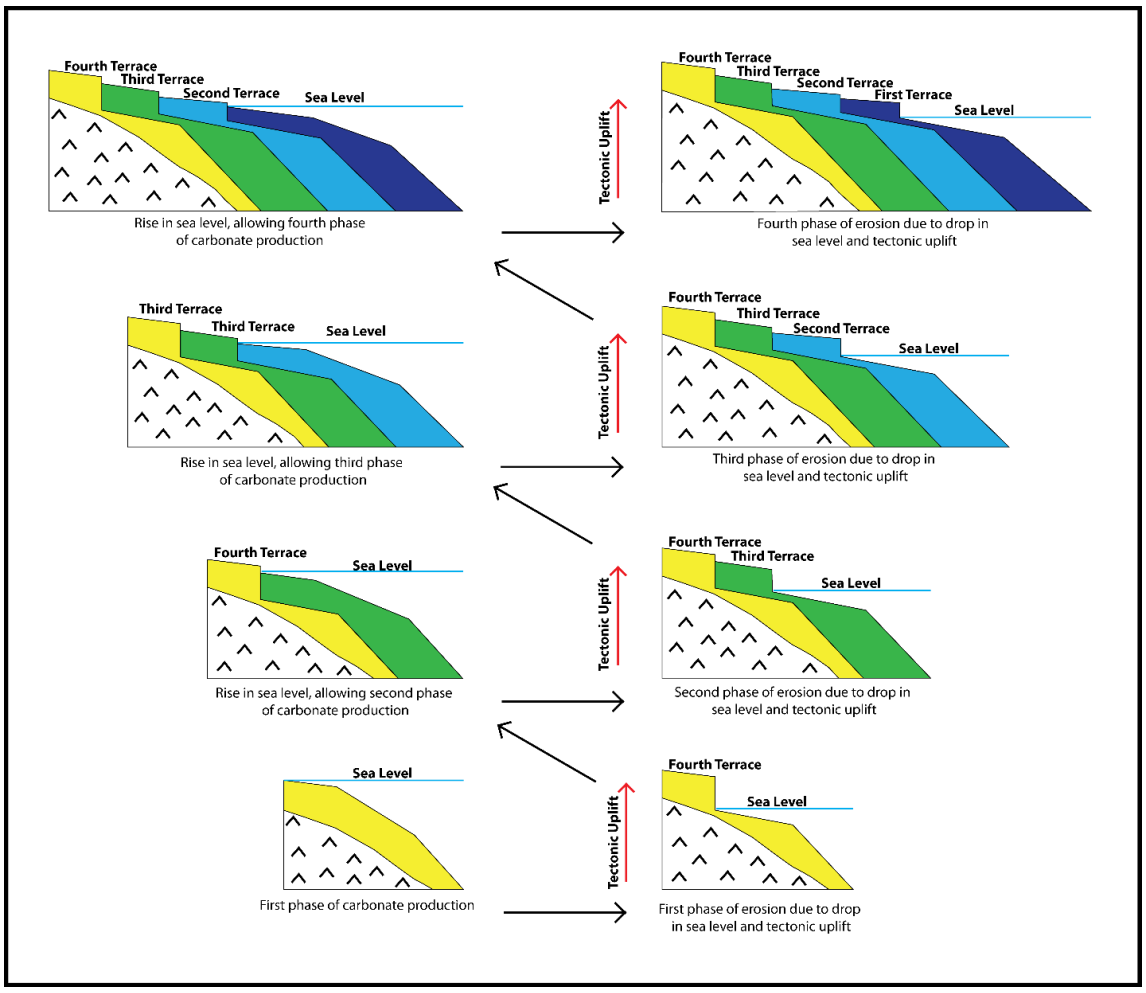

Figure 8: Schematic cross-section illustrating the process of carbonate deposition and terrace formation on Bonaire. Factors contributing to these processes are sea level fluctuation and tectonic uplift.

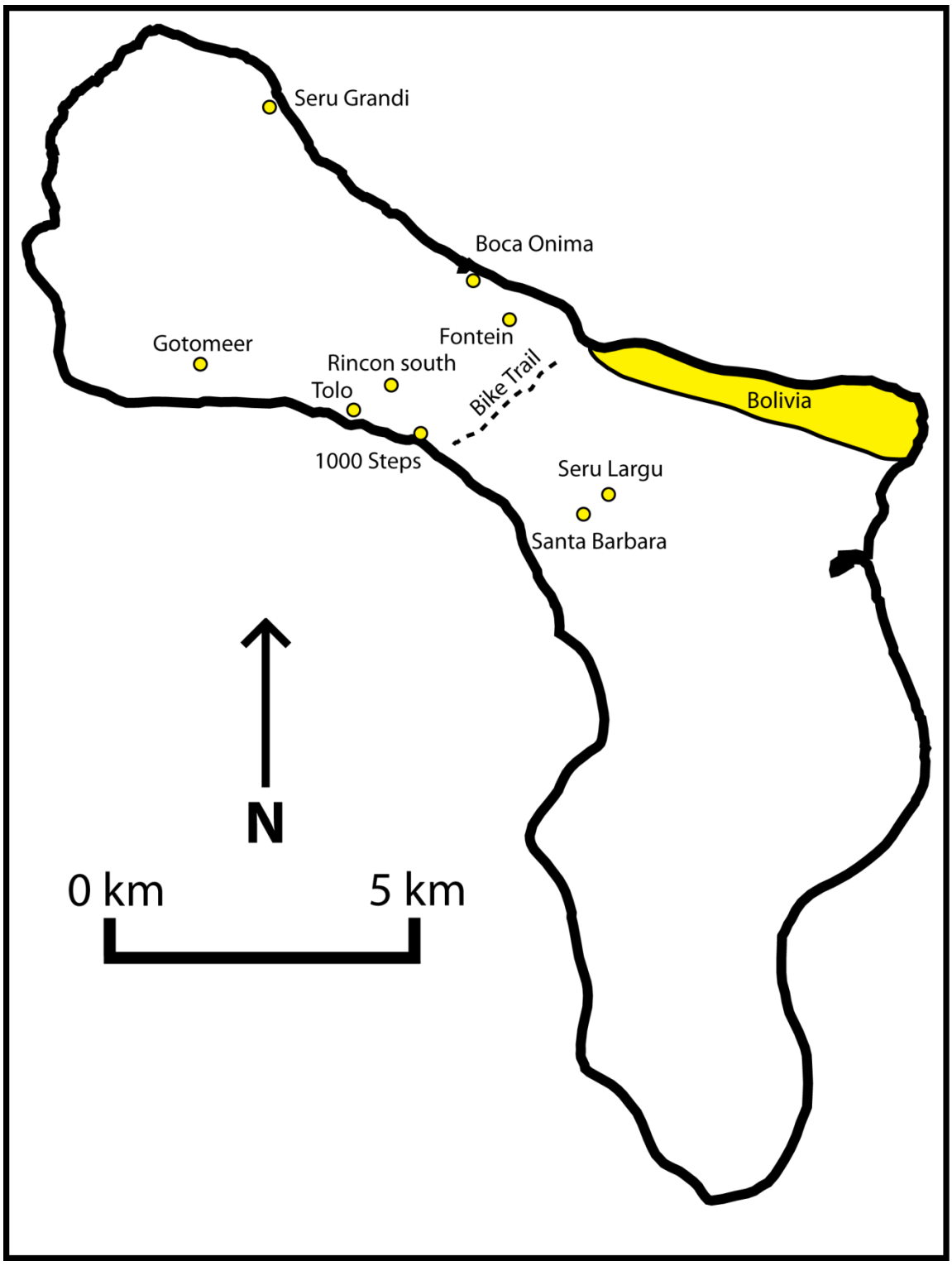

Figure 9: Bonaire outcrop location map.

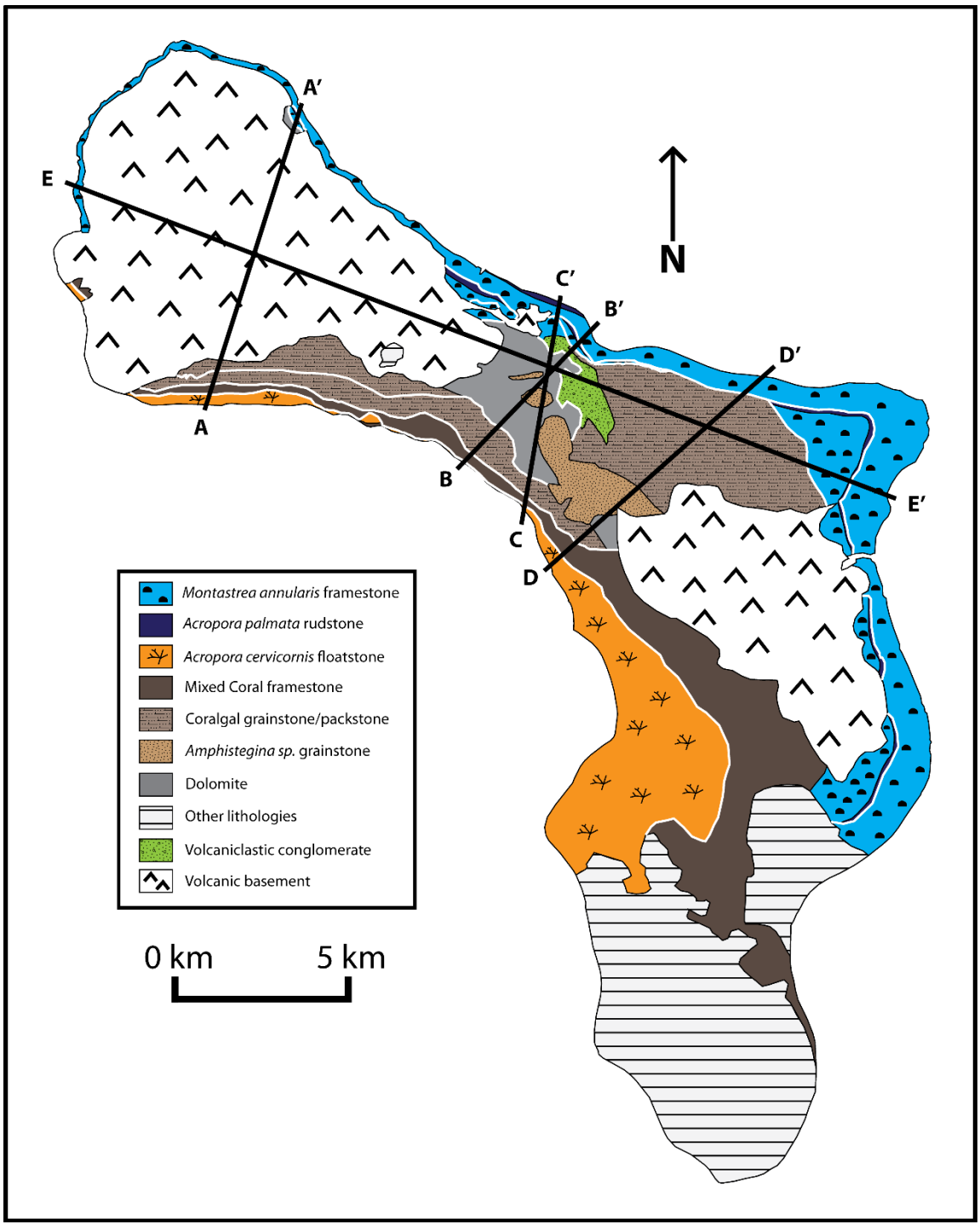

Figure 10: Bonaire facies map including eight carbonate facies. Black boundaries illustrate facies contacts, and white boundaries illustrate facies contacts and boundaries between terraces.

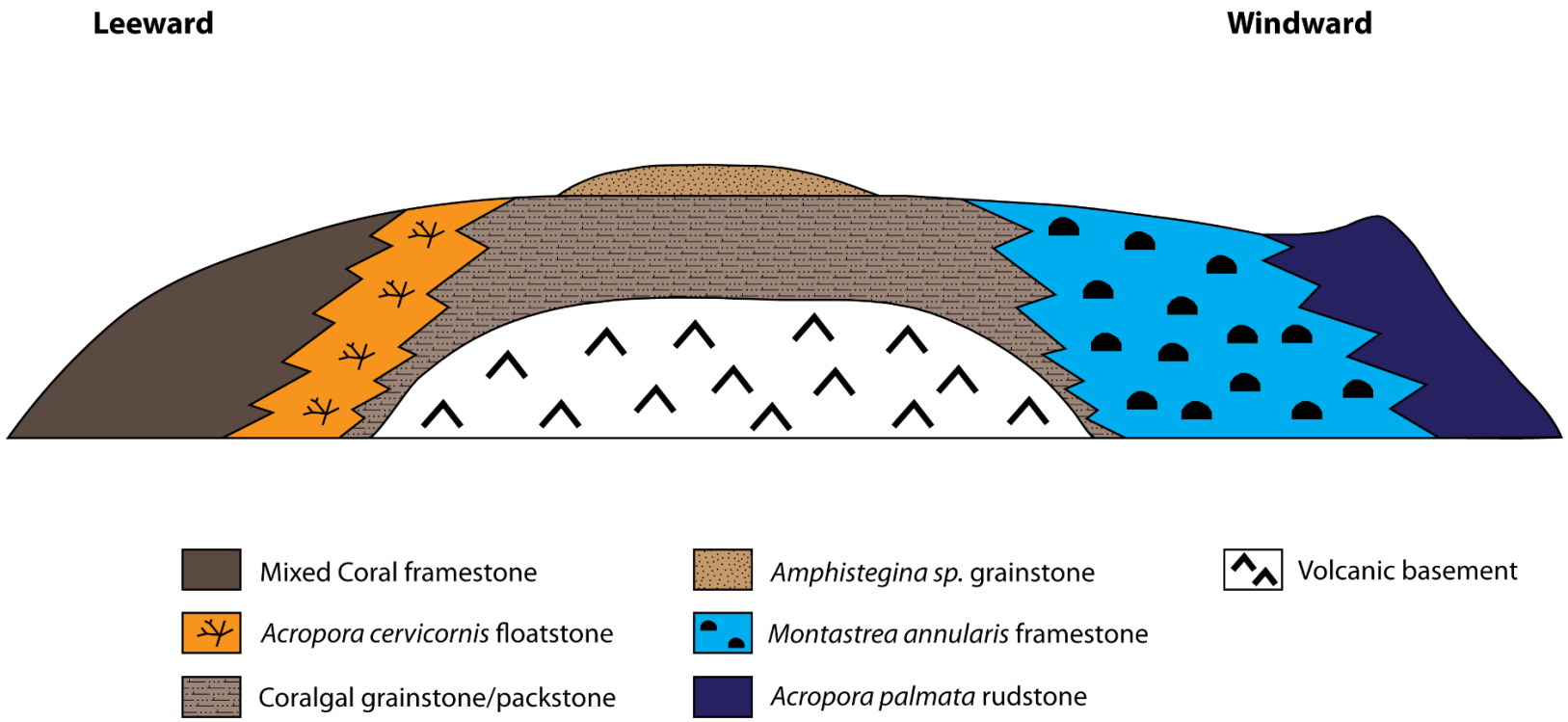

Figure 11: Depositional model illustrating where facies deposited relative to one another on the platform from leeward side to windward side.

Figure 12: Petrographic images that illustrate bioclasts and cements seen within samples. Descriptions of samples are in Table 2. R. alg. – articulated red algae; Encr. R alg. – encrusting red algae; Foram. – foraminifera; G alg. – green algae, Coral – coral fragment or piece of *in-situ* coral. Sample names: A) 12-2-1; B) 26-7-2; C) 26-8-4; D) 16BON2; E) 26-8-3

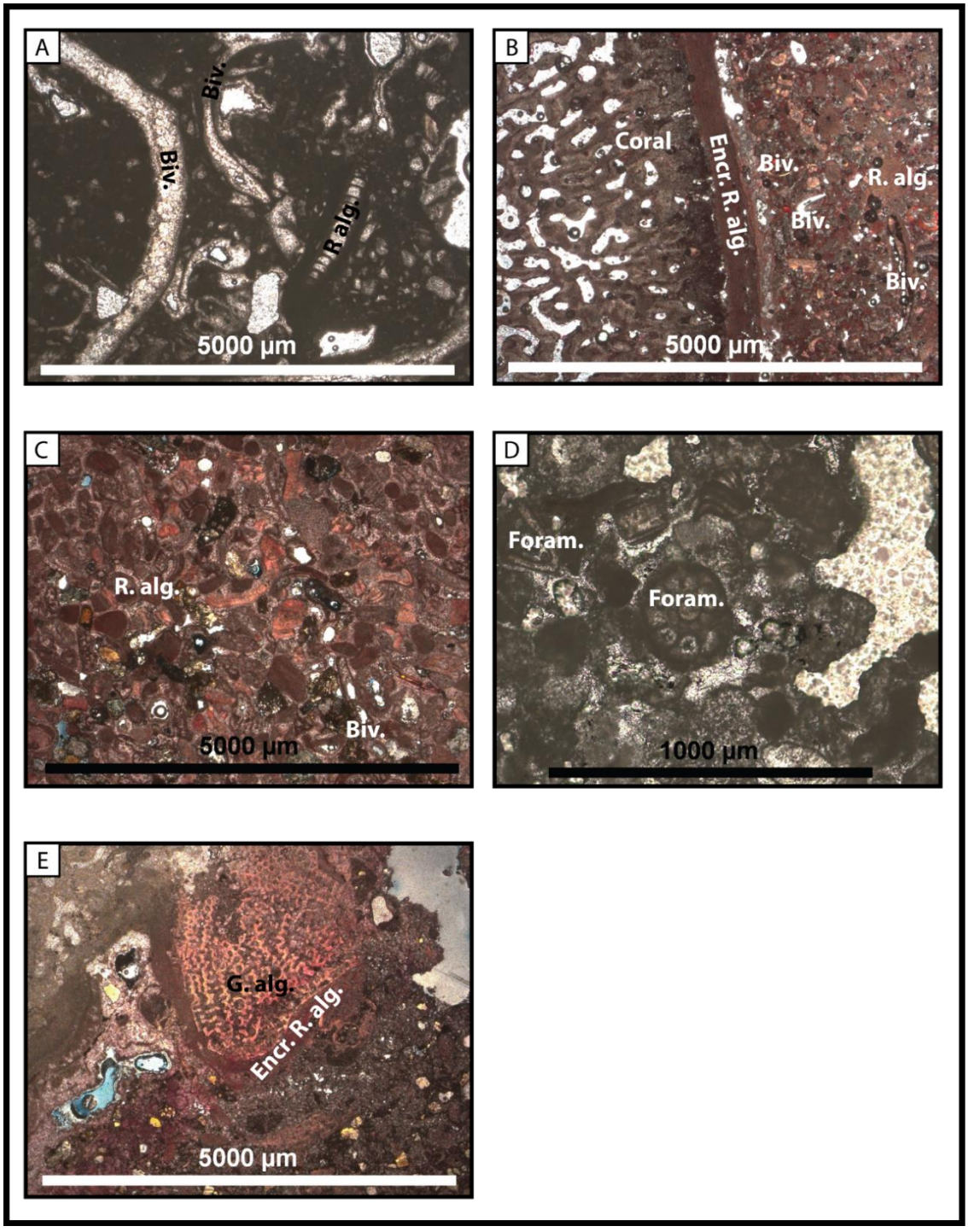
A
Biv.
Biv.
R.alg.
5000 µm
B
Coral
Encr. R. alg.
Biv.
R. alg.
Biv.
Biv.
5000 µm
C
R. alg.
5000 µm
Biv.
D
Foram.
Foram.
1000 µm
E
G. alg.
Encr. R. alg.
5000 µm

Figure 13: Petrographic images from terraces 1-4 comparing cements and dolomite. A) Sample 19BON4 from the terrace 4 strata containing dolomite (Dol) and calcite (Cal). B) Sample 4BON3 from the terrace 3 strata containing bioclasts and cement matrix (Cem), with little porosity. C) and D) Sample 26-8-1 from the terrace 2 strata containing bioclasts with rim cements and equant spar cements filling in porosity (blue stain). E) and F) Sample 26-7-2 from the terrace 1 strata containing cement (Cem) as well as porosity (blue stain). The progression through the different terrace strata reflects a decrease in porosity moving from the youngest strata (Terrace 1, images E & F) to the oldest strata (Terrace 4, image A).

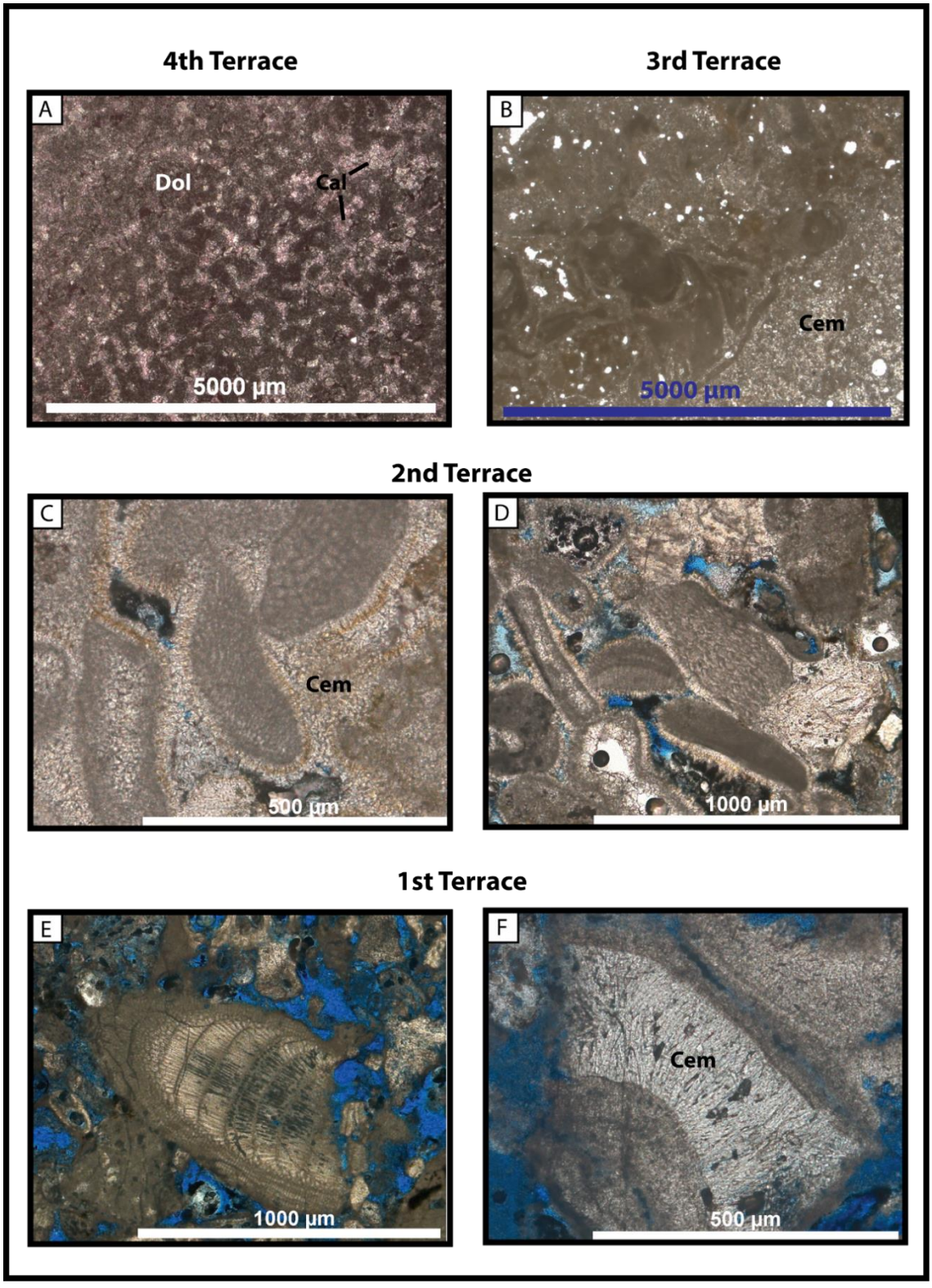
4th Terrace
3rd Terrace
A
Dol
Cal
5000 µm
B
Cem
5000 µm
2nd Terrace
C
Cem
500 µm
D
1000 µm
1st Terrace
E
1000 µm
F
Cem
500 µm

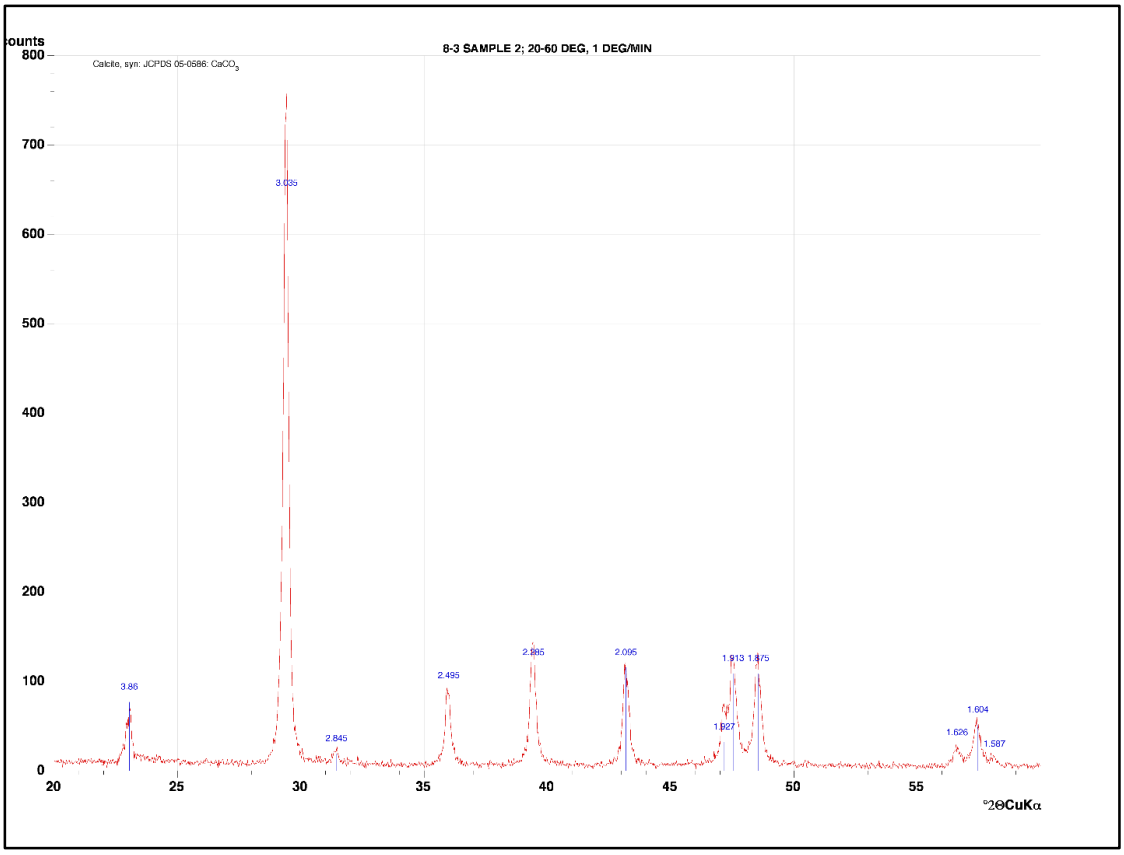

Figure 14: XRD analysis of coral sample 8-3-2 (Bolivia location) where aragonite was completely replaced with calcite.

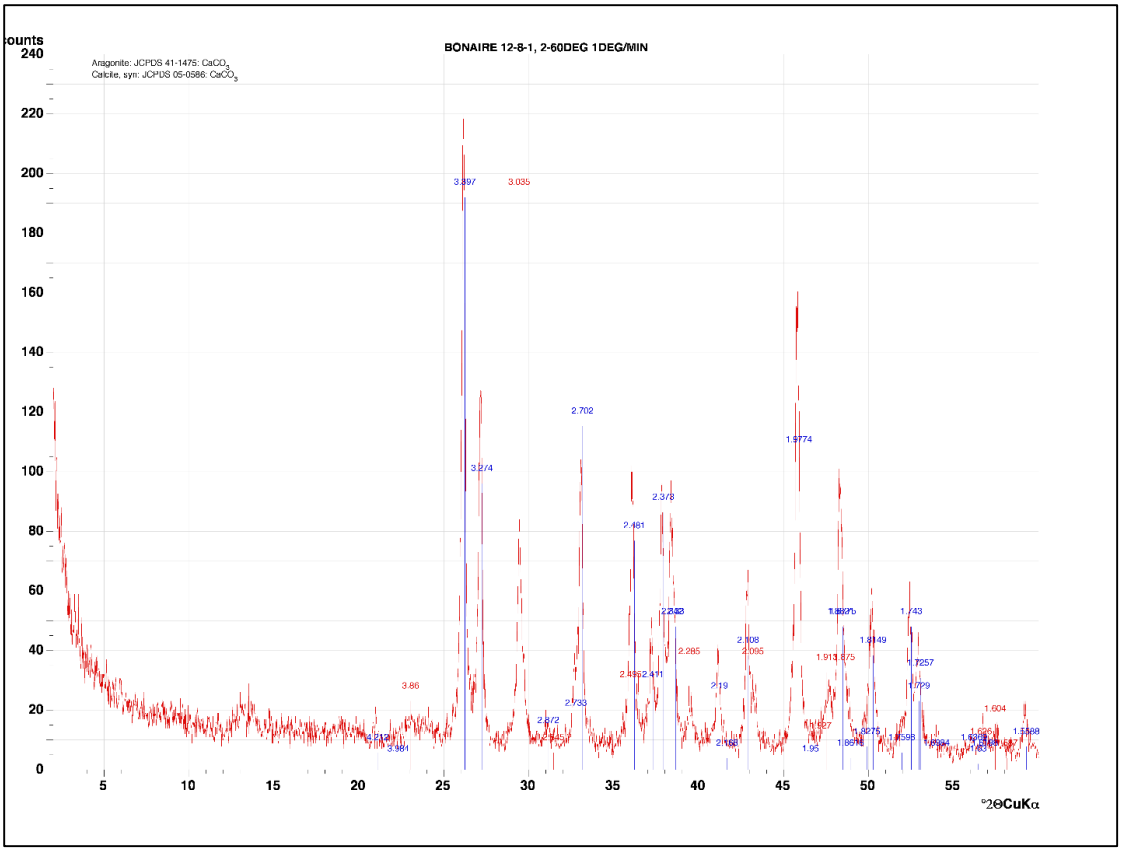

Figure 15: XRD analysis (Sample 12-8-1; Bolivia location) from coral sample illustrating aragonite as the most abundant mineral within sample. A small amount of calcite is also within sample.

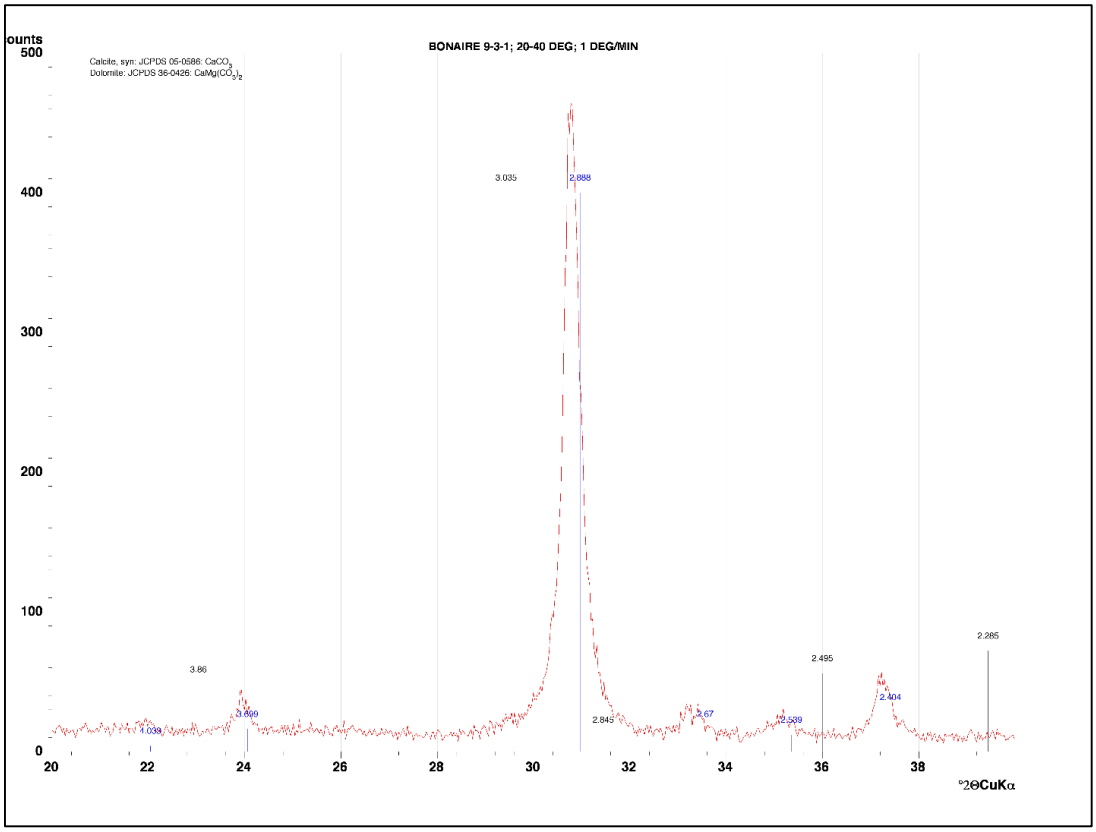

Figure 16: XRD analysis (Sample 9-3-1; Tolo location) illustrating dolomite being sole component of rock sample. Graph is skewed to the left, which may be a result of a trace element in sample or sample thickness was not optimal samples and location.

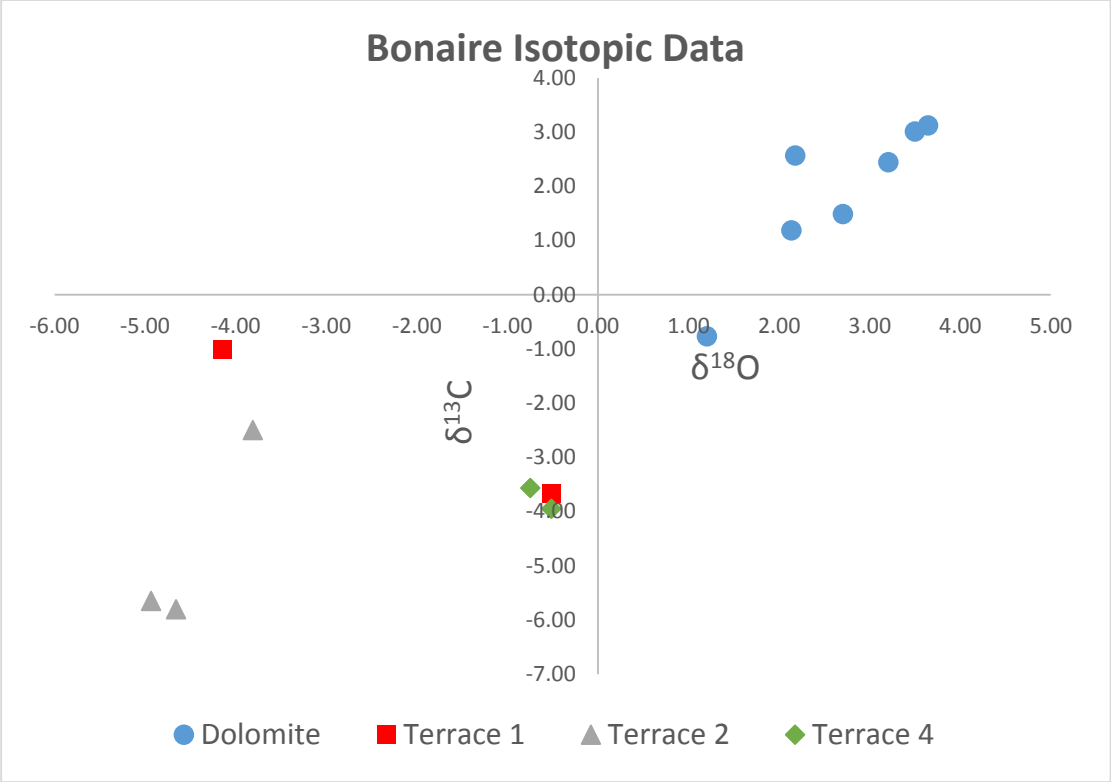

Figure 17: Scatter plot illustrating relationship between $\delta^{18}O$ (y-axis) and $\delta^{13}C$ (x-axis) isotopic results comparing dolomite samples and limestone samples from the strata of terraces 1, 2, and 4.

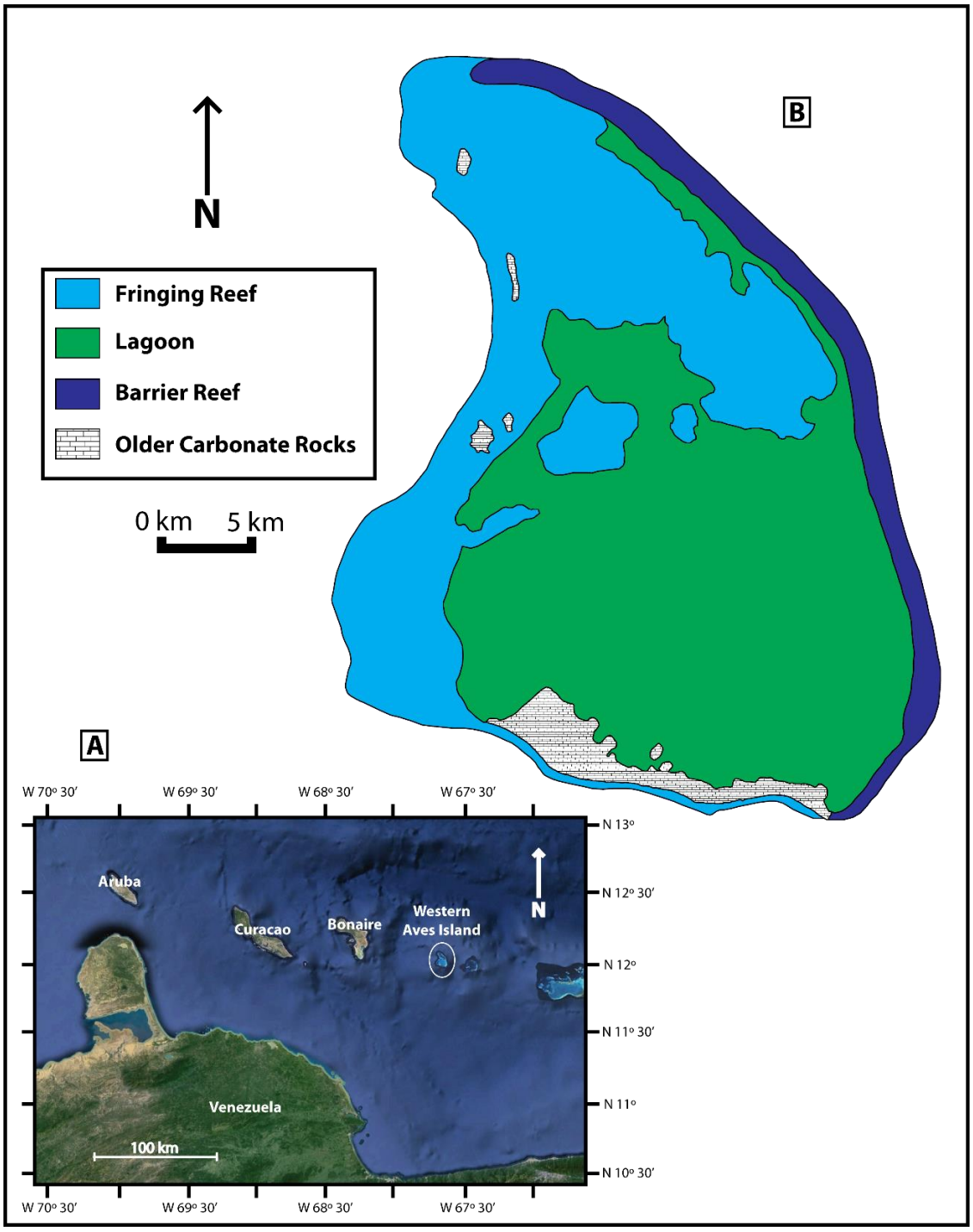

Figure 18: (A) Current facies distribution map of the western Aves Island (60 km east of Bonaire), illustrating present depositional environments. (B) Location of the western Aves Island. Depositional environments delineated by use of aerial photography.

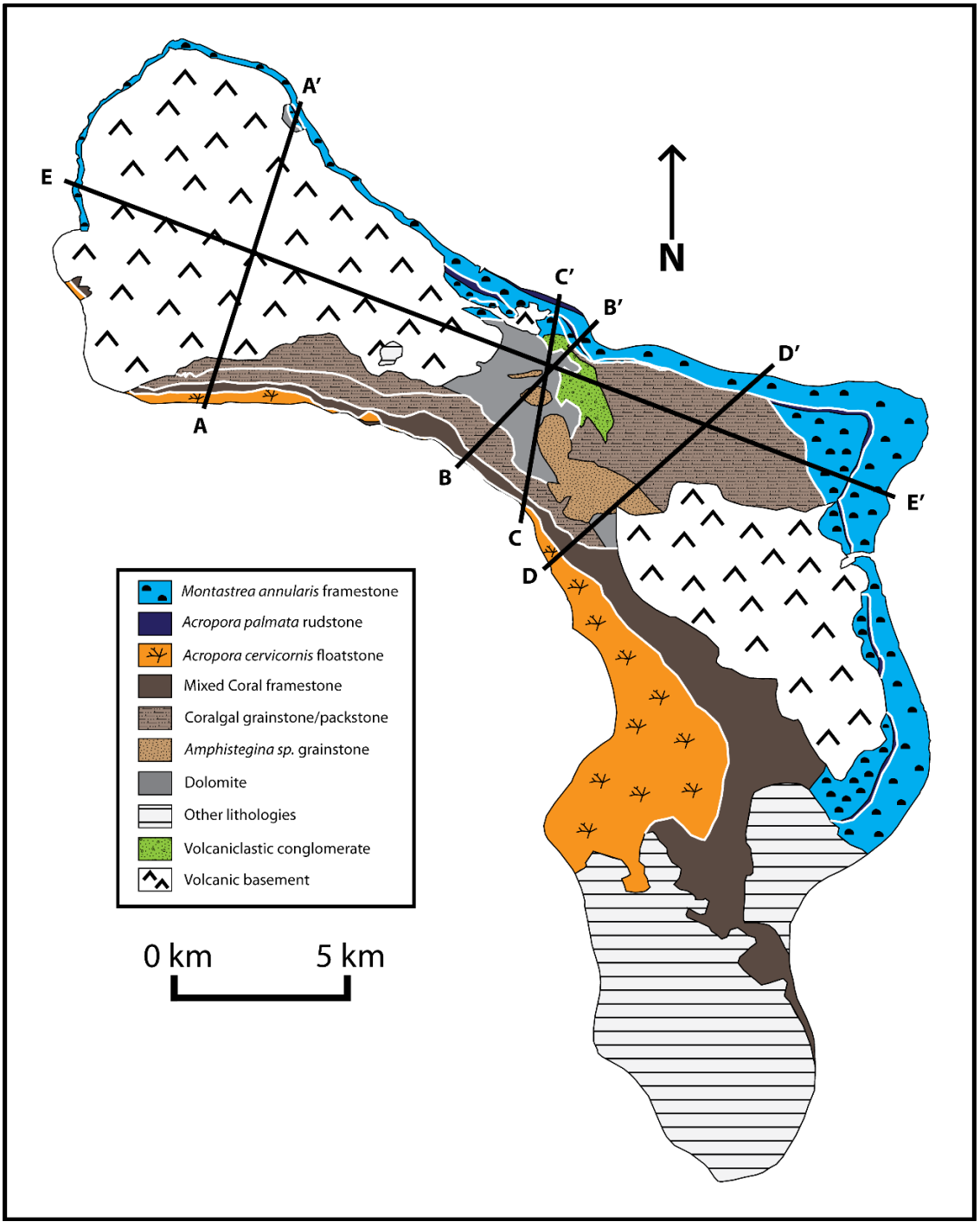

Figure 19: Bonaire facies map illustrating locations of cross-section transects.

Figure 20: Cross sections A-A', B-B', C-C', and D-D' transect across the island in a general north-south to southwest-northeast azimuth, illustrating facies distribution and stratigraphic relationship of the Pleistocene carbonate. Black lines are the contacts between different facies while white lines are boundaries for terrace strata.

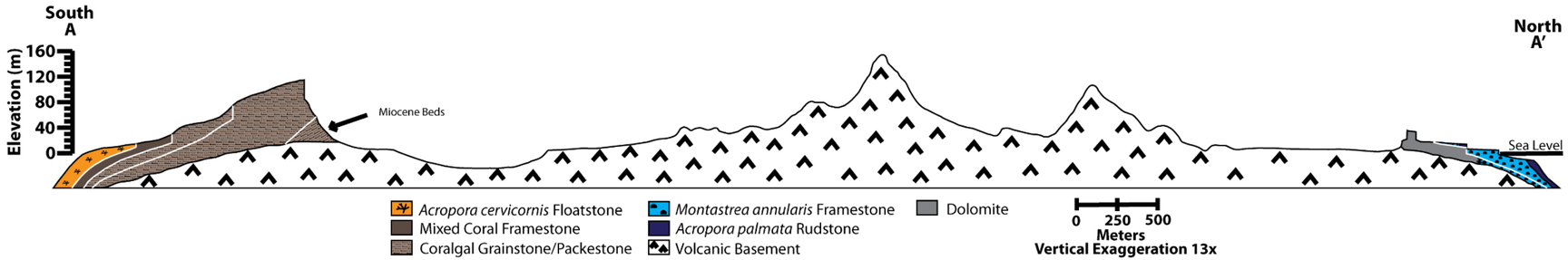
South
A
North
A′
Elevation (m)
160
120
80
40
0
Miocene Beds
Sea Level
Acropora cervicornis Floatstone
Mixed Coral Framestone
Coralgal Grainstone/Packestone
Montastrea annularis Framestone
Acropora palmata Rudstone
Volcanic Basement
Dolomite
0 250 500
Meters
Vertical Exaggeration 13x

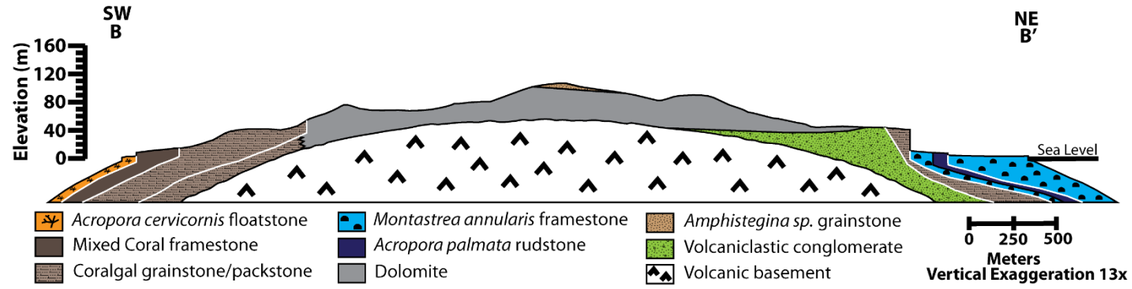
SW
B
NE
B′
Elevation (m)
160
120
80
40
0
Sea Level
Acropora cervicornis floatstone
Mixed Coral framestone
Coralgal grainstone/packstone
Montastrea annularis framestone
Acropora palmata rudstone
Dolomite
Amphistegina sp. grainstone
Volcaniclastic conglomerate
Volcanic basement
0 250 500
Meters
Vertical Exaggeration 13x

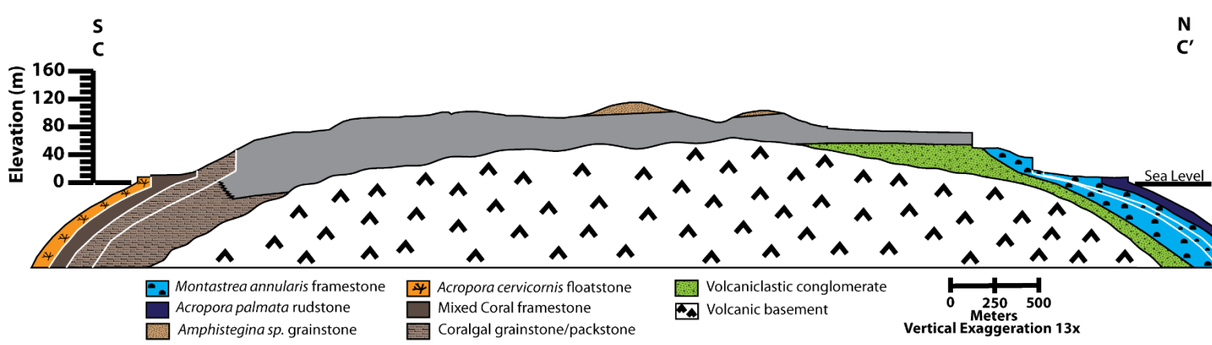
S
C
N
C′
Elevation (m)
160
120
80
40
0
Sea Level
Montastrea annularis framestone
Acropora palmata rudstone
Amphistegina sp. grainstone
Acropora cervicornis floatstone
Mixed Coral framestone
Coralgal grainstone/packstone
Volcaniclastic conglomerate
Volcanic basement
0 250 500
Meters
Vertical Exaggeration 13x

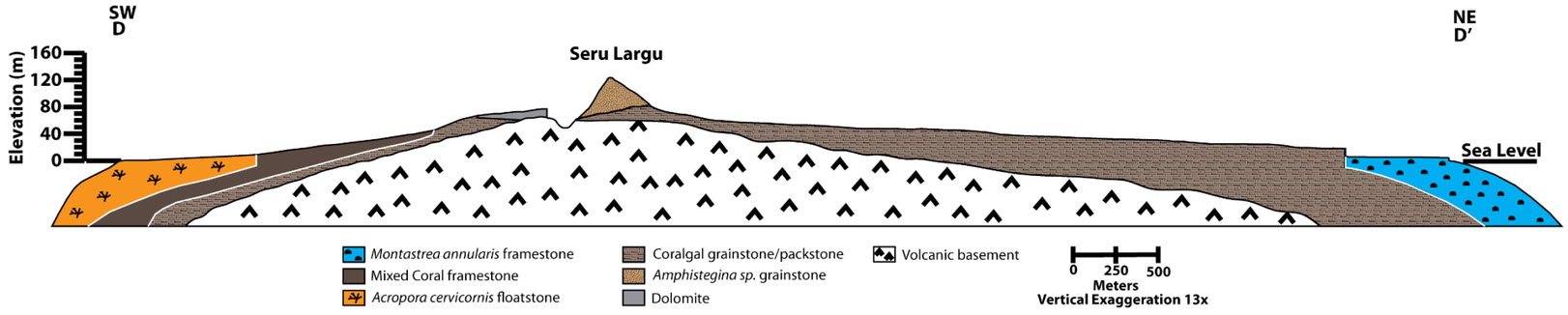
SW
D
NE
D′
Seru Largu
Elevation (m)
160
120
80
40
0
Sea Level
Montastrea annularis framestone
Mixed Coral framestone
Acropora cervicornis floatstone
Coralgal grainstone/packstone
Amphistegina sp. grainstone
Dolomite
Volcanic basement
0 250 500
Meters
Vertical Exaggeration 13x

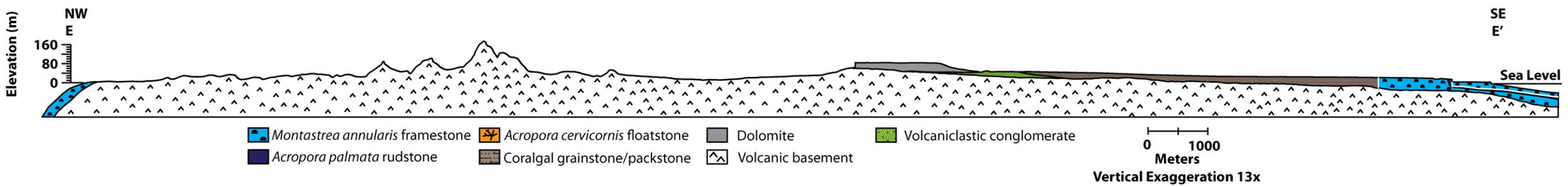

Figure 21: Cross-section E-E' illustrates facies distribution and stratigraphic relationship of the Pleistocene carbonate perpendicular to cross-sections A-D in Figure 20. Black lines are the contacts between different facies while white lines are boundaries for terrace strata.

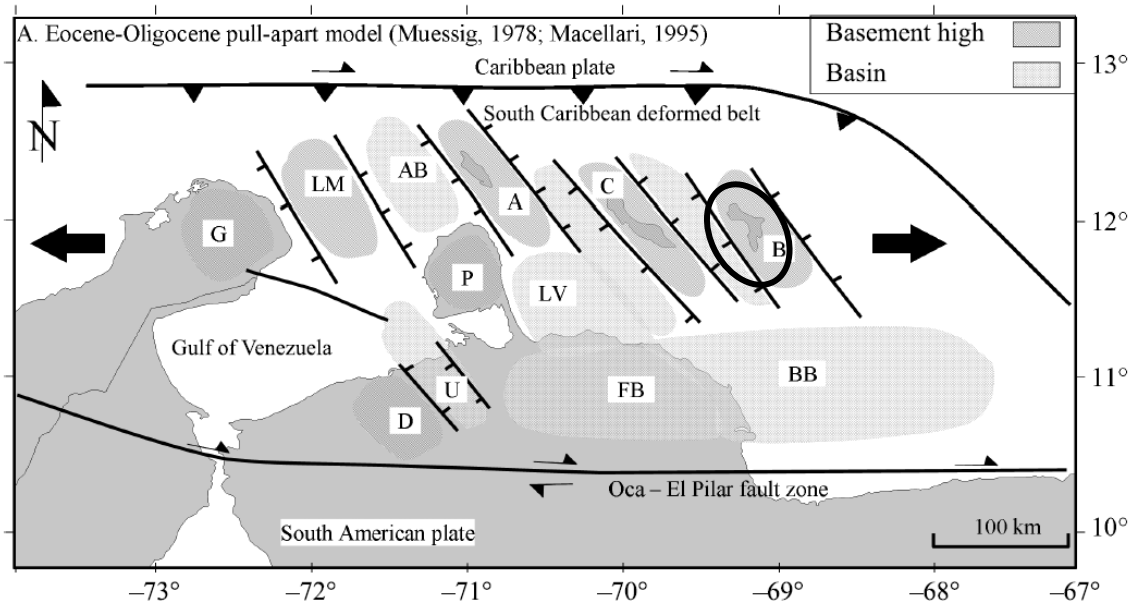

Figure 22: Eocene-Oligocene pull-apart basin related to right-lateral transform plate motion between the Caribbean Plate and South American Plate. Reprinted from Gorney et al. (2007).

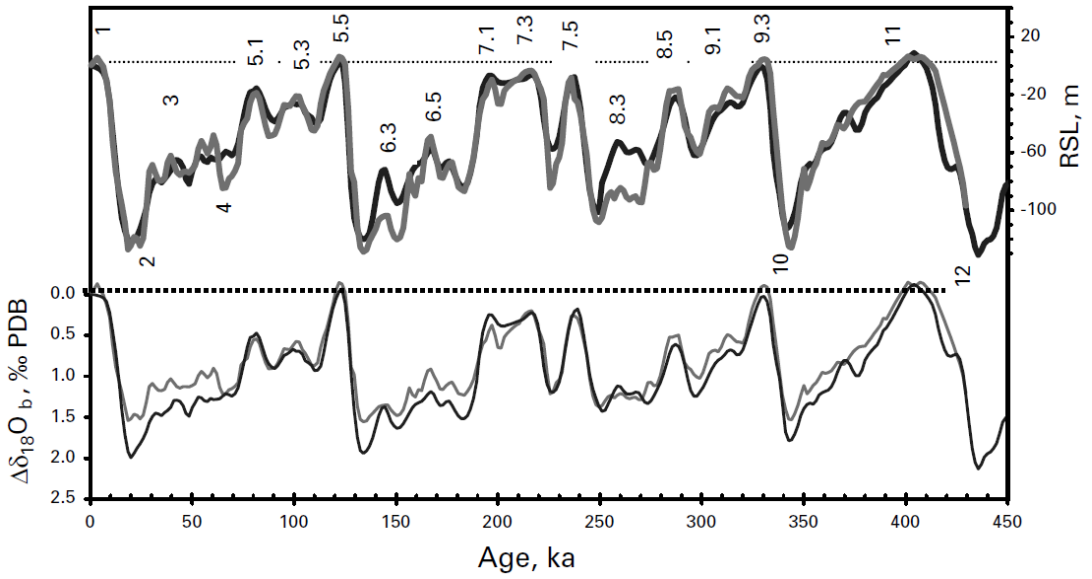

Figure 23: Pleistocene sea-level curve reprinted from Waelbroeck *et al.* (2002) illustrating $\delta^{18}O$ values and interpreted sea levels compared to present sea-level (dotted lines).

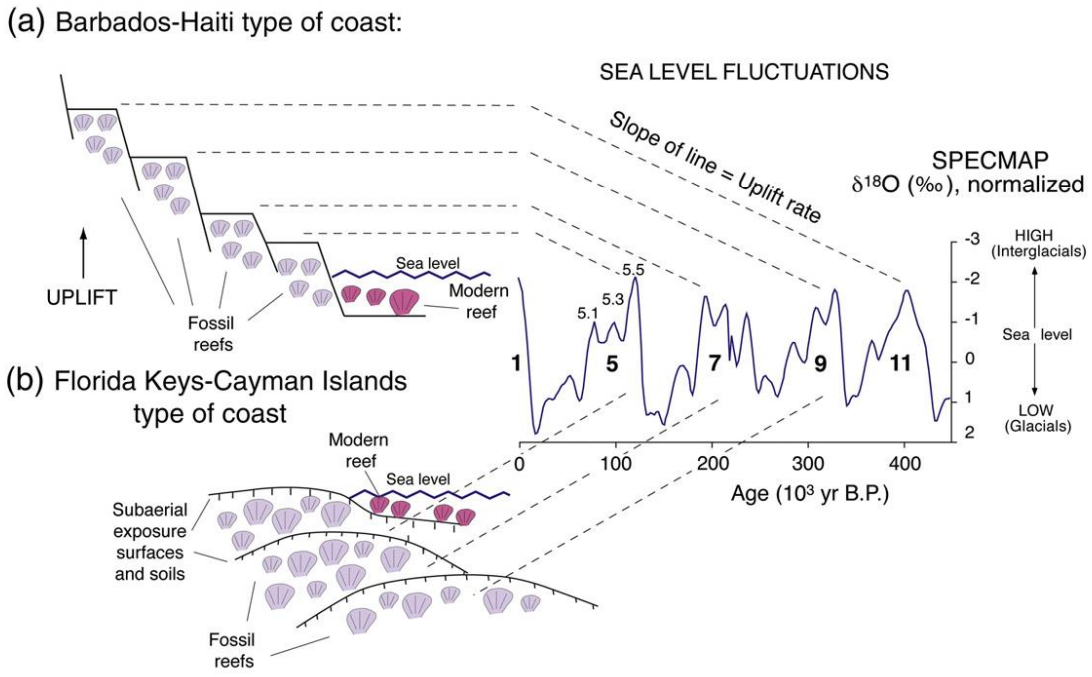

Figure 24: Pleistocene sea-level curve reprinted from Muhs et al. (2012) that illustrates topography influenced by uplift and glacio-eustatic sea-level fluctuation.

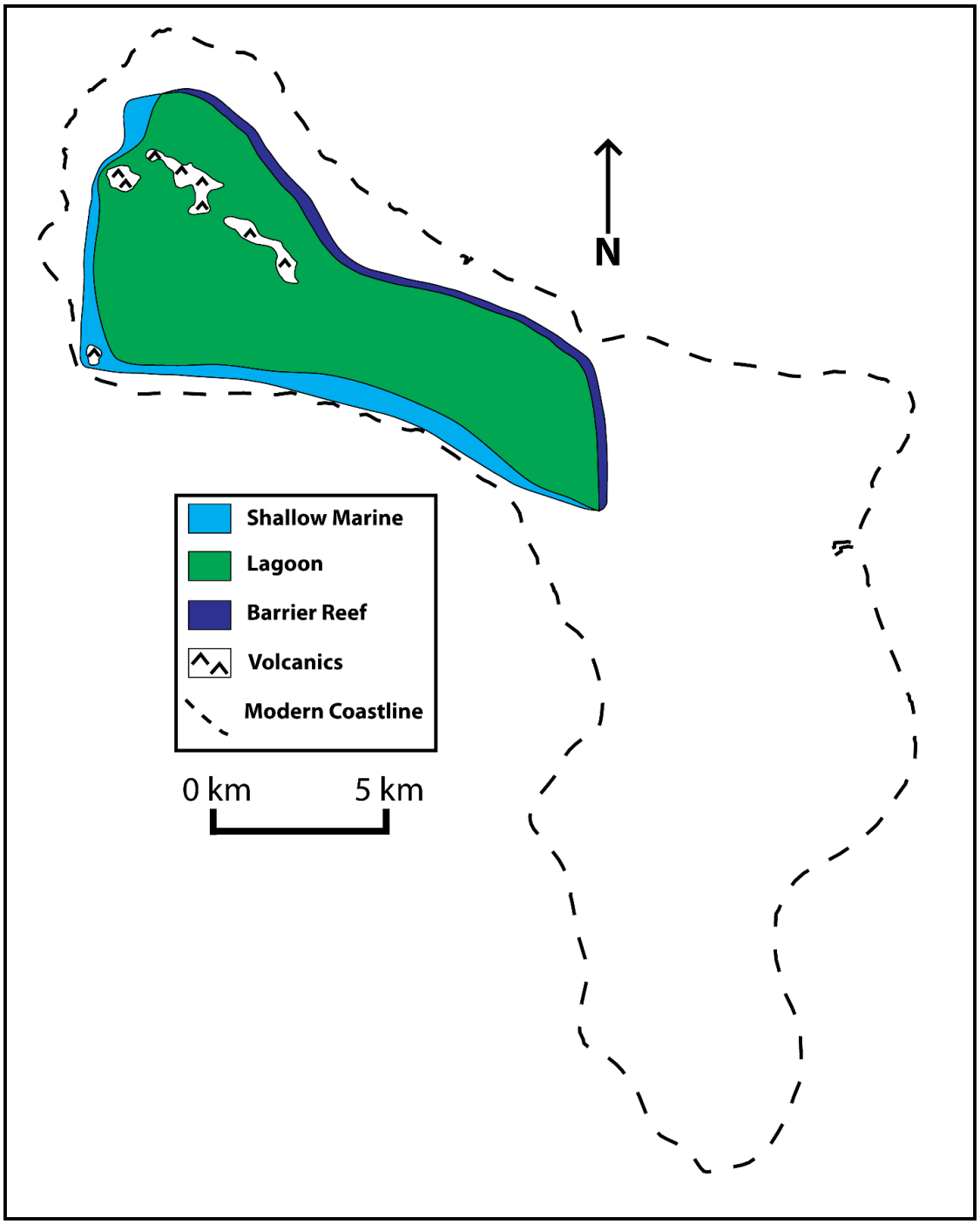

Figure 25: Paleogeography map of 4th terrace strata (MIS 11 interglacial period) depositional environments. The dashed line represents the modern Bonaire coastline.

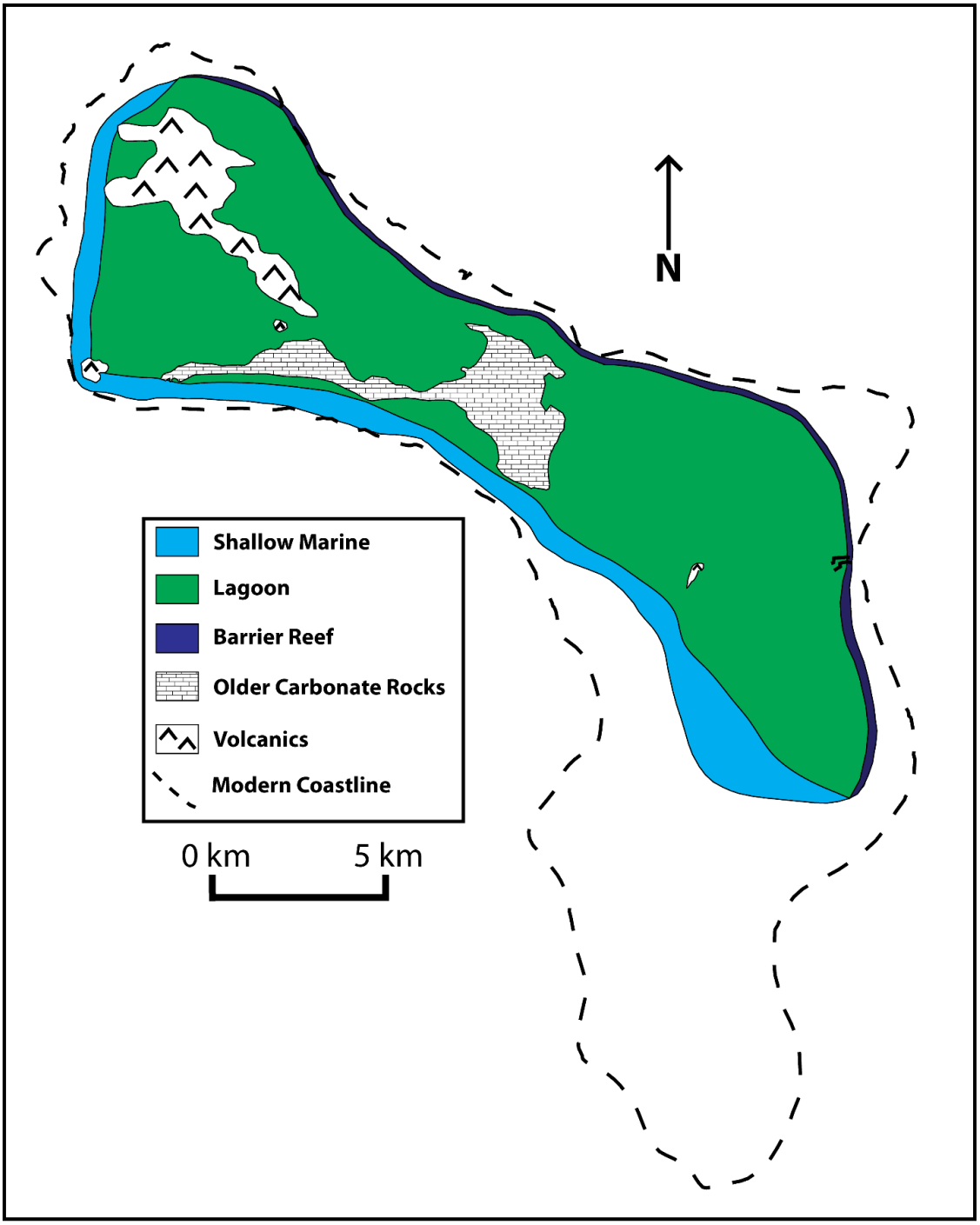

Figure 26: Paleogeography map of 3rd terrace strata (MIS 9 interglacial period) depositional environments. The dashed line represents the modern Bonaire coastline.

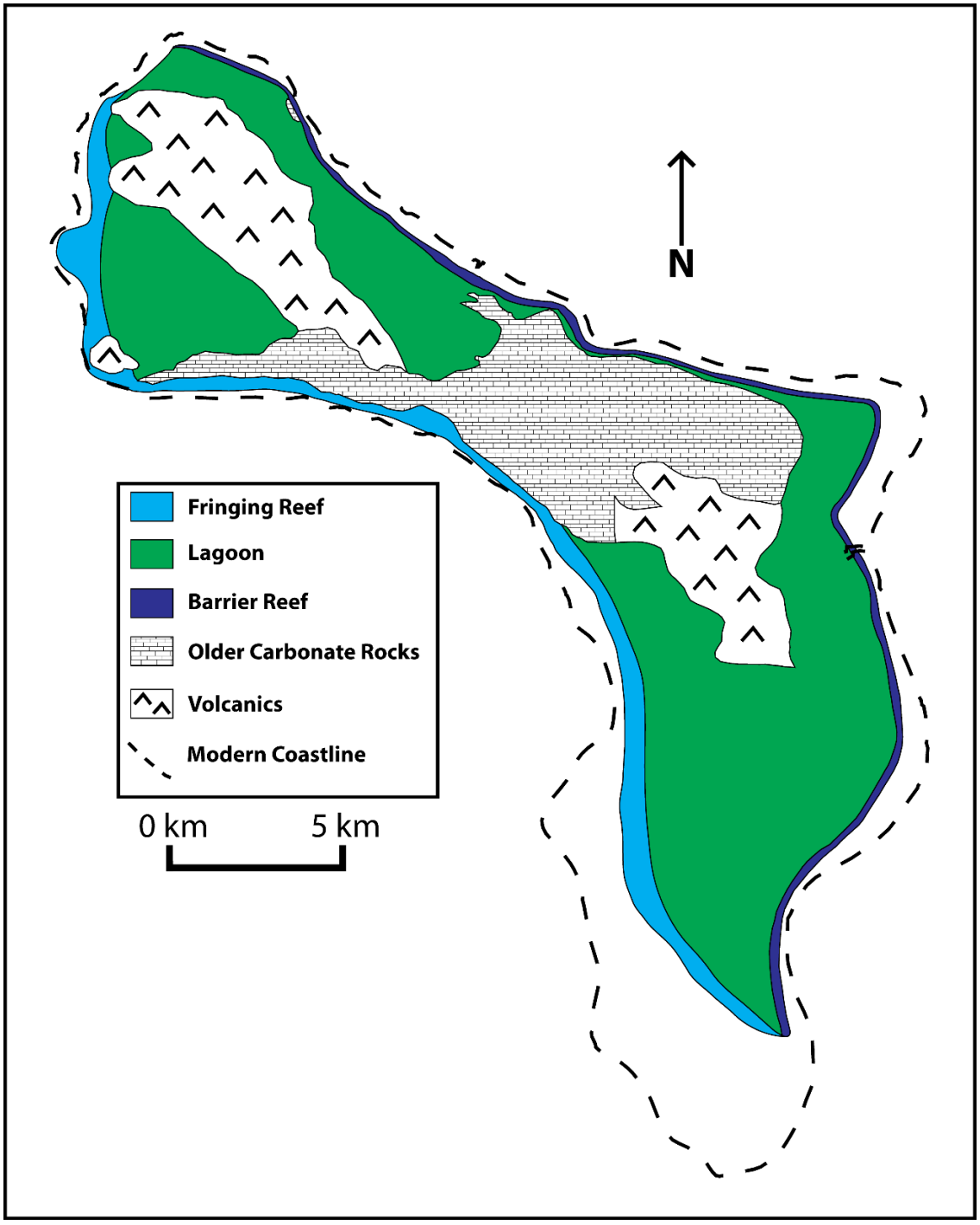

Figure 27: Paleogeography map of 2nd terrace strata (MIS 7 interglacial period) depositional environments. The dashed line represents the modern Bonaire coastline.

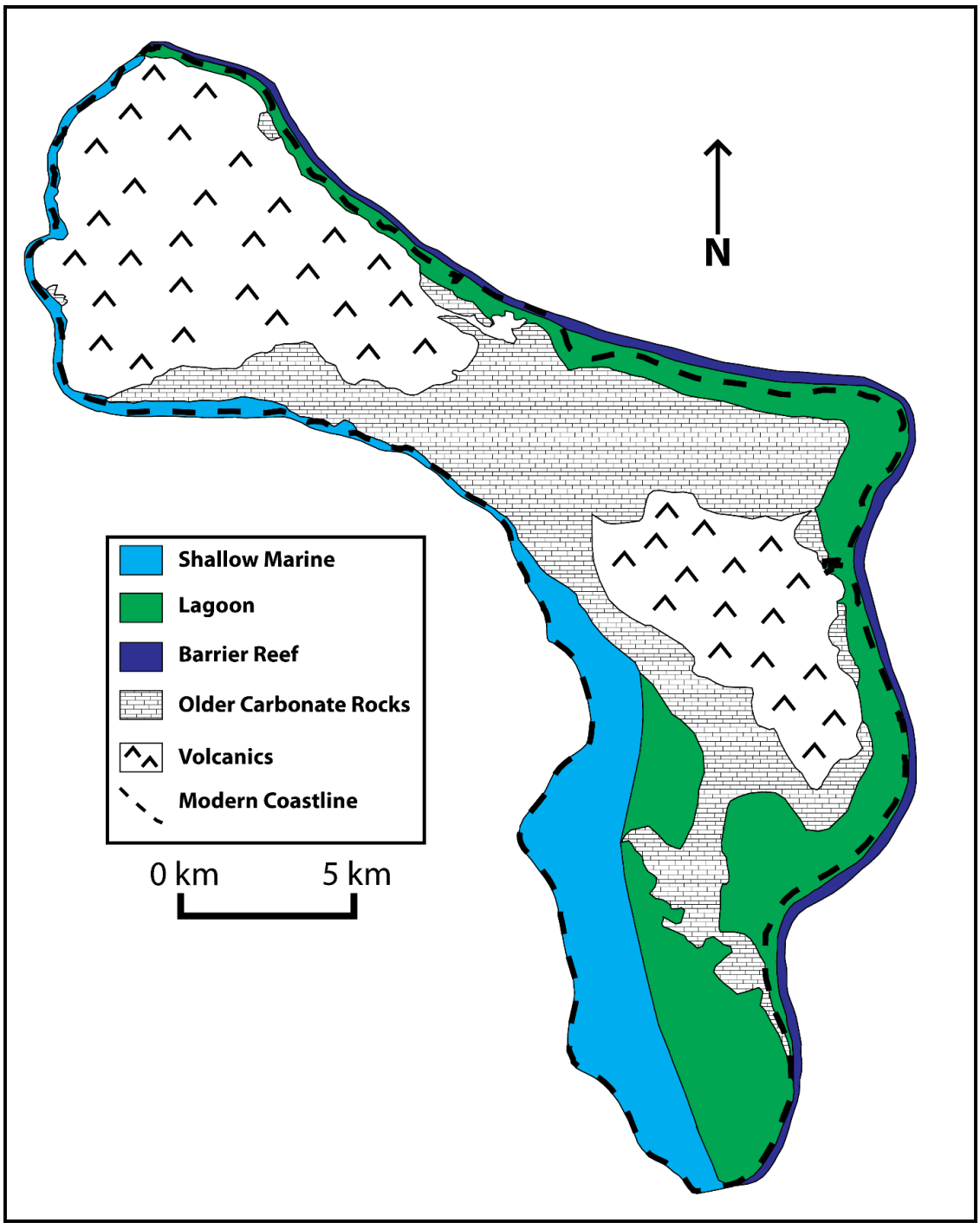

Figure 28: Paleogeography map of 1st terrace strata (MIS 5e interglacial period) depositional environments. The dashed line represents the modern Bonaire coastline.

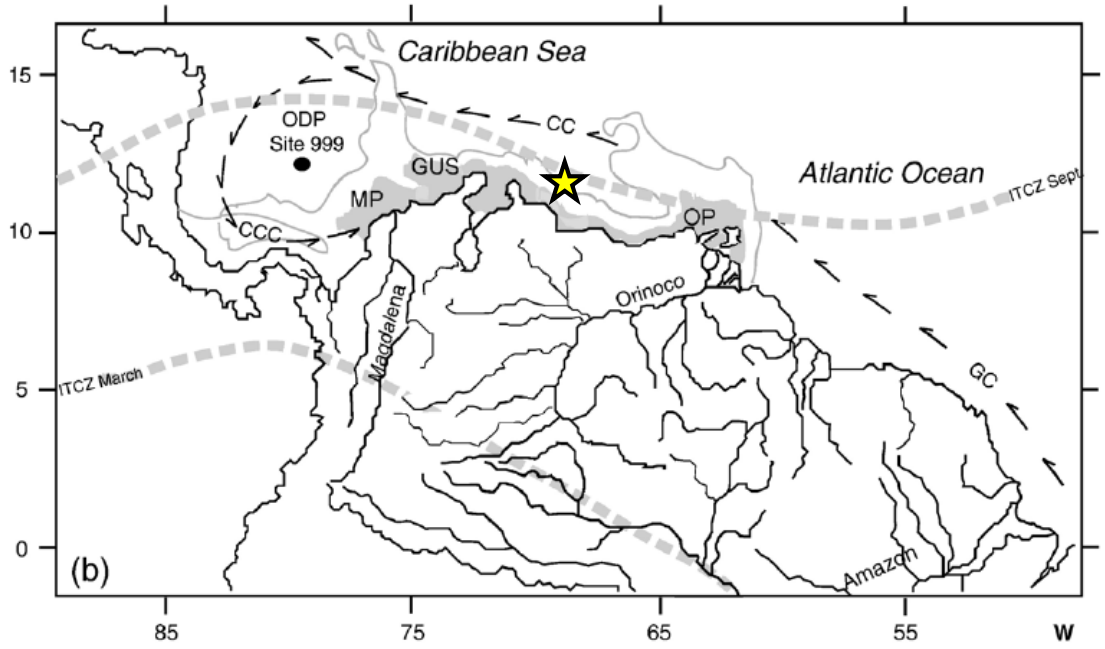

Figure 29: Map illustrating westward flow of the Caribbean Current (CC), average ITCZ locations during the September and March. Generalized locations of the Guajira upwelling system (GUS) and the Orinoco River plume (OP) are also shown. Bonaire's location illustrated by the star. Reprinted from Martinez et al. (2007).

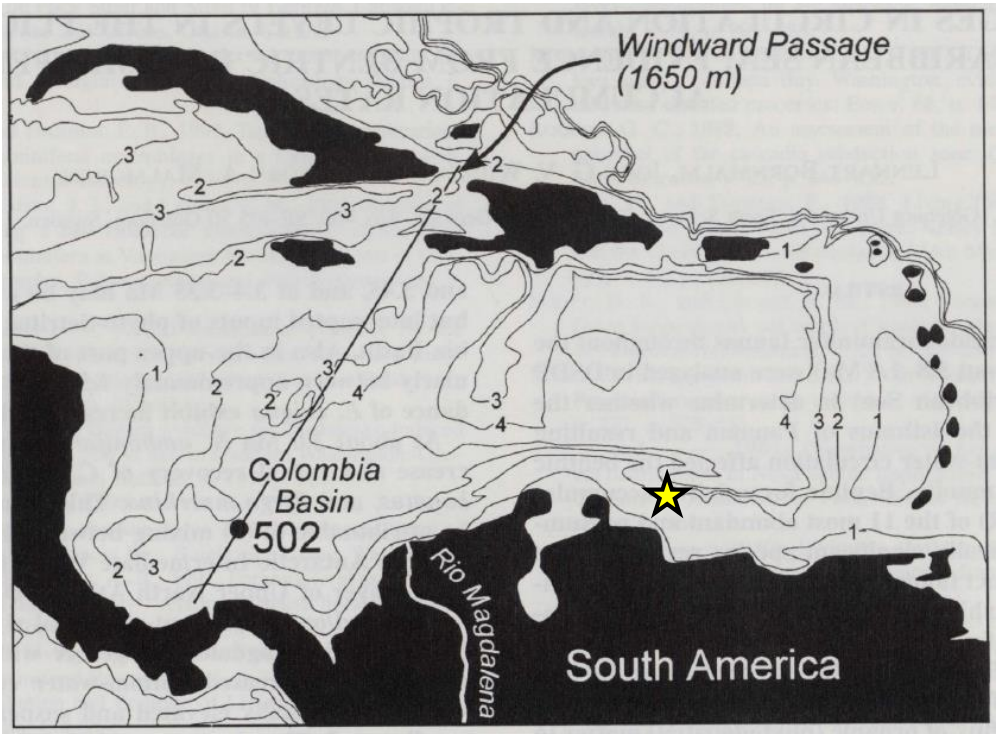

Figure 30: Map referenced to Fig. 31 showing location of cross-section transect Bonaire's location illustrated by the star. Reprinted from Bornmalm et al. (1999).

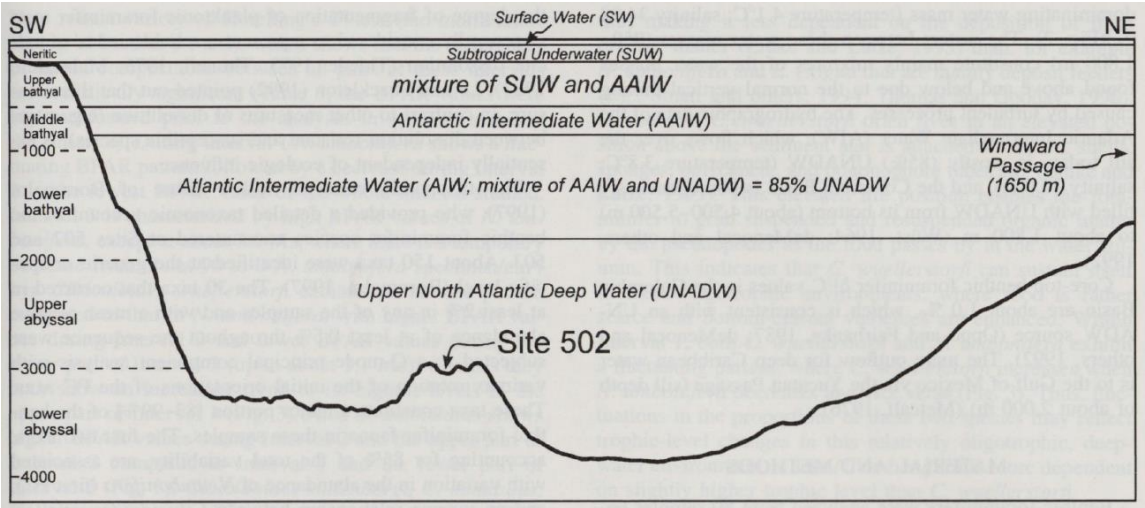

FIGURE 2. Cross section showing generalized water-mass stratification of the Colombia Basin between the Windward Passage and Panama (redrawn after Wüst, 1964) as indicated in Fig. 1.

Figure 31: Cross-section referring to transect in Fig. 30 illustrating generalized water-mass stratification. Reprinted from Bornmalm et al. (1999).

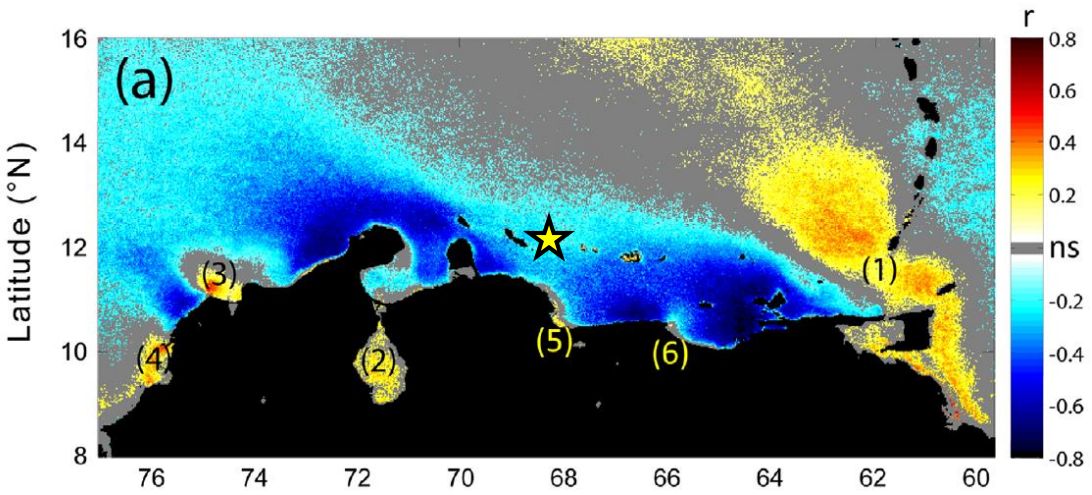

Figure 32: Map illustrating waters influenced by upwelling and fluvial discharge shown by the colors blue (upwelling) and yellow (fluvial discharge). Correlation coefficient (r) is determined by weekly time series of sea-surface temperature and Log(Chl), or concentration of satellite-derived chlorophyll-*a* concentration for the period of 1998-2009. Upwelling has strong inverse correlations with phytoplankton biomass (blue color), while areas of freshwater influence (Orinoco River output) has a direct positive correlation with Chl (yellow). Bonaire's location illustrated by the star. Reprinted from Rudea-Roa and Muller-Karger (2012).

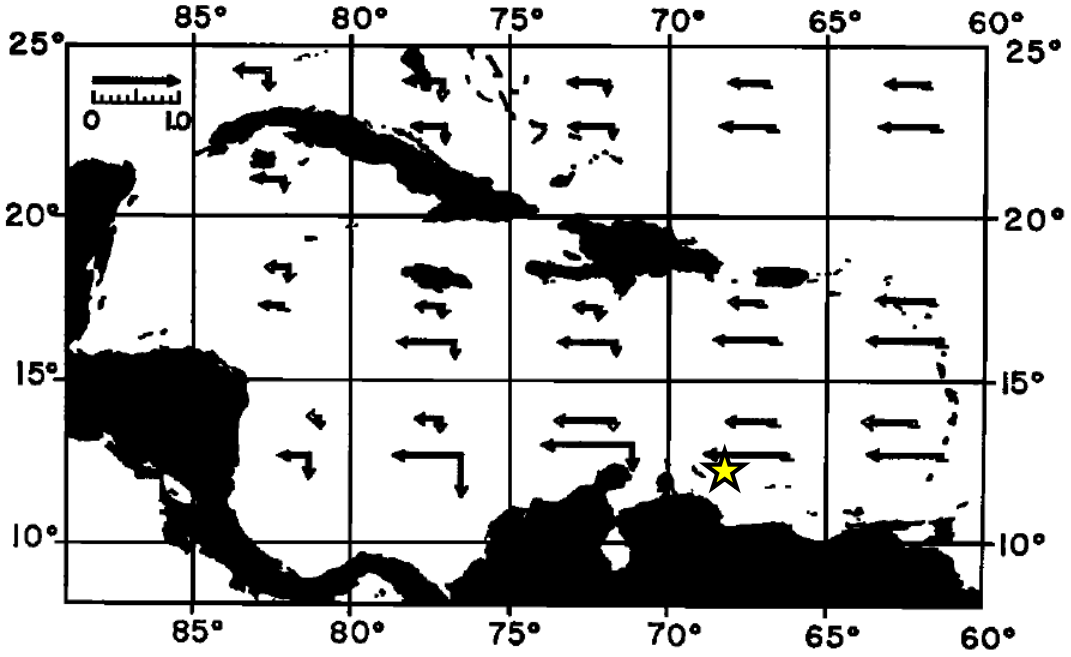

Figure 33: Wind stress on the Caribbean Sea; solid arrows refer to wind stress during March, April, and May, and hollow arrows refer to September, October, and November. Values in dynes/cm^3. Bonaire's location illustrated by the star. Reprinted from Gordon, (1967), (cited originally from Hikada, (1958)).

Table 1: Carbonate facies descriptions with interpretations of depositional environment.

Facies	Description	Interpretation
Amphistegina sp. Grainstone	Abundant with *Amphistegina sp.,* bryozoan fragments present. Fine-grained, well-sorted bioclasts. Gastropods present boring into bedrock. Calcite cement within pores, nucleating from bioclasts.	Fine-grain benthic foraminifera *Amphistegina sp.* grainstone. High-angled beds include cross-stratifications, and are likely eolian. Low-angled cross-stratification is likely from a shallow marine environment, with moderate amount of wave energy to sort sand and allow it to deposit.
Montastrea annularis Framestone	Primarily comprised of *Montastrea annularis,* but other corals such as *Diploria strigose, Diploria clivosa*, and *Montastrea cavernosa* have been observed. *Montastrea annularis* either forms a large singular corallum, which is more common or densely populated columnar corolla. They grow either vertically to form a phaceloid corallum or radiated outward to form a fan-shaped corallum, and can exceed 3m in height. 20-70% coral abundance.	*Montastrea annularis* can be located in low to medium-energy waters. It is likely that this facies deposited in a lagoonal environment, protected from higher energies by a barrier created by branched corals.
Acropora cervicornis Floatstone	Composed of *Acropora cervicornis*, with small amounts of *Diploria sp. Acropora cervicornis* is partially to completely dissolved. Much of the clasts present are *A. cervicornis* rubble broken off from branches. Grainstone-packstone surrounding coral branches. Branch diameter is 2-3 cm.	*Acropora cervicornis* requires decreased amounts of wave energy to thrive and is abundant on the leeward coast. Commonly abundant at depths between 4-12m. Scarcity of secondary branches and abundant rubble suggests *Acropora cervicornis* becomes significantly damaged by occasional storm waves. Most rubble is captured by proximal branches, but some rubble can be observed distally.

Table 1: Continued

Facies	Description	Interpretation
Acropora palmata Rudstone	Composed primarily of *Acropora palmata*, with abundance between 20-50%. Portions of coral has been dissolved out, leaving behind molds. *Acropora palmata* either in-situ, or branches have broken off as broken slabs. Slabs can measure from 10-30 cm wide and 2-6 cm in thickness (Kim and Lee, 1999).	This facies is abundant with *Acropora palmata*, which is commonly located in areas where there is much water turbulence and energy. *Acropora palmata* can be seen in modern reefs along the reef crest, so this is the interpreted depositional environment. This facies can be observed with abundant broken branches along the reef crest of modern reefs.
Mixed Coral Framestone	Abundant in *Montastrea annularis*, *Diploria sp.*, and *Acropora cervicornis*. Coralline algae (Corallinacea family*)* present as bioclastic grains between corals in all beds. *Montastrea annularis* and *Diploria sp.* are in situ.	Abundant in massive corals *Montastrea annularis* and *Diploria sp.*, which is overlain is some areas by *Acropora cervicornis*. Deposited in a low to medium energy environment. This facies is located within second terrace, being protected by the island from high energy waves, so a barrier-type system may not have been present, but instead be deposited between 10-20m depth. This facies in terrace 4 was some of the first carbonate to be produced on Bonaire, and will likely have deposited behind a barrier, and likely deposited within a lagoon.

Table 1: Continued

Facies	Description	Interpretation
Coralgal Grainstone/Packstone	Composed of fine-grained bioclast fragments. Bioclast-rich, composed of red algae (*Corallinacea*), coral fragments (*Acropora sp.*), calcareous green algae, bivalves, gastropods, bryozoans, and foraminifera (*Amphistegina sp.)*. Most abundant bioclasts are coralline red algae and coral fragments. Coralline algae is non-crustose and articulated. Some fine-grained volcaniclastics present. White in color, bioturbated with burrowing. Some root casts infilled with paleosol. Cross-stratification present on windward side.	Grains are well-sorted. This facies is most abundant spatially across the island, and was originally deposited on the island interior in a lagoonal environment. Cross-stratification is well-preserved within the top meter of exposures, which is due to shallow waters with wave influence. This cross-stratification can be located both within the island interior as well as at the most distal part of the terrace strata, at the terrace itself. It is likely this cross-stratification was a result of reworked sediment at a beach environment as sea-level dropped. Leeward Coralgal Gs/Ps does not show cross-stratification as evident as the windward counterparts, and shows some bioturbation.
Dolomite	Microcrystalline dolomite with similar size crystals. Contains Corallinacea red algae (articulated) as only bioclast that is partially recrystallized. Massive bedding in outcrop.	Microcrystalline dolomite with only remnant coralline red algae. Dolomite is located within second terrace on windward side of island, and also the third terrace at Seru Grandi, which located in the northern side of Bonaire. This dolomite formed after the third terrace lithologies deposited. This dolomite is present along the coast, so it is likely that this formed from seepage reflux.

Table 2: Descriptions of thin sections from Pleistocene strata.

Sample	Description
4BON3	Some mud matrix, but mostly composed of calcite cement. Fragments of red algae present
9_1_2	Fragments of foraminifera and articulated red algae within a calcite cement matrix
9_1_3	Calcite and dolomite grains replacing coral
9_2_2	Calcite cement abundant. Bioclasts present include coral fragments and fragments of articulated red algae
9_3_1	Microcrystalline dolomite present with fragments of articulated red algae
12_5_3	Lineations of green algae flakes
12_2_1	Abundance of green alge (*Halimeda sp.)* present within calcareous mud matrix. *Halimeda sp. g*rains have recrysallized as cement
14-6-1	Microcrystalline dolomite with sucrosic texture, no bioclasts present
15-1-1	Bioclasts present include green algae, articulated red algae, and bryozoan fragments. Matrix is composed of mud and calcite cement
15-3-1	Microcrystalline dolomite present with fragments of articulated red algae
15BON1	Presence of green and articulated red algae, foraminifera, and dolomite
15BON3	Coralline red algae present. Matrix is composed of microcrystalline calcite and dolomite cement.
16BON2	Abundance of foraminfera (*Amphistegina sp.*) with some fragments of bryozoans
16BON4	Abundance of foraminfera (Amphistegina sp.) with some fragments of bryozoans
19BON2	Abundance of foraminfera (Amphistegina sp.) with some fragments of bryozoans
19BON3	Microcrystalline sucrosic textured dolomite with some calcite cement present. No bioclasts present
19BON4	Microcrystalline sucrosic textured dolomite with some calcite cement present. No bioclasts present
19BON7	Microcrystalline dolomite present with fragments of articulated coralline red algae present
20BON2	Microcrystalline sucrosic textured dolomite with some calcite cement present. No bioclasts present
24-1-3	Composed of green and red algae, bivalves, foraminifera, and volcaniclastics with calcite cement and calcareous mud matrix
26-1	Presence of calcareous red algae and coral fragments with calcite cement between grains
26-3-1	Dolomite with no bioclasts, porosity ~10-15%

Table 2: Continued

Sample	Description
26-3-2	Tufa composed of calcite, grains radiate out from nucleation points infilling porosity
26-6	Composed of microcrystalline dolomite with few grains of red algae and som e volcaniclastic grains
26-6-1	Composed of microcrystalline dolomite with few grains of red algae
26-6-3	Microcrystaline dolomite present with fragments of articulated red algae. Some red algae partially recrystallized
26-6-4	Microcrystalline dolomite present with few fragments of articulated red algae
26-7-2	Coral specimen present that is encrusted by red algae. Bioclasts such as bivalves, encrusting red algae, foraminifera, and bryozoan fragments present
26-7-2 2	Abundant with coralline red algae, with fragments of bivalves and coral also present. Porosity ~25%
26-8-1	Articulated red algae fragments abundant within sample, with included bryozoan fragments and dissolved bivalves
26-8-2	Bioclasts present include fragments of articulated red algae, bivalves, bryozoans, and foraminifera. Both calcite cement and dolomite are present
26-8-3	Green algae present that is encrusted by red algae. Articulated red algae fragments are present and separated by calcite cement
26-8-4	Microcrystalline dolomite present with fragments of articulated red algae. Porosity ~5-10%
26-8-5	Abundant with green algae
26-8-6	Dolomite replacing all matrix and grains, which include green and red algae, and bivalves
26-8-7	Presence of foraminifera, calcareous articulated red algae, and bivalves. Some bivalves have dissolved and vugs filled with calcite cement. Some microcrystalline dolomite present
27-1-1	Composed of microcrystalline dolomite and with a moderate amount of red algae grains
27-2-1	Repeating consistent structure with may belong to a sponge
27-3-1	Composed of microcrystalline dolomite and abundant with red algae grains
27-4-1	Composed of microcrystalline dolomite and abundant with red algae grains
27-5-1	Foraminifera and red algae with microcrystalline dolomite cement
27-7-1	Composed of red and green algae, dolomite present within matrix, porosity ~25%
27-8-1	Composed of microcrystalline dolomite with few grains of red algae
27-9-1	Composed of microcrystalline dolomite with few grains of red algae

Table 2: Continued

Sample	Description
Boca Chikitu	Only composed of articulated coralline red algae, 30-40% porosity
LS1	Bioclasts include fragments of articulated red algae, bivalves, bryozoans, coral, and foraminifera
LS2	Abundant in bivalves, some coral and red algae, much of the matrix is dolomitized

APPENDIX B: SUPPLEMENTAL FIGURES AND TABLES

(Not referenced in text.)

Table 3

Stable isotope geochemistry results ($\delta^{18}O$ and $\delta^{13}C$) of limestone and dolomite samples.

sample ident 1	sample ident 2	**d18O VPDB**	**d13C VPDB**
T2 dolomite	26-6-3	**3.50**	**3.02**
T2 dolomite	15-3-1	**3.21**	**2.45**
T2 dolomite	9-3-1	**2.18**	**2.57**
T2 dolomite	26-6-4	**3.65**	**3.13**
T3 dolomite	20Bon1-2	**2.14**	**1.19**
T4 dolomite	19BON3	**2.70**	**1.49**
T4 dolomite	19BON8	**1.20**	**-0.77**
T1	0	**-4.15**	**-1.01**
T1	20	**-0.52**	**-3.66**
T2	12-2-1	**-3.81**	**-2.50**
T2	12-2-3a	**-4.66**	**-5.81**
T2	12-2-2a	**-4.93**	**-5.65**
T4	19BON4	**-0.74**	**-3.56**
T4	19BON7	**-0.51**	**-3.95**

Table 4

Geochemical results using electron microprobe analysis. Results are measured by weight percentage and well as molar percentage. Highlighted in yellow are dolomite samples, while other samples are limestone.

	Wt. % carbonate (all elements)									**MOLE % (normalized for Mg, Ca, Fe, Mn, Sr only)**				
Analysis	CaCO3 (wt%)	FeCO3 (wt%)	SrCO3 (wt%)	MnCO3 (wt%)	S(CO3)3 (wt%)	MgCO3 (wt%)	Al2(CO3)3 (wt%)	Na2CO3 (wt%)	Si(CO3)2 (wt%)	Ca (mole%)	Mg (mole%)	Fe (mole%)	Mn (mole%)	Sr (mole%)
5CaCO3_stdck#1	99.06	0.00	0.00	0.05	0.05	0.00	0.00	0.01	0.09	99.95	0.00	0.00	0.05	0.00
3calcite_stdck#1	97.62	0.00	0.02	0.20	0.04	0.00	0.02	0.00	0.19	99.80	0.00	0.00	0.20	0.00
JS_2413_a_pt01	98.37	0.01	0.19	0.00	0.09	0.98	0.06	0.07	0.31	98.69	1.16	0.00	0.00	0.15
JS_2413_a_pt02	98.62	0.03	0.18	0.02	0.06	0.86	0.01	0.04	0.08	98.85	1.00	0.05	0.00	0.10
JS_2413_a_pt03	98.58	0.04	0.14	0.00	0.04	1.05	0.19	0.04	0.35	98.59	1.26	0.05	0.00	0.10
JS_2413_a_pt04	99.13	0.07	0.08	0.02	0.05	0.89	0.00	0.04	0.00	98.85	1.05	0.05	0.00	0.05
JS_2413_b_pt05	97.66	0.04	0.20	0.00	0.02	0.65	0.03	0.08	0.01	99.00	0.80	0.05	0.00	0.15
JS_2413_b_pt06	98.02	0.08	0.05	0.00	0.06	1.91	0.07	0.03	0.08	97.65	2.25	0.05	0.00	0.05
JS_2413_b_pt07	97.76	0.08	0.05	0.01	0.22	1.15	0.03	0.01	0.02	98.55	1.35	0.05	0.00	0.05
JS_2664_c_pt01	62.16	0.03	0.00	0.05	0.24	38.83	0.01	0.09	0.00	57.39	42.56	0.00	0.05	0.00
JS_2664_c_pt02	57.45	0.05	0.02	0.02	0.20	43.13	0.07	0.10	0.01	52.86	47.09	0.05	0.00	0.00
JS_2664_c_pt03	99.46	0.05	0.00	0.00	0.03	1.33	0.00	0.03	0.00	98.40	1.55	0.05	0.00	0.00
JS_2664_c_pt04	98.87	0.06	0.00	0.00	0.07	1.25	0.00	0.02	0.03	98.50	1.45	0.05	0.00	0.00
JS_2664_b_pt05	91.91	0.05	0.02	0.00	0.07	8.54	0.02	0.05	0.03	90.03	9.92	0.05	0.00	0.00
JS_2664_b_pt06	94.19	0.01	0.03	0.00	0.04	5.88	0.00	0.05	0.04	93.09	6.91	0.00	0.00	0.00
JS_2664_b_pt07	94.83	0.07	0.07	0.00	0.13	6.09	0.00	0.06	0.10	92.83	7.07	0.05	0.00	0.05
JS_2664_a_pt08	93.21	0.05	0.04	0.02	0.08	7.37	0.00	0.04	0.04	91.38	8.57	0.05	0.00	0.00
JS_2664_a_pt09	94.58	0.06	0.02	0.01	0.08	4.68	0.00	0.03	0.03	94.39	5.56	0.05	0.00	0.00
JS_2664_a_pt10	59.93	0.07	0.03	0.04	0.26	40.02	0.02	0.08	0.04	55.72	44.18	0.05	0.05	0.00
JS_2664_a_pt12	96.17	0.05	0.02	0.00	0.16	3.82	0.10	0.00	0.09	95.44	4.51	0.05	0.00	0.00
JS_2664_a_pt13	97.24	0.01	0.04	0.01	0.03	2.44	0.04	0.00	0.07	97.10	2.90	0.00	0.00	0.00
JS_2672_a_pt01	96.97	0.09	0.11	0.00	0.07	2.13	0.04	0.06	0.02	97.25	2.55	0.10	0.00	0.10
JS_2672_a_pt02	95.91	0.08	0.21	0.00	0.16	2.86	0.02	0.07	0.17	96.39	3.41	0.05	0.00	0.15
JS_2672_a_pt03	94.14	0.06	1.37	0.00	0.73	0.33	1.80	0.89	0.96	98.54	0.42	0.05	0.00	0.99
JS_2672_b_pt04	96.32	0.07	0.18	0.00	0.24	2.92	0.02	0.11	0.02	96.39	3.46	0.05	0.00	0.10
JS_2672_b_pt05	94.49	0.08	0.18	0.00	0.24	4.27	0.08	0.09	0.34	94.77	5.08	0.05	0.00	0.10
JS_2672_b_pt06	96.04	0.10	0.29	0.00	0.73	2.96	0.08	0.31	0.17	96.16	3.54	0.10	0.00	0.20
JS_2672_d_pt07	96.06	0.09	0.11	0.00	0.25	2.93	0.00	0.15	0.03	96.34	3.46	0.10	0.00	0.10
JS_2672_d_pt08	95.88	0.05	0.13	0.00	0.09	2.99	0.02	0.05	0.03	96.29	3.56	0.05	0.00	0.10

Table 4:Continued

	Wt. % carbonate (all elements)									MOLE % (normalized for Mg, Ca, Fe, Mn, Sr only)				
Analysis	CaCO3 (wt%)	FeCO3 (wt%)	SrCO3 (wt%)	MnCO3 (wt%)	S(CO3)3 (wt%)	MgCO3 (wt%)	Al2(CO3)3 (wt%)	Na2CO3 (wt%)	Si(CO3)2 (wt%)	Ca (mole%)	Mg (mole%)	Fe (mole%)	Mn (mole%)	Sr (mole%)
JS_2672_d_pt09	97.13	0.04	0.09	0.01	0.23	3.45	0.00	0.12	0.00	95.84	4.06	0.05	0.00	0.05
JS_2672_d_pt10	96.98	0.06	0.16	0.00	0.31	2.91	0.04	0.17	0.06	96.43	3.42	0.05	0.00	0.10
JS_2681_a_pt01	98.61	0.03	0.03	0.00	0.04	0.86	0.02	0.00	0.37	98.95	1.00	0.05	0.00	0.00
JS_2681_a_pt02	98.90	0.07	0.07	0.00	0.01	0.81	0.01	0.01	0.00	98.95	0.95	0.05	0.00	0.05
JS_2681_a_pt03	96.97	0.10	0.03	0.00	0.09	1.28	0.32	0.04	0.73	98.38	1.51	0.10	0.00	0.00
JS_2681_b_pt04	97.14	0.03	0.10	0.02	0.07	0.76	0.02	0.03	1.66	98.99	0.91	0.05	0.00	0.05
JS_2681_b_pt05	99.72	0.08	0.06	0.01	0.02	0.80	0.00	0.08	0.01	98.95	0.95	0.05	0.00	0.05
JS_2681_b_pt06	98.13	0.11	0.10	0.00	0.01	1.01	0.18	0.01	0.27	98.65	1.20	0.10	0.00	0.05
JS_2681_c_pt07	100.29	0.08	0.09	0.01	0.04	0.80	0.00	0.07	0.01	98.95	0.95	0.05	0.00	0.05
JS_2681_c_pt08	97.80	0.05	0.02	0.00	0.04	2.07	0.00	0.05	0.01	97.50	2.45	0.05	0.00	0.00
JS_2681_c_pt09	97.91	0.11	0.11	0.01	0.00	1.03	0.44	0.04	1.39	98.63	1.22	0.10	0.00	0.05
JS_2681_c_pt10	98.89	0.03	0.11	0.00	0.07	0.98	0.00	0.05	0.04	98.75	1.15	0.05	0.00	0.05
JS_2682_a_pt01	98.28	0.00	0.01	0.00	0.00	1.27	0.02	0.02	0.02	98.50	1.50	0.00	0.00	0.00
JS_2682_a_pt02	98.15	0.01	0.09	0.00	0.04	1.56	0.04	0.04	0.14	98.10	1.85	0.00	0.00	0.05
JS_2682_a_pt03	97.55	0.02	0.21	0.01	0.06	1.47	0.04	0.02	0.45	98.09	1.76	0.00	0.00	0.15
JS_2682_a_pt04	98.23	0.03	0.01	0.00	0.00	1.01	0.03	0.04	0.14	98.75	1.20	0.05	0.00	0.00
JS_2682_b_pt05	98.35	0.05	0.20	0.02	0.09	1.64	0.00	0.28	0.03	97.84	1.96	0.05	0.00	0.15
JS_2682_b_pt06	98.52	0.04	0.25	0.02	0.06	0.98	0.01	0.24	0.14	98.64	1.16	0.05	0.00	0.15
JS_2682_b_pt07	98.65	0.03	0.18	0.00	0.08	1.22	0.01	0.06	0.00	98.45	1.45	0.00	0.00	0.10
JS_2682_b_pt08	98.06	0.06	0.18	0.02	0.09	1.48	0.00	0.04	0.52	98.09	1.76	0.05	0.00	0.10
JS_2682_c_pt09	99.46	0.05	0.12	0.00	0.03	1.32	0.01	0.02	0.00	98.30	1.55	0.05	0.00	0.10
JS_2682_c_pt10	99.25	0.06	0.01	0.00	0.02	1.16	0.00	0.03	0.00	98.60	1.35	0.05	0.00	0.00
JS_2682_c_pt11	97.81	0.03	0.16	0.02	0.01	1.29	0.00	0.02	0.07	98.30	1.55	0.05	0.00	0.10
JS_2682_c_pt12	96.74	0.00	0.23	0.01	0.05	1.25	0.19	0.04	0.59	98.34	1.51	0.00	0.00	0.15
3dolomite_stdck#1	54.16	0.12	0.01	0.03	0.02	45.24	0.01	0.00	0.13	50.15	49.75	0.10	0.00	0.00
JS_2663_c_pt01	62.88	0.02	0.08	0.03	0.20	38.60	0.00	0.12	0.01	57.82	42.13	0.00	0.00	0.05
JS_2663_c_pt02	59.66	0.01	0.00	0.00	0.10	42.97	0.04	0.06	0.05	53.91	46.09	0.00	0.00	0.00
JS_2663_c_pt03	48.90	0.01	0.01	0.01	0.19	36.73	0.01	0.08	0.07	52.89	47.11	0.00	0.00	0.00
JS_2663_c_pt04	61.92	0.02	0.04	0.02	0.31	38.42	0.13	0.09	0.12	57.59	42.41	0.00	0.00	0.00
JS_2663_c_pt05	57.55	0.01	0.06	0.01	0.12	43.14	0.05	0.05	0.07	52.91	47.04	0.00	0.00	0.05
JS_2663_a_pt06	61.54	0.04	0.02	0.01	0.13	38.95	0.03	0.07	0.00	57.06	42.89	0.05	0.00	0.00
JS_2663_a_pt07	60.32	0.07	0.01	0.01	0.09	40.18	0.04	0.06	0.00	55.81	44.14	0.05	0.00	0.00

Table 4:Continued

	Wt. % carbonate (all elements)									MOLE % (normalized for Mg, Ca, Fe, Mn, Sr only)				
Analysis	CaCO3 (wt%)	FeCO3 (wt%)	SrCO3 (wt%)	MnCO3 (wt%)	S(CO3)3 (wt%)	MgCO3 (wt%)	Al2(CO3)3 (wt%)	Na2CO3 (wt%)	Si(CO3)2 (wt%)	Ca (mole%)	Mg (mole%)	Fe (mole%)	Mn (mole%)	Sr (mole%)
JS_2663_a_pt08	57.45	0.04	0.01	0.01	0.25	42.91	0.23	0.06	0.27	52.99	46.96	0.05	0.00	0.00
JS_2663_a_pt09	58.84	0.02	0.05	0.01	0.51	38.86	1.26	0.12	2.39	56.02	43.92	0.00	0.00	0.05
JS_2663_a_pt10	57.67	0.00	0.09	0.02	0.27	41.75	0.25	0.07	0.91	53.76	46.18	0.00	0.00	0.05
JS_2683_a_pt01	99.23	0.06	1.11	0.00	0.00	1.11	0.03	0.02	0.00	97.90	1.30	0.05	0.00	0.75
JS_2683_a_pt02	78.79	0.00	1.81	0.00	0.00	0.32	0.02	0.03	0.17	97.95	0.50	0.00	0.00	1.55
JS_2683_a_pt03	98.82	0.08	0.24	0.00	0.02	1.05	0.01	0.01	0.21	98.55	1.25	0.05	0.00	0.15
JS_2683_a_pt04	100.31	0.06	0.08	0.00	0.01	0.82	0.02	0.01	0.05	98.95	0.95	0.05	0.00	0.05
JS_2683_b_pt05	97.85	0.01	0.05	0.02	0.06	2.64	0.05	0.02	0.31	96.84	3.11	0.00	0.00	0.05
JS_2683_b_pt06	100.53	0.05	0.04	0.00	0.00	0.69	0.01	0.00	0.05	99.15	0.80	0.05	0.00	0.00
JS_2683_b_pt07	96.46	0.63	0.07	0.00	0.12	2.17	1.99	0.02	4.90	96.85	2.58	0.53	0.00	0.05
JS_2683_b_pt08	100.60	0.07	0.05	0.00	0.00	1.26	0.01	0.02	0.03	98.45	1.45	0.05	0.00	0.05
JS_2683_c_pt09	99.73	0.05	0.08	0.25	0.01	0.01	0.00	0.02	0.01	99.70	0.00	0.05	0.20	0.05
JS_2683_c_pt10	99.54	0.49	0.05	1.68	0.01	0.34	0.00	0.02	0.01	97.70	0.40	0.40	1.45	0.05
JS_2683_c_pt11	99.95	0.11	0.12	0.00	0.03	0.69	0.00	0.02	0.00	99.00	0.80	0.10	0.00	0.10
JS_2683_c_pt12	96.59	0.47	0.04	0.00	0.07	1.66	0.87	0.03	2.81	97.53	2.00	0.41	0.00	0.05
JS_2683_d_pt13	97.06	1.90	0.07	0.02	0.11	1.27	0.90	0.04	2.05	96.83	1.48	1.64	0.00	0.05
JS_2683_d_pt14	99.79	0.09	0.10	0.00	0.06	0.78	0.02	0.01	0.13	98.95	0.90	0.10	0.00	0.05
JS_2683_d_pt15	100.23	0.08	0.10	0.00	0.00	0.96	0.01	0.01	0.00	98.80	1.10	0.05	0.00	0.05
LS_1_a_pt01	100.52	0.03	0.04	0.01	0.14	0.57	0.01	0.10	0.00	99.30	0.65	0.05	0.00	0.00
LS_1_a_pt02	99.76	0.03	0.08	0.00	0.00	0.99	0.04	0.02	0.15	98.80	1.15	0.00	0.00	0.05
LS_1_a_pt03	99.36	0.03	0.00	0.03	0.04	0.86	0.13	0.02	0.33	98.95	1.00	0.05	0.00	0.00
LS_1_a_pt04	99.63	0.02	0.04	0.00	0.00	0.90	0.03	0.02	0.07	98.90	1.05	0.00	0.00	0.05
LS_1_b_pt05	97.70	0.00	0.01	0.00	0.11	0.66	0.00	0.06	0.05	99.20	0.80	0.00	0.00	0.00
LS_1_b_pt06	101.06	0.01	0.03	0.00	0.01	0.59	0.00	0.05	0.08	99.30	0.70	0.00	0.00	0.00
LS_1_b_pt07	99.50	0.02	0.03	0.01	0.07	0.76	0.00	0.01	0.06	99.10	0.90	0.00	0.00	0.00
LS_1_b_pt08	99.81	0.00	0.00	0.03	0.04	0.58	0.04	0.02	0.18	99.30	0.70	0.00	0.00	0.00
LS_1_c_pt09	88.74	0.00	0.00	0.00	0.04	0.81	0.02	0.02	0.01	98.95	1.05	0.00	0.00	0.00
LS_1_c_pt10	98.47	0.00	0.00	0.04	0.11	0.56	0.00	0.04	0.01	99.30	0.65	0.00	0.05	0.00
LS_1_c_pt11	98.04	0.17	0.00	0.04	0.11	0.84	0.76	0.03	2.06	98.77	1.02	0.15	0.05	0.00
LS_1_d_pt12	98.43	0.01	0.02	0.02	0.07	0.34	0.03	0.03	0.30	99.60	0.40	0.00	0.00	0.00
LS_1_d_pt13	97.47	0.40	0.01	0.01	0.08	0.71	0.36	0.06	0.97	98.79	0.86	0.35	0.00	0.00
LS_1_d_pt14	98.88	0.17	0.02	0.00	0.07	1.02	0.81	0.04	1.55	98.63	1.22	0.15	0.00	0.00
JS_2687_a_pt01	100.18	0.06	0.06	0.00	0.03	1.51	0.03	0.03	0.01	98.15	1.75	0.05	0.00	0.05

Table 4:Continued

	Wt. % carbonate (all elements)									MOLE % (normalized for Mg, Ca, Fe, Mn, Sr only)				
Analysis	CaCO3 (wt%)	FeCO3 (wt%)	SrCO3 (wt%)	MnCO3 (wt%)	S(CO3)3 (wt%)	MgCO3 (wt%)	Al2(CO3)3 (wt%)	Na2CO3 (wt%)	Si(CO3)2 (wt%)	Ca (mole%)	Mg (mole%)	Fe (mole%)	Mn (mole%)	Sr (mole%)
JS_2687_a_pt02	100.25	0.09	0.03	0.00	0.02	0.55	0.04	0.03	0.09	99.25	0.65	0.10	0.00	0.00
JS_2687_a_pt03	100.80	0.08	0.04	0.01	0.04	0.48	0.00	0.01	0.01	99.35	0.55	0.05	0.00	0.05
JS_2687_a_pt04	99.34	0.06	0.06	0.01	0.00	2.08	0.01	0.02	0.00	97.50	2.40	0.05	0.00	0.05
JS_2687_b_pt05	100.52	0.05	0.00	0.00	0.00	1.56	0.00	0.01	0.06	98.15	1.80	0.05	0.00	0.00
JS_2687_b_pt06	100.25	0.07	0.00	0.00	0.02	1.04	0.08	0.03	0.36	98.74	1.20	0.05	0.00	0.00
JS_2687_b_pt07	100.84	0.07	0.11	0.00	0.01	0.40	0.13	0.07	0.10	99.40	0.45	0.05	0.00	0.10
JS_2687_b_pt08	99.66	0.02	0.09	0.00	0.05	0.75	0.02	0.03	0.60	99.05	0.90	0.00	0.00	0.05
JS_2687_c_pt09	98.72	0.02	0.03	0.02	0.15	0.95	0.02	0.10	0.37	98.84	1.16	0.00	0.00	0.00
JS_2687_c_pt10	101.10	0.15	0.05	0.39	0.01	0.58	0.00	0.02	0.09	98.85	0.65	0.10	0.35	0.05
JS_2687_c_pt11	100.67	0.07	0.06	0.00	0.00	0.25	0.01	0.03	0.00	99.60	0.30	0.05	0.00	0.05
JS_2687_c_pt12	99.23	0.03	0.06	0.00	0.00	1.87	0.02	0.04	0.04	97.75	2.20	0.00	0.00	0.05
JS_2687_c_pt13	100.48	0.04	0.07	0.00	0.02	1.43	0.02	0.02	0.05	98.25	1.65	0.05	0.00	0.05
JS_2687_d_pt14	99.68	0.05	0.13	0.01	0.04	0.74	0.00	0.02	0.02	99.00	0.85	0.05	0.00	0.10
JS_2687_d_pt15	100.19	0.08	0.08	0.01	0.04	0.77	0.01	0.02	0.09	99.00	0.90	0.05	0.00	0.05
JS_2687_d_pt16	101.11	0.08	0.06	0.00	0.00	0.58	0.01	0.02	0.07	99.25	0.65	0.05	0.00	0.05
3dolomite_stdck#1	53.71	0.12	0.00	0.01	0.05	45.44	0.04	0.00	0.15	49.82	50.08	0.10	0.00	0.00
JS_2684_a_pt01	59.96	0.03	0.02	0.01	0.32	39.03	0.02	0.10	0.15	56.40	43.60	0.00	0.00	0.00
JS_2684_a_pt02	61.30	0.03	0.06	0.03	0.35	37.43	0.01	0.07	0.06	57.92	41.98	0.00	0.05	0.05
JS_2684_a_pt03	61.28	0.07	0.00	0.05	0.31	37.55	0.07	0.09	1.29	57.81	42.08	0.05	0.05	0.00
JS_2684_a_pt04	98.06	0.05	0.02	0.01	0.16	2.83	0.07	0.05	0.19	96.64	3.31	0.05	0.00	0.00
JS_2684_b_pt05	58.32	0.02	0.03	0.02	0.24	40.39	0.05	0.08	0.04	54.89	45.11	0.00	0.00	0.00
JS_2684_b_pt06	36.58	12.89	0.00	0.41	0.12	31.33	9.83	0.84	116.62	42.90	43.62	13.07	0.41	0.00
JS_2684_b_pt07	59.31	0.07	0.02	0.01	0.21	39.32	0.02	0.05	0.00	55.94	44.01	0.05	0.00	0.00
JS_2684_b_pt08	58.76	0.01	0.00	0.00	0.22	40.44	0.02	0.07	0.05	55.04	44.96	0.00	0.00	0.00
JS_2684_c_pt09	60.44	0.06	0.00	0.02	0.42	38.47	0.02	0.11	1.16	56.93	43.02	0.05	0.00	0.00
JS_2684_c_pt10	58.61	0.02	0.03	0.01	0.17	40.38	0.03	0.05	0.05	54.99	45.01	0.00	0.00	0.00
JS_2684_c_pt11	58.22	0.00	0.00	0.00	0.13	40.65	0.02	0.09	0.01	54.69	45.31	0.00	0.00	0.00
JS_2684_c_pt12	59.42	0.03	0.08	0.03	0.13	39.13	0.00	0.09	0.06	56.12	43.83	0.00	0.00	0.05

Table 5

Sample names with facies type, name of outcrop location collected from, and coordinates of sample location.

Location	Facies	Sample	Waypoint	Longitude	Latitude	Elevation (m)
1000 Steps	*Acropora cervicornis* floatstone	26-1	273	-68.321653	12.21093	7.82
Bike Trail	Coralgal grainstone/packstone	4BON1	5	-68.31203	12.21164	43
Bike Trail	Coralgal grainstone/packstone	4BON2	6	-68.31236	12.21146	44
Bike Trail	Coralgal grainstone/packstone	4BON3	7	-68.31272	12.2113	40
Bike Trail	Coralgal grainstone/packstone	4BON4	8	-68.313	12.21109	39
Bike Trail	Coralgal grainstone/packstone	19BON1	78	-68.3109	12.21226	43
Bike Trail	*Amphistegina sp.* grainstone	19BON2	79	-68.29456	12.22399	94
Bike Trail	Dolomite	19BON3	80	-68.30119	12.22023	102
Bike Trail	Dolomite	19BON4	81	-68.30158	12.21982	94
Bike Trail	Dolomite	19BON5	83	-68.30206	12.21933	91
Bike Trail	Dolomite	19BON6	84	-68.30465	12.21663	82
Bike Trail	Dolomite	19BON7	85	-68.30763	12.21359	80
Bike Trail	Dolomite	19BON8	86	-68.30868	12.21296	71
Bike Trail	Coralgal grainstone/packstone	19BON9	87	-68.30914	12.21288	60
Bike Trail	*Amphistegina sp.* grainstone	15-5-1	459	-68.290225	12.229172	58.04
Bike Trail	*Amphistegina sp.* grainstone	15-2-1	461	-68.292046	12.227762	68.62
Boca Onima	*Montastrea annularis framestone*	26-7-1	295	-68.311362	12.253295	13.82
Boca Onima	*Montastrea annularis framestone*	26-7-2	295	-68.311362	12.253295	13.82
Boca Onima	*Montastrea annularis framestone*	26-8-1	296	-68.309407	12.248896	12.62
Boca Onima	Dolomite	26-8-2	296	-68.309407	12.248896	12.62
Boca Onima	*Montastrea annularis framestone*	26-8-3	296	-68.309407	12.248896	12.62
Boca Onima	Dolomite	26-8-4	296	-68.309407	12.248896	12.62
Boca Onima	*Montastrea annularis framestone*	26-8-5	296	-68.309407	12.248896	12.62
Boca Onima	Dolomite	26-8-6	296	-68.309407	12.248896	12.62
Boca Onima	Dolomite	26-8-7	296	-68.309407	12.248896	12.62
Bolivia	Dolomite	20BON1	88	-68.28689	12.23526	25
Bolivia	Coralgal grainstone/packstone	8-3_1	365	-68.337996	12.217329	21.27

Table 5: Continued

Location	Facies	Sample	Waypoint	Longitude	Latitude	Elevation (m)
Bolivia	Coralgal grainstone/packstone	8-3_2	365	-68.337996	12.217329	21.27
Bolivia	Coralgal grainstone/packstone	13-6-1	372	-68.333004	12.264884	15.75
Bolivia	*Acropora palmata* rudstone	12-2_1	428	-68.210291	12.212714	10.46
Bolivia	*Acropora palmata* rudstone	12-2_2	429	-68.210743	12.217417	9.98
Bolivia	*Acropora palmata* rudstone	12-2_3	429	-68.210743	12.217417	9.98
Bolivia	*Acropora palmata* rudstone	12-2_4	429	-68.210743	12.217417	9.98
Bolivia	*Acropora palmata* rudstone	12-2_5	429	-68.210743	12.217417	9.98
Bolivia	*Acropora palmata* rudstone	12-3_1	430	-68.225047	12.219576	5.65
Bolivia	*Acropora palmata* rudstone	12-3_2	430	-68.225047	12.219576	5.65
Bolivia	*Acropora palmata* rudstone	12-3_3	430	-68.225047	12.219576	5.65
Bolivia	Coralgal grainstone/packstone	12-4_1	431	-68.237411	12.221696	11.9
Bolivia	Coralgal grainstone/packstone	12-4_4	431	-68.237411	12.221696	11.9
Bolivia	Coralgal grainstone/packstone	12-5_1	432	-68.255795	12.226326	6.13
Bolivia	Coralgal grainstone/packstone	12-5_2	432	-68.255795	12.226326	6.13
Bolivia	*Montastrea annularis framestone*	12-6_1	433	-68.276073	12.233363	13.58
Bolivia	*Montastrea annularis framestone*	12-7_1	434	-68.257085	12.231567	2.53
Bolivia	*Montastrea annularis framestone*	12-8_1	435	-68.238875	12.227245	10.22
Bolivia	*Montastrea annularis framestone*	12-8_2	435	-68.238875	12.227245	10.22
Bolivia	Dolomite	15-3-1	464	-68.276913	12.230173	29.21
Bolivia	Coralgal grainstone/packstone	15-4-1	465	-68.279132	12.230351	28.72
Bolivia	Coralgal grainstone/packstone	12-4_2	-	-	-	-
Bolivia	Coralgal grainstone/packstone	12-4_3	-	-	-	-
Fontein	*Montastrea annularis framestone*	26-2-1	275	-68.300061	12.239426	32.33
Fontein	(Tufa)	26-3-1	276	-68.299959	12.23963	24.88
Fontein	(Tufa)	26-3-2	276	-68.299959	12.23963	24.88
Goto Meer	Dolomite	25-4	260	-68.375169	12.231382	59.73
Goto Meer	Dolomite	25-5	261	-68.37518	12.231345	50.84
Goto Meer	Coralgal grainstone/packstone	25-6	262	-68.374596	12.230864	43.38
Goto Meer	Coralgal grainstone/packstone	25-7	263	-68.374621	12.230794	29.21
Goto Meer	Coralgal grainstone/packstone	25-8	264	-68.374489	12.230733	19.59
Goto Meer	Coralgal grainstone/packstone	25-9	264	-68.374489	12.230733	19.59

Table 5: Continued

Location	Facies	Sample	Waypoint	Longitude	Latitude	Elevation (m)
Goto Meer	Coralgal grainstone/packstone	25-10	265	-68.374358	12.230567	8.06
Goto Meer	Coralgal grainstone/packstone	25-11	266	-68.374453	12.230882	1.57
Goto Meer	Coralgal grainstone/packstone	25-12	267	-68.374539	12.230971	2.05
Goto Meer	Coralgal grainstone/packstone	25-13	268	-68.374646	12.231553	27.76
Goto Meer	Coralgal grainstone/packstone	25-14	269	-68.374797	12.231773	18.39
Goto Meer	Coralgal grainstone/packstone	25-15	270	-68.374832	12.231621	15.51
Rincon south	Coralgal grainstone/packstone	13-8-1	447	-68.329132	12.226513	102.75
Santa Barbara	Dolomite	20BON2	89	-68.27593	12.19124	70
Seru Grandi	Dolomite	15BON1	53	-68.35737	12.29171	12
Seru Grandi	*Montastrea annularis* framestone	15BON2	54	-68.35772	12.2924	10
Seru Grandi	*Montastrea annularis* framestone	15BON3	55	-68.35819	12.29415	10
Seru Grandi	*Montastrea annularis* framestone	15BON4	57	-68.35847	12.2947	10
Seru Grandi	Dolomite	26-6-1	288	-68.356883	12.291249	18.39
Seru Grandi	Dolomite	26-6-3	288	-68.356883	12.291249	18.39
Seru Grandi	Dolomite	26-6-4	288	-68.356883	12.291249	18.39
Seru Grandi	*Montastrea annularis* framestone	27-1-1	298	-68.358301	12.295969	10.7
Seru Grandi	*Montastrea annularis* framestone	27-2-1	301	-68.358745	12.295473	4.21
Seru Grandi	*Montastrea annularis* framestone	27-3-1	302	-68.358477	12.29468	13.58
Seru Grandi	*Montastrea annularis* framestone	27-4-1	303	-68.358139	12.293848	26.8
Seru Grandi	Dolomite	27-5-1	305	-68.357425	12.292118	22.48
Seru Grandi	*Montastrea annularis* framestone	27-7-1	306	-68.358275	12.289565	37.86
Seru Grandi	Dolomite	27-8-1	307	-68.358545	12.290161	29.21
Seru Grandi	Dolomite	27-9-1	309	-68.35725	12.2899	27.52
Seru Grandi	Dolomite	27-10-2	310	-68.35725	12.2899	-0.6
Seru Grandi	*Montastrea annularis* framestone	13-1-1	437	-68.356522	12.290214	15.99

Table 5: Continued

Location	Facies	Sample	Waypoint	Longitude	Latitude	Elevation (m)
Seru Grandi	Dolomite	13-2-1	438	-68.356754	12.289906	12.86
Seru Grandi	Dolomite	13-2-2	438	-68.356754	12.289906	12.86
Seru Grandi	*Montastrea annularis* framestone	13-3-1	440	-68.358181	12.289801	40.26
Seru Grandi	*Montastrea annularis* framestone	13-3-2	440	-68.358181	12.289801	40.26
Seru Grandi	Dolomite	13-4-1	441	-68.358876	12.290511	44.83
Seru Grandi	*Montastrea annularis* framestone	13-5-1	442	-68.358787	12.290594	37.38
Seru Grandi	*Montastrea annularis* framestone	13-5-2	442	-68.358787	12.290594	37.38
Seru Grandi	*Montastrea annularis* framestone	14-1-1	449	-68.357088	12.289933	24.4
Seru Grandi	Dolomite	14-1-2	449	-68.357088	12.289933	24.4
Seru Grandi	Dolomite	14-2-1	450	-68.356867	12.289964	20.55
Seru Grandi	*Montastrea annularis* framestone	14-3-1	451	-68.35697	12.290966	24.88
Seru Grandi	*Montastrea annularis* framestone	14-4-1	452	-68.35806	12.291121	30.89
Seru Grandi	Dolomite	14-5-1	453	-68.35936	12.291108	40.02
Seru Grandi	Dolomite	14-6-1	454	-68.359756	12.291041	45.55
Seru Grandi	Dolomite	14-7-1	455	-68.359576	12.293661	31.85
Seru Grandi	Dolomite	14-8-10	456	-68.360058	12.293381	59.49
Seru Grandi	*Montastrea annularis framestone*	14-9-1	457	-68.358898	12.294064	36.66
Seru Grandi	Dolomite	26-6-unlabeled	-	-	-	-
Seru Largu	*Amphistegina sp.* grainstone	16BON1	61	-68.27079	12.19332	102
Seru Largu	*Amphistegina sp.* grainstone	16BON2	64	-68.27076	12.19331	101
Seru Largu	*Amphistegina sp.* grainstone	16BON3	64	-68.27076	12.19331	101
Seru Largu	*Amphistegina sp.* grainstone	16BON4	71	-68.27082	12.19342	112
Seru Largu	*Amphistegina sp.* grainstone	16BON5	74	-68.2693	12.19349	113
Seru Largu	*Amphistegina sp.* grainstone	16BON6	75	-68.27014	12.19332	115
Seru Largu	*Amphistegina sp.* grainstone	16BON7	76	-68.2702	12.19328	108

Table 5: Continued

Location	Facies	Sample	Waypoint	Longitude	Latitude	Elevation (m)
Tolo	Mixed Coral Framestone	9-1_3	366	-68.339001	12.218228	23.92
Tolo	Mixed Coral Framestone	9-1_4	367	-68.340412	12.21799	26.8
Tolo	Mixed Coral Framestone	9-2_1	368	-68.341516	12.217329	11.9
Tolo	Mixed Coral Framestone	9-2_2	368	-68.341516	12.217329	11.9
Tolo	Mixed Coral Framestone	9-2_3	368	-68.341516	12.217329	11.9
Tolo	Mixed Coral Framestone	9-2_4	369	-68.341276	12.217704	28.48
Tolo	Dolomite	9-3_1	371	-68.323218	12.25842	13.34
Tolo	Mixed Coral Framestone	9-4_1	374	-68.281251	12.203296	119.33
Tolo	Mixed Coral Framestone	15-5-1	469	-68.258949	12.033917	8.06
Tolo	Mixed Coral Framestone	9-1_1	-	-	-	-
Tolo	Mixed Coral Framestone	9-1_2	-	-	-	-

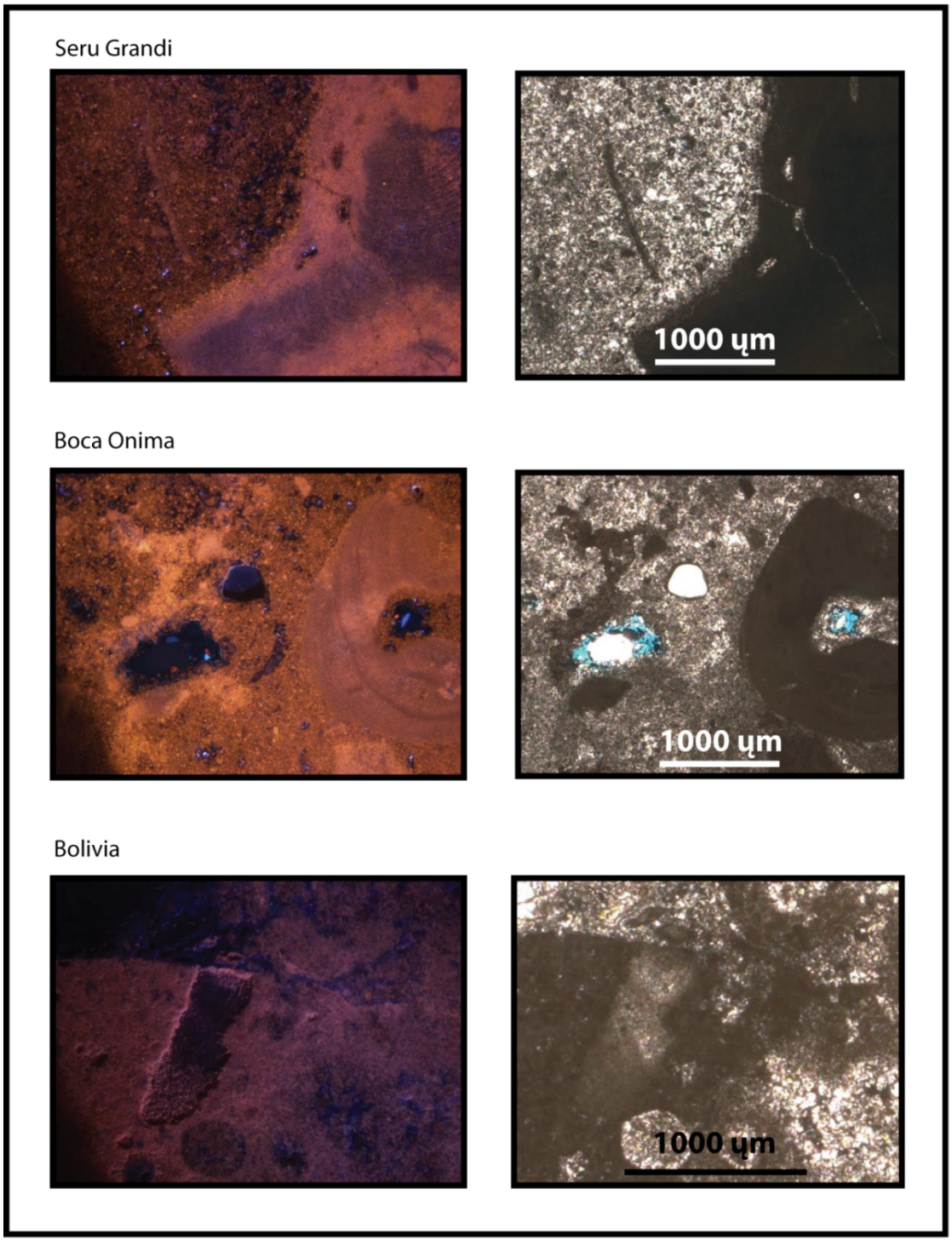

Figure 34: Comparing dolomite samples using paired Cathodoluminescence (CL) and plain light images. Seru Grandi, Sample 26-6-3; Boca Onima, Sample 26-8-4; Bolivia, Sample 15-3-1; Tolo, Sample 9-3-1; Santa Barbara, Sample 20BON2.

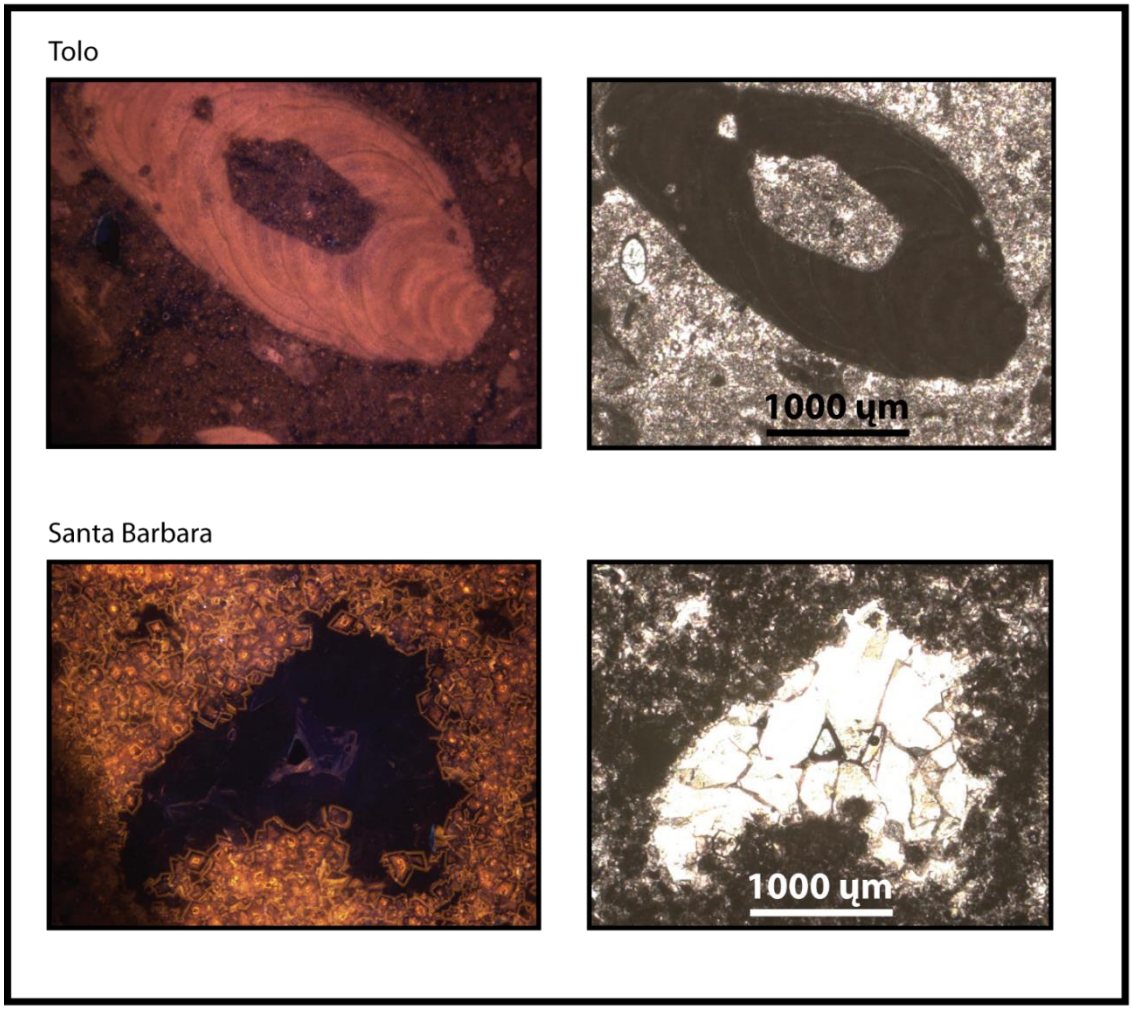

Figure 34 continued: Paired Cathodoluminescence (CL) and plain light images. Tolo, Sample 9-3-1; Santa Barbara, Sample 20BON2.

Seru Grandi – Sample has luminescence, with both matrix and bioclasts (red algae) luminescing. The matrix is composed of microcrystalline quartz and luminesces to a dull to moderate intensity of orange. The red algae is of moderate intensity of orange-pink color [Fig. 1]. Sample 26-6-3.

Boca Onima - This sample luminesces more strongly than Seru Grandi's samples with the matrix being medium to bright orange and the red algae medium orange-red in color. Matrix is still microcrystalline so any growth pattern within the grains is not obvious. Dolomite near pores do not luminesce as bright as dolomite away from pores [Fig. 1]. Sample 26-8-4.

Bolivia – This sample has red algae present which luminesces to a dull orange-pink color. Microcrystalline dolomite grains do not luminesce, or are a very dull blue [Fig.1]. Sample 15-3-1.

Tolo - Sample has very dull luminescence in the microcrystalline matrix, with a brown color. Red algae is much brighter, with medium intensity and a red-orange color. No observable growth patterns within matrix dolomite [Fig. 2]. Sample 9-3-1.

Santa Barbara – Sample is much coarser than all of the second terrace microcrystalline dolomite, and exhibits a sucrosic texture. Grain boundaries are euhedral and rhombic. Luminescence ranges from a low intensity to a very high intensity, with colors from brown to yellow. The larger grains contain the most luminescent (yellow) thin bands within the grains, with one per grain if present. These are located varying from within the middle to halfway within the crystals. The dull brown luminescence is located on

the outside of the grains. The smallest grains are entirely dull brown, or black due to no luminescence [Fig. 2]. Sample 20BON2.